EVALUATION OF PHOTON IMAGING DEVICES

A final technical report for
Contract: N00014-68-A-0215-0007
Project: NR015-732/6-29-71

SPONSORED BY THE
Office of Naval Research
with funding from
ARPA Order No. 1938

SUBMITTED BY

UNIVERSITY OF RHODE ISLAND
DEPARTMENT OF ELECTRICAL ENGINEERING
KINGSTON, RHODE ISLAND 02881

Principal Investigators: S. Nudelman
J. A. Hall

DISCLAIMER NOTICE

THIS DOCUMENT IS THE BEST QUALITY AVAILABLE.

COPY FURNISHED CONTAINED A SIGNIFICANT NUMBER OF PAGES WHICH DO NOT REPRODUCE LEGIBLY.

EVALUATION OF PHOTON IMAGING DEVICES

a final technical report for

Contract: N00014-68-A-0215-0007

Project: NR015-732/6-29-71

sponsored by the

Office of Naval Research

with funding from

ARPA Order No. 1938

submitted by

The Department of Electrical Engineering
University of Rhode Island
Kingston, Rhode Island 02881

Principal Investigators: S. Nudelman
J. A. Hall

TABLE OF CONTENTS

1. Introduction

The research conducted at the University of Rhode Island under this contract, the first phase of a larger program, was concentrated on the establishment of procedures for evaluation of photon imaging devices and subsystems, with emphasis on television pickup tubes. The results may be grouped into three main categories. First, we have re-examined the basic criteria now used for rating the performance of photon imaging devices and systems and propose consideration of detective quantum efficiency (DQE) as a more significant figure of merit. This criterion recognizes that photoelectronic imaging devices basically count photons, and that for an ideal device or system, every incident photon should result in a countable event at the output of the device. DQE is simply, for the entire device or entire system, the ratio of the number of countable output events to the number of incident photons. For an ideal device or system, DQE = 1. Hence measured DQE provides a convenient figure of merit showing by what margin the device fails to count all incident photons. For an otherwise ideal device with a real photocathode, the DQE will equal the quantum efficiency of the photocathode for the radiant flux spectral distribution incident on the device or system input. The DQE concept and some examples of its use are discussed at length in the body of this report and expecially in the first appendix.

Second, a basic test equipment for the evaluation of television camera tubes was set up in the laboratories of the Department of Electrical Engineering at the University of Rhode Island. This basic equipment is being augmented with separate "heads" optimised for each major camera tube type, following the teaching of Hall that a tele-

vision camera tube cannot really be tested by itself, but that one can meaningfully test as a unit the tube together with an optimum combination of focus and deflection coils, shielding and decoupling networks, video preamplifier, and the objective lens required to form an image on the input photocathode. At this date, we can evaluate vidicons, silicon target vidicons, and SEC camera tubes.

Because the determination of DQE, as well as other figures of merit, depends on an accurate measure of video signal and of noise in the video channel, or later in the image at the system output, much effort has been devoted to obtaining meaningfully accurate measurements of signal and of noise and of their spectral distribution. Because the widely used analog methods described by Hall[1] are of very limited accuracy, we have made much use of digital techniques which permit measuring signal in noise accurately down to signal to noise ratios of the order of 1:10. RMS noise was measured by a direct sampling technique which makes no assumptions on the type of noise statistics and which can provide that extreme accuracy needed to separate the camera tube noise contribution from that of the video amplifier. The techniques used are described in the body of this report, and in the second appendix. As far as we are aware, these techniques have already provided measurement accuracy better than any previous methods.

Third, the measurement techniques are now being extended to evaluate signal and noise directly in the output image presented to the human observer. The performance of electro-optical systems has in general been predicted in terms of the characteristics of the video signal. Rosell, for example, predicts observer performance from the display signal to noise ratio, SNR_D, but derives SNR_D from the characteristics of the video signal, without regard to the degradations

introduced by the display. A direct measurement of output image quality both includes the display characteristics, but also may help to clarify the effect of control settings, of the choice of gain (contrast) and brightness (background) settings on the performance of the decision making human who is the final link in most electro-optical systems. Candidate procedures and some initial results are described in the body of this report. The methods being developed will be effective on any type of display, including television displays, directly viewed image intensifier output images, and electromechanically scanned displays as used in some FLIR systems. The resulting data, described at first in terms of DQE or of SNR_D, should provide a far better understanding of the factors which make for effective observer performance in using each type of photon imaging system.

2. Detective Quantum Efficiency

Since Albert Rose first applied the fluctuation theory of vision to predicting the "seeing" performance which a man might achieve if aided by an image intensifier tube, workers have used various yardsticks to evaluate the performance of photo-electronic imaging devices. Most, but not all, are based on a measurement of the contrast and brightness (signal) in the display and of the fluctuation in that brightness (noise), or for television systems on the signal to noise ratio measured in the video channel. Most are geared primarily to predicting human observer performance, an important goal, but inappropriate for use with systems in which a computer, rather than an observer, undertakes recognition or tracking tasks. None, so far as we know, establishes an absolute yardstick against which actual system or sensor performance can be compared to show by what margin it fails to be ideal. To provide a figure of merit which fills this need, we are working with the concept of Detective Quantum Efficiency, (DQE).

All electro-optical imaging sensors in a sense count photons, at higher rates in brighter parts of the picture. An ideal system would produce an observable or recordable event for each incident photon. The DQE of a system or a sensor is simply the ratio of the number of observable events presented at the output to the number of photons incident on the input, both referred to an appropriate area and an appropriate sampling interval. For an ideal image intensifier, say, with a real photocathode irradiated at very low intensity with an image in monochromatic light, since each photo-electron leaving the first photocathode would result in an observable flash of light at a corresponding spot in the image on the output phosphor screen, the

DQE would be simply the quantum efficiency of the photocathode for irradiation of that wavelength.

Unfortunately, for many systems, including image intensifiers operating with larger input photon fluxes, it is essentially impossible to count the number of observable events in an appropriate area of the output display, or the number of observable events per second in a video signal. It is, however, possible to measure the signal to noise or signal to fluctuation ratio in a suitable area of the output image for an appropriate sampling time and to compare it with the signal to fluctuation ratio (or the video signal to noise ratio) which an ideal device would have produced if every incident photon had resulted in a countable output event. And as shown in Appendix I,

$$DQE = \frac{(\text{SNR out of real device})^2}{(\text{SNR out of ideal device})^2}$$

For an ideal device, DQE = 1. For one with a real photocathode, DQE = η , where η is the effective quantum efficiency for the spectral distribution of light in the input image.

As shown in Appendix I, the DQE figure of merit seems applicable to photon imaging devices as diverse as television camera tubes and photographic film, and hence should serve as a basic yardstick to permit comparing the effectiveness of widely different imaging systems, thus unifying the rating of such devices or systems against each other and against an absolute standard, against the performance of an ideal device. Realizing this goal would be a tremendous contribution to the art and to those armed services agencies which use imaging devices.

The status of this part of the program is described in Appendix I. Because this is an on-going program, and because much of the analysis has been performed by Dr. S. Nudelman of these laboratories during a

Sabbatical year in Germany, and latest modification are not available, Appendix I in its present form must be regarded as a status report only. Some points are still being refined, and the experimental application will be developed during phase III of this program. We expect that a final version of Appendix I with significant experimental data will appear as part of the phase III final report from these laboratories.

Sabbatical year in Germany, and latest modification are not available, Appendix I in its present form must be regarded as a status report only. Some points are still being refined, and the experimental application will be developed during phase III of this program. We expect that a final version of Appendix I with significant experimental data will appear as part of the phase III final report from these laboratories.

3. Digital Techniques for the Evaluation of Television Cameras and Sensors.

3.1 General

The basic equipment used for evaluation of television sensors at this University is a television camera tube test apparatus built by the Westinghouse Electronic Tube Division. Similar to equipments used by Westinghouse to evaluate SEC camera tubes, vidicons, and SIT camera tubes, this equipment has proven highly reliable, and is seldom out of service, despite the large number of accessories with which it has been interfaced as new evaluation methods were developed. The basic equipment provides well regulated ripple free power supplies to the tube under test, normally set with aid of a digital voltmeter, is normally used with a choice of back illuminated transparency test patterns mounted on a mirror tunnel light box designed after MacRae et.al., and provides both for display of the video information on a high quality Conrac monitor and for examination of the video signal on a Tektronix 547 or similar oscilloscope. To provide an optimum interface with the rest of the equipment, the tube under test is housed in a specially designed "head" which provides a light tight enclosure, and which contains a video preamplifier mounted close to the tube output terminal and matched for tube output electrode capacitance, a set of the focus, alignment, and deflection coils specified by the tube maker as optimum for that tube, an objective lens of appropriate focal length and known m.t.f., and electrode decoupling circuits to provide proper a.c. grounds close to the tube electrode leads to avoid unwanted cross coupling and prevent any tendency toward oscillation. A separate head has been designed for each tube type, and use of a built-in plug and socket arrangement means that one may change tube types in

a few minutes time with assurance of optimum conditions by simply changing heads with the tubes inside, and of course resetting electrode voltages and coil currents.

The video amplifier channel has a basic bandwidth of 12 to 15 MHz. Signal and noise currents are normally measured with respect to a calibrating pulse generated in the equipment and injected at the ground end of the camera tube load resistor, as taught by Hall. Preamplifiers include both the traditional TV camera head amplifier, typically using a 50Kohm load resistor without compensation for the effects of shunting tube and circuit capacitance, but with a 6 db. per octave rising gain vs. frequency characteristic in the preamplifier to provide an overall flat response, and the recently popular operational type preamplifier in which inverse feedback is used to reduce the effective input impedance to a few thousand ohms so that shunt capacitance effects may be ignored. In both cases the equivalent rms input noise current in a 10 MHz video bandwidth, with camera tube in place but not operating is about 3 to 4 na., about at the theoretical limit.

The general philosophy in our program to develop procedures for image evaluation has been to use manual setup of each test sequence for flexibility and accuracy, and to use our digital computer capability, where needed, for more effective analysis of the video signal and therefore to permit obtaining more accurate measurements. The approach was described early in the program in a paper "Methods for Evaluating Camera Tubes" by Fisher, Lee, McCollough, Nudelman, Tufts and Wilkinson of these laboratories, which appears with some revisions as Appendix II of this report. As indicated there, the traditional scheme of measuring signal amplitude by viewing the video display on a line selector scope is of satisfactory accuracy for most purposes

when the light level is high and the test pattern coarse so that signal to noise ratio is high, but completely unsatisfactory for the cases of most interest where low light levels or a fine (high spatial frequency) test pattern and falling m.t.f. reduce the video signal to noise ratio far below unity, yet where the observer still sees a useable picture on the display. Further, the low signal to noise ratio experienced in nearly all television signals has made it nearly impossible to determine the signal waveform accurately, and has, for example, prevented investigators from measuring m.t.f. in the definitive manner by measuring the line spread function and determining its Fourier transform. To obtain better video signal information, we have made use of the repetitive character of the television signal of a stationary scene, sampling signal plus noise in a number of successive frames and averaging out the noise. The implementations, described in Appendix II, have involved a box car integrator, a sampling scope, and the combination of an analogue storage terminal to reduce the effective video bandwidth, followed by an A/D converter. The digital output from either the sampling scope or the storage terminal was then fed to a DEC PDP-9 digital computer for analysis. Results obtained are reported in the following sections.

Noise in the presence of signal in the video channel has traditionally been measured by viewing the display on a line selector scope, estimating the height of the apparant noise envelope, and dividing by 6. Other possible methods are described in Appendix III. The video sampling and digital processing equipment used for the second and third signal measuring schemes listed above may also be used to obtain far more definitive noise measurements, as described in Appendix II and in the following sections.

3.2 Computer Aided Television System Evaluation

This section will basically describe the status of the computer aided image tube evaluation system described in a paper presented at the 5th Symposium on Photo-electronic Imaging Devices. The paper is enclosed for reference, as Appendix II.

TEST CHARTS

In the paper, the design of a test chart better suited to the computer aided system was mentioned. In particular, we were trying to develop a chart which had the following properties.

1. Large value of spectrum (when scanned at the TV rate) in the regions of interest and low outside that region, to minimize the possibility of aliasing or other effects in later calculations.
2. A smooth spectrum in the region of interest, preferably uniform, so that the tube MTF's could be directly computed.
3. One which would enable a large signal to be generated by the tube to minimize noise effects.

For ease of fabrication, we constrained ourselves to two-level charts (black and white).

The spectra of the Westinghouse ET-1702 and Limansky charts were analytically computed for reference and compared to two classes of candidate charts; Those based on M-sequences and those based on Barker sequences.

When considered as periodic functions, M-sequences have desirable spectra. Unfortunately, when considered as aperiodic sequences, the spectral qualities deteriorate and depend on the phase of the sequence selected. The only Barker sequence which looked promising was that of length = 13, but it had no significant advantages over the two reference

charts. The conclusion was that the improvements in the charts considered over the ET-1702 or Limansky charts were not substantial enough to warant further investigation.

We have some ideas for other possibilities and have derived a general formula for the spectra of the charts, but its solution for other than trivial cases is itself a non-trivial task and has been given a lower priority than other work, some of which is described below

COMPUTER SYSTEM

A number of hardware modifications have been made to the system since the writing of the paper to make its operation more reliable, and it can now be controlled from the computer. Hardware development is considered to be virtually complete and current work is in the following 3 areas:

1. Software development
2. Analysis of accuracy of data processing
3. Calibration of the system

Software Developments

The major accomplishment here is the writing of a program to process data from the photo-imaging laboratory. This program provides the following information:

1. Signal (as a function of time) displayed on graphics display terminal
2. Fixed pattern noise due to target structure of storage terminal, and also a slight curvature of its pedestal
3. Signal (1) corrected for fixed pattern noise (2)
4. Power spectrum of signal

5. Power spectral density of noise from storage terminal as well as in signal
6. Effective sampling frequency

Below are photographs showing 1, 2 and 3.

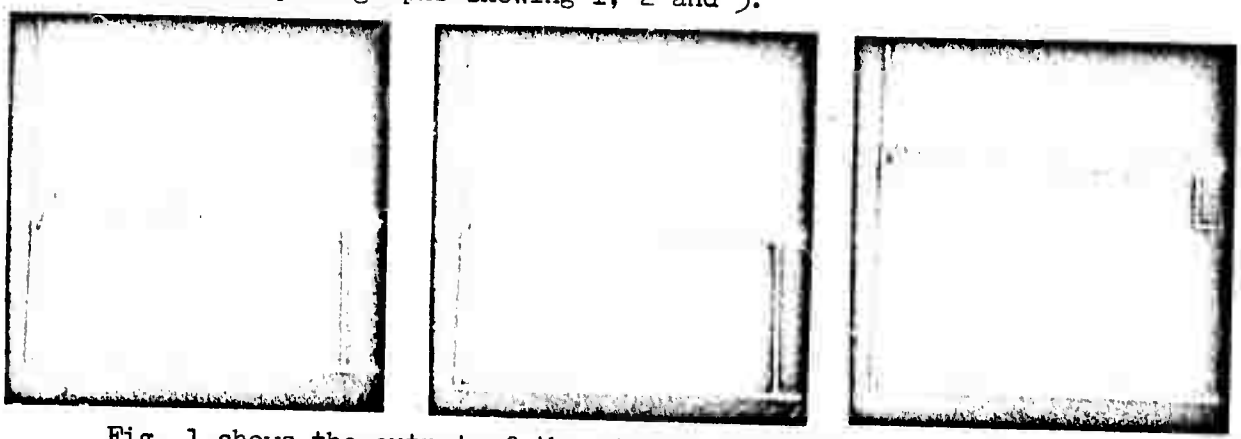

Fig. 1 shows the output of the storage terminal. The input was a sine wave.

Fig. 2 shows the fixed pattern noise which was present.

Fig. 3 is the sine wave with the fixed pattern noise subtracted out. (the apparent change in the pedestal height is not significant, but was done for display purposes).

Power spectral densities for white noise through a low pass filter and band limited noise are shown in the figures below;

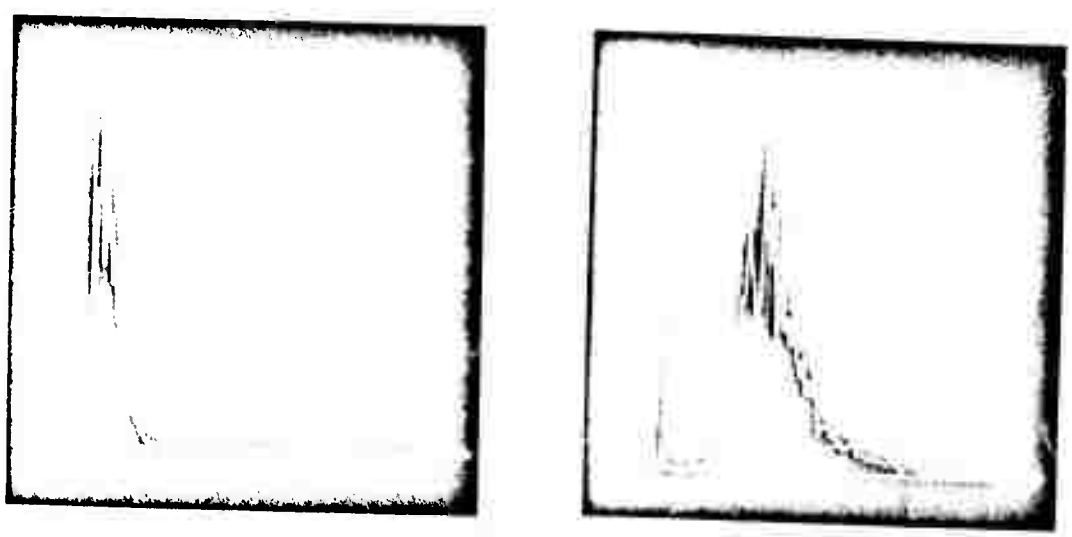

There are a number of important points to be made about the program. It is interactive and affords a great deal of flexibility for the user, both in selecting what processing is to be done, and displaying the results of that processing. The program is quite fast; the analysis and display to generate the above pictures was completed in approximately 20 minutes. A final, important feature of the program is the fact that it runs in 16k of core. This is accomplished by using an overlay structure in the programming, and shows how such processing is feasible on small machines. One final development in the software area is a program to do a linear least square fit of experimental data using the graphics display terminal. Data from the photo imaging lab is displayed on the terminal, the user selects the end points of the fit with the light pen and the program tells the number of points used and the rms error. This has been used for example to determine that the linearity of the read out sweeps is 0.2°/o (including compensation for quantization error in A/D converter).

Accuracy Analysis

This is the analysis which establishes what the accuracy and error bounds on the above processing are. It is being concluded at the present time, as is the calibration and use of an Ultra Fast Fourier Transform which runs in approximately 15-25°/o of the time usually required to perform the FFT. The use of data weighting windows to smooth the data and improve the spectral estimates is also being investigated.

The selection of weighting windows will eventually be another option in the main processing program.

System Calibration

The final calibration of the system is contingent upon the completion of the latter two areas. We have determined that the bandwidth of the storage terminal is $\approx$ 10mHz. A method for measuring its linearity which is more rigorous than the usual staircase or ramp approach is being developed and several methods of determining the MTF of the terminal are under consideration.

We hope to develop the above programs and calibration procedures into a set of tests which can be run each time before data is collected.

3.3 Sampling Scope Techniques for Measuring Signal and Noise

The sampling scope techniques described in Appendix II were developed largely in these laboratories by Mr. H. D. Fisher, now of the Naval Electronics Laboratory Center. The details of his most recent work are given in a separate report from NELC, but a general estimate of the value of this technique is given in Appendix IV. In the sampling technique, a single sample is taken from the same point in each frame of a television signal. If the signal is truly stationary, the average value of many samples gives accurately the value of the signal at that point in the frame, while the r.m.s. deviation of the samples from that average may be calculated easily by the computer and is accurately the r.m.s. value of the noise present in the bandwidth of the video amplifier. Our principal problems were with small variations in the signal due to circuit instabilities in the 67 second interval required to accomodate 2000 samples. Provided that the instabilities can be kept very small compared to the noise currents, this method seems capable of measuring r.m.s. noise currents in the presence of the video signal to an accuracy of one or two percent. As indicated in Appendix III, this accuracy is actually required if one wishes to measure typical tube noise contributions in the presence of the omnipresent pre-amplifier noise.

3.4 Signal Measurements with a Box-Car Integrator

The basic concept of boxcar integrator signal measurements is described in Appendix II. Results of recent measurements, and considerations of measurement accuracy vs. measurement time are discussed in this section.

In order that the boxcar integrator be utilized effectively, two aspects of its operation must be given careful consideration, namely the Minimum Scan Rate (MSR) actually given in seconds or minutes per scan, and Signal to Noise Improvement Ratio (SNIR). Both are necessarily interelated and therefore proper weighting must be assigned to each according to the experimenter's needs and the restrictions under which he may be working.

MSR and SNIR are expressed mathematically by the following

$$MSR = \left(\frac{TB}{AT}\right)\left(\frac{OTC}{12}\right)$$

$$SNIR = [2(OTC)f]^{\frac{1}{2}}$$

where: TB = time base setting of boxcar integrator in seconds

OTC = observed time constant

AT = Aperture time (size of sampling window)

f = frequency of sampling.

The observed time constant mentioned here is a function of the settings of the time constant switches on the PAR model 160 boxcar integrator and of the sampling gates (normal resolution - wide window, high resolution - narrow window). OTC is expressed by the following:

$$OTC = \frac{1}{f}\left[\left(\frac{TC_{HR}}{AT}\right)^2 + \left(\frac{TC_{NR}}{ST}\right)^2\right]^{\frac{1}{2}}$$

where: TC_{HR} = high resolution time constant

TC_{NR} = normal resolution time constant

f = sampling frequency

AT = aperture time

ST = stretch time (normal gate width)

The OTC affects both the MSR and the SNIR, and therefore plays an important part in weighting one or the other. SNIR is proportional to the square root of OTC. And because it is desirable, for signal extraction from noise, to make SNIR large it becomes necessary to make OTC large also. Unfortunately OTC is directly proportional to MSR. This means that the larger OTC is made the slower the boxcar integrator must scan to produce a dependable output. This has the effect of increasing the experiment time necessary to make measurements.

From experience gained, the following settings have been chosen:

1. aperture time (AT) = $10(10^{-9})$ sec.
2. time base (TB) = $5(10^{-6})$ sec.
3. stretch time (ST) = $10(10^{-6})$ sec.
4. sampling freq. (f) = 30/sec.
5. high res. time const. (TC_{HR}) = $100(10^{-9})$ sec.

The aperture time was chosen from resolution requirements and is the narrowest sampling gate width available with this model boxcar integrator. The sampling frequency was chosen because it is the TV frame rate and allows the boxcar integrator to be synchronized with the scanning pattern for the tube under test. It is well to note here also that a short time base was chosen because MSR is directly proportional to the time base duration.

The above settings were always used and were not to be varied to

weight either MSR or SNIR.

It is now of interest to determine the maximum SNIR available at these settings. To do this, it will be assumed that the slowest scan rate of 1000 minutes experiment time for a 5μ second time base will be utilized. Then:

$$MSR = \frac{TB}{AT} \quad \frac{OTC}{12}$$

$$= \frac{5(10^{-6})}{10(10^{-9})} \quad \frac{OTC}{12}$$

or MSR in minutes = 42 OTC in seconds

Setting MSR = 1000 minutes:

$$1000 = 42(OTC)$$

$$OTC \approx 24 \text{ seconds}$$

Since:

$$SNIR = [2 f (OTC)]^{\frac{1}{2}}$$

$$SNIR = 7.75 (OTC)^{\frac{1}{2}}$$

Then we have for a maximum practical signal to noise improvement:

$$SNIR_{MAX} = 7.75 \sqrt{24} = 38$$

To show how this affects the experiment time, assume that it is desired to scan across eight lines of a 800 TVL/Ph bar pattern, (four black and four white lines). At 800 TVL/PH, one bar corresponds to a video signal duration of approximately 50 nanoseconds. The scan rate tells in minutes the time required to scan across the complete time base. Therefore with a scan rate of 1000 minutes and a time base of 5μ sec. we obtain

$$\frac{1000}{5(10^{-6})} = 200 \text{ min/μsec of signal}$$

or

.2 min/nanosec.

Since a group of 8 alternating black and white bars takes a total of 400 nanoseconds. The experiment time is:

.2 min/n sec. x 400 nsec = 80 min.

It will therefore take a total of 80 minutes "real time" to scan across these 8 bars while realizing the maximum signal to noise improvement ratio available at the prescribed settings.

This is a stiff price to pay in time for obtaining a relatively noise free trace of the video waveform associated with just one group in the test pattern, and shows why a tradeoff between MSR and SNIR must be made.

In practice it is not necessary to operate the boxcar integrator in a manner which will yield the maximum SNIR possible. In fact experience has shown that SNIR of 20 or less yields good results. This is a boon for the experimenter because by decreasing the SNIR by a factor of $\frac{1}{2}$, one decreases the MSR and thus the experiment time to 1/4 of the original value, to about 20 minutes for the example given.

Measurements were made using a WX30893 SEC camera tube manufactured by Westinghouse Electric Corp. Results showed that it was possible to obtain valid measurements of signal strength at spatial frequencies up to 700 TVL/PH. This serves to illustrate the substantial advantage of the boxcar integrator as compared to the "A" scope. Measurements with the latter were difficult at 500 TVL/PH and impossible for any spatial frequency above 500 TVL/PH. Although no video signal was measured at spatial frequencies higher than 700 TVL/Ph, this was due to resolution limitations of the camera tube and not of the boxcar integrator. Because of the narrow 10/nsec sampling gate obtainable

with the model 160 boxcar integrator it is possible to achieve meaningful results for horizontal spatial frequencies as high as 2000 TV lines per pattern height with standard US broadcast scanning standards.

The experiment times with the boxcar integrator are sufficiently long, so that obtaining an accurate trace for the video waveform from an entire scanning line is impractical. The inherently long experiment time can in a sense be blamed on the extremely low information gathering duty cycle, only 10 nanoseconds in every 1/30 second, one part in 3,000,000. But despite its slowness, the boxcar integrator does offer the possibility of determining accurately such waveforms as a black to white transition and hence of providing data which was completely inaccessible through the earlier A-scope technique.

4. Measurement of Signal to Noise Ratio Directly from the Display

Recent theories predicting observer performance are based on an assumed signal to noise ratio at the display, in terms of a noise which is a time varying brightness fluctuation for a viewer-determined display area and sampling time, and of signal which is the difference in brightness of adjoining small areas in the image. To permit measuring signal and noise independently at the display on the pattern detail which the viewer is using for recognition, all with minimum disturbance to the viewer, we are setting up the following method in these laboratories.

4.1 The pattern is viewed by a Model 1980 Spectra Pritchard spot photometer. The optical system of this device images the display on a mirror within the device. A small calibrated aperture in the mirror permits light from a small area of the display to pass through the mirror to a multiplier photo-tube for measurement of brightness or of fluctuations in brightness. The operator views an area of the image in the mirror through an eyepiece. A small dark spot, the aperture, shows exactly the small area being measured in the operator's field of view.

4.2 The instrument is provided with a series of interchangeable mirrors in a turret to provide a range of aperture sizes, and with a series of lenses of various focal lengths to permit measuring brightness and brightness fluctuations for image areas as small as 0.001" in diameter.

4.3 The averaged photomultiplier output is normally fed through an appropriate low pass filter and an A/D converter to a digital indicator or to a computer. For our purpose the signal is processed at full bandwidth through a sampling scope, A/D converter or our other peri-

pheral equipment. For a direct view device, average brightness is measured either by computer averaging of a large number of samples or by the normal integrating circuits in the photometer, which can operate simultaneously with the sampling process. The fluctuation current is measured and recorded as a function or sampling aperture size and the sampling time, and digital techniques are used to determine the rms. fluctuation for sampling times of 0.1 or 0.2 sec like that of the eye, or for any other desired averaging/sampling time. The same sample and hold technique is also readily useful for measurement of displays with moving test patterns.

4.4 With TV displays or scanner displays, the signal from the spot photometer consists of a pulse of light as the electron beam in the display scans across the sample area. Depending on the size of the sampled area, there may be several such pulses repeating at the line scan rate if several raster lines cross the area. Each will have a quasi exponential tail due to display phosphor decay. Bursts of pulses will recur at the frame rate, or field rate if interlaced scanning is used. Current thinking is that the observer integrates the brightness vs time function for each small area over the 0.1 to 0.2 second integration time of his eye to determine the brightness of that area, and that it is the fluctuation in this short time average which the observer sees as noise.

By use of our peripherals, we will sum the charge represented by each light pulse from a sample area and store the values of these sums for many frames to determine their average value and their fluctuations from the average value as a function of sample area, sample time, display brightness and of input signal parameters. The resulting data should provide the first direct measure of signal to noise ratio at

the TV display, will include the image degrading effects of the display, and should permit a more direct correlation of display parameters with observer performance than ever achieved before. The use of the telescopic instrument which can view the display in real time without displacing the human observer, seems to us an important advantage in this search for correlation.

4.5 The attached figure shows a typical waveform as measured from a small area of a television display with a model 1970 Spectra-Pritchard Photometer. This signal was fed to an A/D converter with a 1MHz clock rate, whose output was then summed in a digital computer to approximate the area under the curve, therefore the total light output from each TV field. As shown, the time constant of the P-4 phosphor screen is long enough so that the 1MHz sampling rate is fast enough to provide an accurate measure of the total light output. The print out beneath the figure shows that fluctuations for this display were very small. The experiments are now bing extended to cases of lower camera tube illumination where higher amplifier gain will make preamplifier noise obvious on the display.

4.6 The present scheme appears fully adaptable to other types of scanning pattern, including the linear array scan used in some FLIR systems, since we are measuring integrated brightness from a small area of the display, and it is only necessary that the A/D converter be gated on for an appropriate sampling time interval.

In this method, the display and the spot photometer will be mounted in one solid unit to avoid relative motion between them. Sampling of various areas will be accomplished either by moving the photometer or by electrically moving the pattern on the display. Since the collection of noise statistics will require taking a large number of samples

at one place in the picture, we do not now see a need for rapid motion of the sampling instrument. On the other hand the performance of the system against moving scenes seems best presented in terms of the data from a stationary observing instrument.

At present, we expect that the interface between this instrument and a computer will be relatively modest. In any event, if a Biomation data recorder is available for processing video signals, the same interface equipment should be more than adequate to process the narrower bandwidth data taken from the phosphor screen of the display.

APPENDIX I

Detective Quantum Efficiency

The pages of the following appendix are not numbered consistently with the rest of this report, because it is a working draft representing the status of an on-going project, being conducted by Professor S. Nudelman.

I. Introduction

A. The Study and Preliminary Findings

This report presents the status of a study to seek improved ways for evaluating and specifying the performance of photoelectronic imaging devices, with emphasis on components rather than complete systems. Soon after beginning work, it became clear that the problem led to solutions that could be in conflict with the ways in which one evaluates passive optics, film and elemental photodetectors. Accordingly, the study was expanded to seek solutions that were compatible for all imaging devices.

Detailed analysis of various models of optics, elemental photodetectors and photoelectronic imaging devices reveals that Detective Quantum Efficiency (DQE) is a compatible concept. DQE is simply the fraction of incident photons that result in usable output information. At best it is equal to the quantum efficiency of the photosensor; it is degraded from this value by noise limiting device performance. Thus it is a simple concept and shown to be adaptable for easy use.

DQE (which can be considered as a function of spatial frequency) and MTF are shown to be related in a simple manner, that is, this spatial frequency dependent DQE is proportional to MTF^2. This permits making use of conventional procedures for obtaining MTF to calculate DQE as a function of frequency. Replacing MTF by DQE for device evaluation in essence provides a corresponding evaluation, but based on an absolute scale.

The DQE discussed in this paper is considered to be dependent on spatial frequency. Accordingly, one can establish the fraction of incident photons that will result in usable output signal as a function of frequency. Further, when used in a system analysis, it can be used in the manner that is customary for MTF, that is in the multiplication of component DQE's to obtain the system DQE.

This first report covers theoretical concepts. At the time of its writing, the section dealing with film was incomplete. It will be included in the second report.

Data is being collected from our test facility at the University of Rhode Island to evaluate image tubes in terms of DQE vs. spatial frequency. It will be used to test the theory, and hopefully to demonstrate improvement in the evaluation and specification of these devices.

B. General Comments

Photoelectronic imaging devices are generally not rated by criteria similar to those used for most photoelectronic devices, such as quantum efficiency, noise equivalent power or detectivity star as applied to phototubes or elemental detectors. In fact they are not rated at all in any absolute manner, or referenced to any absolute standard. A user is provided with engineering information about device operation such as signal, noise, signal to noise ratio, the modulation transfer function, transfer characteristics with either photometric and radiometric units. Problems remain, however, in

that even with such abundant information, a scientist trying to design a system for imaging and reproducing some incident photon flux cannot select the proper tube for his purpose without tremendous experience or education in dealing with these devices. He still lacks a quantity (such as quantum efficiency when applied to photocathodes) which can provide some measure at a glance of the fraction of incident photons that are converted to countable electronic events, and a measure of limiting performance capability.

Today one of the most important measurements made on all imaging devices is the modulation transfer function (MTF). It offers a measure of the performance of the device as a function of spatial frequency, which in turn is a measure of resolution. Unfortunately for photoelectronic imaging devices, this quantity is based entirely on the measurement of signal and excludes any considerations of noise or quantum efficiency. MTF measurements are customarily normalized to unity, which means that other basic information is deliberately omitted. In a system or device comprising a series of imaging components and devices such as lenses, image tubes and photographic film, it is customary to multiply the MTF's of each device in the system to arrive at an MTF for the system as a whole. This is done even though the first device might have a quantum efficiency of 100 percent, the second of 50 percent and the third of one percent. They are treated equally well, with the result that one obtains a system MTF curve which is of limited usefulness. It is common experience to find predictions of system performance

based on using MTF to be far different than that actually observed, particularly when faced with noise limiting conditions.

Detective Quantum Efficiency (DQE) is a concept which includes all of those factors missing from MTF. It was created by Rose in 1947[1] and used by R. Clarke Jones to evaluate elemental photosensors, photoelectronic imaging devices and film in a major publication of 1959[2]. Since that time other researchers have used the concept to evaluate devices, but with relatively little acceptance in the engineering community utilizing imaging devices. Its lack of application is based probably on some general confusion about its meaning and ways in which it can be used.

The introduction and application of MTF to optics, which was quite successful, was carried over to photoelectronic imaging devices and photographic media. Thus, it became part of established practice. Once firmly established and included in a voluminous literature which grew out of the applications of this concept, it became increasingly difficult, if not nearly impossible, to make use of other concepts. Thus there is considerable investment in MTF which all are reluctant to lose, considering the large expenditure in human endeavor and funds poured into this concept. Fortunately, it appears that this spatial frequency dependent DQE and MTF are related in a simple analytical manner, which makes it possible to make use of both concepts.

The success of MTF in optics was due to its application to lenses and mirrors having essentially 100 percent transmission

or reflection in the spectral regions used. Considered as ideal devices, they provide a number of recordable events in the image (photons) equal to those incident on the optics from the object. Accordingly they perform like an ideal photoelectronic imaging device whose quantum efficiency is unity. When one multiplies the MTF's of a series of lenses having essentially perfect transmission characteristics, the result can be accurate and predict satisfactorily a system's performance. Unfortunately, this does not follow for photoelectronic imaging devices and film, whose quantum efficiencies vary widely and where noise limiting conditions prevail.

The wordage used by Jones to describe Rose's concept grew out of the considerations of the infrared detector community of research scientists during the 1950's. At that time it became clear that progress in the field required quantitatively correct measurement procedures together with precise definitions in the concepts used to evaluate detectors. Many concepts were being explored and in some cases a word was used such as "sensitivity" which suffered from having many different meanings. A similar situation exists today with the word "contrast" which recently was pointed out to have at least 11 meanings by P. Pryor[3]. Out of the morass and arguments in the 1950's grew the accepted concepts of noise equivalent power (NEP), detectivity (D) and detectivity star (D*) applied to infrared detectors. These concepts provided an evaluation of detectors using absolute measurement procedures based on a blackbody being used as the test source of irradiation. These

concepts are firmly established and still in use today. The quantities NEP, D and D* now precisely defined, completely replaced loose words such as "sensitivity" and various figures of merit explored at that time. Further, they are now associated with specific devices and provide a rating easily related to Detective Quantum Efficiency (see Section II, B3).

Detective Quantum Efficiency then was applied by Jones to evaluate a variety of devices. The word "detectivity" which had been earlier established as a measure of quantitative performance of infrared detectors was carried over to this new way of evaluating devices. Unfortunately, the name seems to have given the impression of being a somewhat mysterious quantity and treated by workers in the field as something useful only in the research laboratory. Yet it is a simple concept indeed.

II. Detective Quantum Efficiency

A. Interpretation

A way in which DQE can be related to the simpler concept of quantum efficiency can be estimated with reference to Fig. 1. There is shown schematically an arrangement of photoelectronic devices comprising an elemental photosensor (non-imaging), followed by imaging devices. Each of these devices has in common a material which converts photons to some recordable event. These range from the photoemissive cathode of the phototube or photomultiplier, to photon sensitive semiconductors and to photographic media. All of these can be evaluated when used in a non-imaging way in terms of the simple concept of quantum efficiency. A rating in this term is simply a measure of the number of recordable events out of the device per incident photon. This concept can be applied also to optical media and mirrors where their transmittance and reflectance respectively are treated as a type of quantum efficiency.

A rating in terms of quantum efficiency, however, is inaccurate for devices limited by electronic noise. An infrared photodetector, for example, is made of a semiconducting material which is sensitive to light and has an intrinsic quantum efficiency. Yet, when this same material is made into a seemingly perfect photodetector, the device quantum efficiency is generally less than that measured for the semiconductor. The explanation lies in the inclusion of new sources of electronic noise when the device is fabricated and connected to its preamplifier. These sources of noise might be inherent in the detector, its

contacts, in the coupling network or the preamplifier[4]. Such noise has been called excess (1/f), shot and Johnson noise depending on its character and source. When electronic noise is significant compared to that generated by photon noise from the background (Photoelectronic), it causes a reduction in the number of recordable output events (electrons) per incident photon, or in terms of current, there is caused a reduction in output signal current per incident photon flux. Thus electronic noise causes the device quantum efficiency to be less than that for the basic photosensing material. It is this device quantum efficiency which is known as "Detective Quantum Efficiency" or DQE.

Image tubes also have commonly a DQE less than the quantum efficiency of their photocathodes. The explanation is the same as for elemental detectors, being the result of additive electronic noise degrading photosensor performance (see Section IIID).

Lenses and mirrors are not subject to electronic noise, so that their transmission or reflection are unaffected in application. Accordingly, their DQE suffers no degradation when perfectly transparent or reflective, respectively. The spatial frequency dependent DQE is then just the MTF^2.

B. Analysis

An understanding of DQE and its applications can be obtained by analysis of simple theoretical models of several ideal photoelectronic devices. It is a relatively simple matter to establish such a model for a semiconductor functioning as a photodetector. This was done during the 1950's by researchers

trying to understand the performance of newly evolving detectors, and to predict the performance expected from an ideal device[5]. They were remarkably successful in both establishing theoretical "ideals" and in the development of devices approaching ideal performance.

Beginning in 1962, a series of three papers evolved with the intention of first clearly delineating those factors responsible for device performance and identifying those factors in various figures of merit[4, 6, 7]. The first dealt with semiconducting detectors and sought to expose particularly those modifications in device performance caused by different sources of noise, and to reveal more clearly the dependence of figures of merit on device area and the bandwidth of the measurement. The second and third publications dealt with intensifiers and signal generating tubes respectively, and evolved from the same approach as used in the first paper for elemental detectors. It was pursued because the additional factors of area involved in direct imaging and readout using an electron beam were readily accommodated by easily understood extensions of the differential equation used as a model for the elemental photodetector. Further, it had the attribute of linking elemental detectors with imaging devices. The result was the derivation of signal and noise expressions applicable to these devices, which led to predictions of the best performance that could be expected. It was hoped that this approach would stimulate research efforts to compare actual performance with "ideal" predictions, improve the accuracy and procedures involved in testing and establish absolute

criteria on which to compare their performances. These aspirations have yet to be achieved, partly because explanations to date of absolute criteria have been unsuccessful in establishing their basis and usefulness.

The purpose of the two subsections that follow is to first define Detective Quantum Efficiency and then to show its relationship to MTF. The following section covers the derivation of expressions for DQE applicable to the simple circular window and mirror, the elemental photodetector and then imaging devices. Comparison of these expressions will reveal:

(1) DQE can be expressed in a form that comprises multiplication of the photosensor quantum efficiency η, with three spatial frequency dependent factors, and a constant.

(2) The multiplying factors all have a maximum value of unity. They can be associated with:

   a. The effective aperture

   b. A roll-off function when the device is limited by electronic noise (excess, shot, Johnson). This function predicted by theory has not yet been identified experimentally.

   c. Image motion

   d. There are other signal degrading factors that can well be included such as those associated with multiple reflections, granularity and scattering. These additional factors, as well as image motion, are not treated here. They are important, but not necessary for the purposes of this study.

(3) The value of the constant, noted in (1) above, is determined by the role of various parameters and properties influencing performance, such as electrical bandwidth, the area of a resolution element, gain and integration time.

1) Definition of Detective Quantum Efficiency (DQE)

Detective Quantum Efficiency is designed so that it provides a rating for a real device compared to that obtained from an ideal device by the expression:

$$DQE = \frac{(S_{P-P}/N_{RMS})^2_{ORD}}{(S_{P-P}/N_{RMS})^2_{OID}} \qquad (1)$$

where:

S_{P-P} is the peak to peak value of signal

N_{RMS} is the RMS value of noise

ORD indicates output from a real device

OID indicates output from an ideal device.

Note it is not a trivial matter that signal is measured peak to peak and noise RMS. This forces DQE always to relate directly to the photosensor's quantum efficiency. The first indication of this appears in the general treatment of section B2, and then for a number of specific devices analyzed in part III.

The treatment of signal and noise throughout this text is easily explained by reference to Figure 2. Input is given by the number of photons per unit area.time (flux) irradiating the device and is indicated throughout by J. Further, input

signal is indicated by J_S. All other incident photons not contributing to signal are referred to as background photons and denoted by J_B.

Input signal is indicated in Figure 2 as being a sinusoid having a peak to peak value J_{SO}. For discussions of elemental detectors, this input signal would be irradiance from a sinusoidally modulated standard light source, such as from a light chopper and a blackbody. Here the abscissa would be measured in time, and the input signal expressed in the form:

$$J_S = J_{SO}e^{i\omega t} \tag{2}$$

where: $\omega = 2\pi f$

f = frequency

t = time

Imaging devices also will be analyzed making use of a sinusoidal irradiance, where the variable is distance rather than time, since our interest here is in the number of sinusoids (periods) across the face of the device. Accordingly, the input signal is now given by:

$$J_S = J_{SO}e^{i\omega x} = J_{SO}e^{i2\pi x/\lambda} \tag{3}$$

where: $\omega = 2\pi/\lambda$

λ = the spatial wavelength of the sinusoidal test pattern and the abscissa in Figure 2 is now given by distance.

Dynamic response from an imaging device could be examined by making use of the traveling waveform, that is

$$J = J_{SO} e^{2\pi i (X/\lambda = v/T')} \tag{4}$$

where: v = velocity of the wave

T' = time it takes the wave to progress through a distance of one wavelength

Photon noise and photon background will be used in an interchangeable manner. The photosensors in imaging devices are responsive to individual photons, as distinct from thermal sensors. Accordingly, the treatment that follows assumes that photons arrive individually in a random manner in accordance with Bose-Einstein statistics, and that for spectral wavelengths less than approximately 10 microns, can be assumed Poissonian. The fluctuation corresponding to the random arrival of photons is given by $\Delta J_B = J_B(t) - J_{ave}$, and the mean square fluctuation denoted by $\overline{\Delta J_B^2}$. Since Poissonian statistics prevail, the mean value of the input photon flux is given by:

$$J_B = \overline{\Delta J_B^2} \tag{5}$$

The question of units arises since DQE makes use of the RMS value of the noise. Clearly this corresponds to making use of $\overline{\Delta J_B^2}$, which has units of $(\text{area} \cdot \text{time})^{-2}$. Often to simplify equations, the photon noise will be expressed in terms of its equivalent J_B which has the units $(\text{area} \cdot \text{time})^{-1}$.

By relating the fluctuation to the mean value which for photons becomes the ambient, or background, it is possible to relate DQE directly to the background flux which offers considerable utility. This is shown next below.

The ideal device is assumed to accept all incident photons both signal and noise (or background) and record them exactly as they appear incident on the face of the device. Assuming the device to have a photosensor with surface area A, and that the device provides an integration time T, the ideal peak to peak signal recorded would be proportional to $J_{SO} \cdot A \cdot T$, and the RMS value of the noise proportional to $(J_B \cdot A \cdot T)^{\frac{1}{2}}$. Accordingly the signal to noise ratio from an ideal device is given by:

$$\frac{S_{P-P}}{N_{RMS}}_{OID} = \frac{J_{SO}(AT)^{\frac{1}{2}}}{J_B^{\frac{1}{2}}} \qquad (6)$$

and insertion in Equation 1 gives (2):

$$DQE = \frac{(S_{P-P} \; / \; N_{RMS})^2_{ORD}}{J_{SO}^2 \; T \; A \; / \; J_B} \qquad (7)$$

Note that this treatment for the ideal device presumes that its photosensor has a quantum efficiency of 100 percent, and that the shape of its limiting aperture does not deteriorate device performance in terms of its spatial frequency response. It's simply perfect. Since it is perfect, the output signal to noise ratio is the same as the input flux signal to noise ratio, multiplied by the square root of the device area and integration time.

Contrast does not appear directly in the definition or subsequent expressions for DQE, nor will it appear anywhere in this text. There are so many ways of expressing contrast that care in its definition must be exercised to maintain its usefulness[3]. All the definitions represent various ratios of some maximum and minimum value. For photoelectronic devices, if signal and noise, or signal and background are properly treated, there is little need to use contrast. Recent conversations with P. Pryor, however, point out that continuing to use "contrast" is necessary in some aspects of image forming systems. He notes the following:

"Contrast is an important concept in the evaluation and analysis of a complete imaging system including the object and its background, all intermediate components, elements and devices, as well as the final display. One must, however, define carefully the type of contrast under discussion (there have been at least 15 different definitions used). The object and its background can often be usefully referred to as having a specific contrast (measured in terms of reflectance or transmission). This "contrast" is independent of "Signal to Noise" at an unspecified level of radiance.

It is also often useful to refer to the contrast reducing effect of the atmosphere (sometimes referred to as contrast transmission). When "modulation contrast" (max minus min divided by max + min) is used to describe a repetitive target such as a bar target, the square wave response function is a measure of contrast reduction as a function of spatial frequency.

It is true that the Signal to Noise out at the display is a very important measure of performance. There is, however, a contrast threshold for the human observer and the contrast out as well as the Signal to Noise out has a significant bearing on the ease at which an observer can detect and recognize detail in a display. It is often possible to adjust the "contrast" without noticeably affecting the Signal to Noise out."

Lenses and mirrors which are non-integrating devices have a DQE given by:

$$DQE = \frac{(S_{P-P} / N_{RMS})^2_{ORD}}{J_{SO}^2 A/J_B} \tag{8}$$

This follows since the ideal device output signal is now $J_{SO}A$ and the noise is $(J_B A)^{\frac{1}{2}}$ in a unit time. This corresponds to the signal to noise ratio of the ideal photodetector improving as the well known function of the square root of its area.

Photoelectronic devices and film generally include some form of integration, so that DQE as expressed in Equation 7 is used most frequently.

Output signal and noise can be recorded in various forms, that is, in terms of light as for intensifiers and displays, as a voltage across a load resistor in a coupling network as for elemental photoconductive detectors, or current as expressed in terms of beam current for TV type camera tubes. The notation used will express output signal and noise for light as L_S and L_N, for voltage V_S and V_N, and current I_S and I_N, respectively.

In the sections that follow, signal to noise ratios will be examined for simple models of devices. These in turn will be used to calculate their DQE. Apertures, windows and mirrors will be examined first, followed by photoelectronic devices (Section III). Photoelectronic imaging devices will begin with the elemental photoconductive detector followed by intensifiers and then signal generating TV type pick-up tubes.

Only passive optics can be said to be non-integrating devices. They do not convert photons to electrons, but accept photons and redirect them to form an image[8]. Photoelectronic devices such as detectors and intensifiers have their performance governed by internal electronic carrier lifetimes τ in their photosensor and phosphor materials, respectively. The degree of integration depends upon τ and increases with increasing lifetime. TV type signal generating tubes have an intrinsic integration requirement identified with their raster period.

Associated with photogenerated carriers in semiconductors, and with the scanning electron beam in TV type tubes, are electron carrier dynamics. Lifetime, displacement and motion of carriers symbolize a time requirement to carry out their mission. This in turn results in a limitation of device frequency response, less than that anticipated from ideal optics and a limiting aperture. Not too surprisingly, difficulty and failure arise in evaluating image tubes when one tries to oversimplify evaluation and apply MTF to image tubes in the same manner as for optics, in part because carrier dynamics are ignored.

Film, by its very nature, is an integrating and storage media.

2. Relationship Between DQE and MTF

The Modulation Transfer Function is normally derived from the line spread function by use of the Fourier transform. However, our approach will be to make use of a sinusoidal signal of infinite extent plus a constant as shown in Figure 2, to

establish a working expression of MTF. This approach simplifies the arithmetic and suffices for the purposes of this treatment. Accordingly, MTF is defined here as:

$$MTF = \frac{\dfrac{\text{Peak Signal Output}}{\text{Average Background Output}}}{\dfrac{\text{Peak Signal Input}}{\text{Average Background Input}}} \tag{9}$$

where the numerator is called the output modulation and the denominator the input modulation. The equivalence of this MTF determined as noted above, to that derived rigorously from line spread functions is well established. It is treated in detail and a simple manner by Levi[9]. Reference to Figure 2 gives:

$$MTF = \frac{\dfrac{V_2 - V_1}{2} \Big/ \dfrac{V_2 + V_1}{2}}{\dfrac{J_2 - J_1}{2} \Big/ \dfrac{J_2 + J_1}{2}} \tag{10a}$$

$$MTF = \frac{V_2 - V_1}{J_2 - J_1} \cdot \frac{J_2 + J_1}{V_2 + V_1} = \frac{V_{SO}}{J_{SO}} \cdot \frac{J_B}{V_B} \tag{10b}$$

where: $V_{SO} = V_2 - V_1$

$J_{SO} = J_2 - J_1$

$J_B = (J_2 + J_1)/2$ = average of Input Background

$V_B = (V_2 + V_1)/2$ = average of Output Background

Now rewrite Equation 7 in the form:

$$DQE = \frac{(S_{P-P})^2_{ORD}}{(J_{SO})^2} \cdot \frac{(J_B)}{(N_{RMS})^2_{ORD}} \cdot \frac{1}{TA} \tag{11}$$

Inserting Equation 10 into 11,

$$DQE = (MTF)^2 \left(\frac{V_B}{J_B}\right)^2 \cdot \frac{J_B}{(N_{RMS})^2_{ORD}} \cdot \frac{1}{TA} \qquad (12)$$

where:

$$(N_{RMS})^2_{ORD} = V_B$$

$$(S_{P-P})_{ORD} = V_{SO}$$

$$DQE = (MTF)^2 \frac{V_B}{J_B} \cdot \frac{1}{TA} \qquad (13)$$

$$DQE = \eta\,(MTF)^2 \qquad (14)$$

where:

$$V_B = \eta\, J_B TA \qquad (15)$$

Equation 14 is a remarkably simple relationship and offers the opportunity to take full advantage of evaluating devices in an absolute manner from DQE while making full use of evaluation procedures based on MTF. True, this derivation has been derived on the simplest of concepts, but was arrived at in a direct manner without recourse to approximations. It was assumed that the background level V_B was established by the background (or noise) from the incident flux. However, the relationship has more general applicability and is useful in other noise limiting conditions, subject to the inclusion of an additional factor. Thus for limiting noise cases in general, Equation 14 can be modified to:

$$DQE = c\eta(MTF)^2 \tag{16}$$

where c is a constant whose maximum value is unity for the background noise limiting case. The product $c\eta$ will be shown to be the maximum value of DQE at low spatial frequency in subsequent sections of part III.

We note that the reason for this particular association lies in the way in which signal, background and noise are defined in DQE and MTF. That is, in DQE, the signal is defined in terms of its peak to peak value; and in MTF, the signal is denoted by its peak value. Further, DQE uses the concept of noise which is defined in terms of its RMS value; whereas MTF uses an average value of the background defined in terms of the minimum and maximum values of signal. Finally, in Equation 11 we inserted the complete expression for the signal ratio in terms of MTF from Equation 10. The result points out that information pertaining to the photosensors quantum efficiency is not available in MTF, whereas DQE has the advantage of including both η and MTF. It is not a serious matter for optics, but is a problem in application to photoelectronics.

3. Relationship Between DQE and NEP-D*

Noise Equivalent Power (NEP) is defined according to the expression:

$$NEP = \frac{HA}{(S/N)_{RMS}} \tag{17}$$

where:

H is the irradiance at the detector in watts/cm^2

S_{RMS} is the rms value of output signal from the photodetector

N_{RMS} is the rms value of output noise from the photodetector, regardless of its source

A is the area of the detector in cm^2

Since DQE uses the $signal_{P-P}$ to $noise_{RMS}$ ratio, Equation 17 can be rewritten as:

$$\frac{S_{P-P}}{N_{RMS}} = \frac{HA}{.707 \times NEP} \tag{18}$$

Substitution of 18 into Equation 7 gives:

$$DQE = \frac{H^2 A}{(.707)^2 \times NEP^2 \times H_{PH} \cdot \tau} \tag{19}$$

where:

H_{PH} = Irradiance in Photons/cm^2 sec

τ = Device time constant

This derivation assumes that the input signal to noise ratio is determined by:

$$J_{S_{P-P}} = H_{PH}(\text{photons/cm}^2\text{sec})$$

$$J_{N_{RMS}} = \sqrt{H_{PH}} \quad (\text{photons/cm}^2\text{sec})$$

and the device time constant is the integration time.

If one uses the relationship between irradiance and emittance expressed in watts and photon flux:

$$H_{PH} = \frac{N_{O-\lambda}}{R_{O-\lambda}} \cdot H \tag{20}$$

Then substitution into Equation 19 gives:

$$DQE = \frac{R_{O-\lambda}}{N_{O-\lambda}} \cdot \frac{H}{NEP^2} \cdot \frac{A}{(.707)^2 \times \tau} \qquad (21)$$

where:

$N_{O\rightarrow\lambda}$ is the total radiant emittance from the unit surface of a blackbody in terms of photon flux (photons/cm^2 sec), extending from zero wavelength to the cut-off wavelength of the photodetector.

$R_{O\rightarrow\lambda}$ is the total radiant emittance as for $N_{O\rightarrow\lambda}$, but expressed in power density (watts/cm^2).

DQE can be calculated for the photodetector whose specifications were given in an NOLC data sheet[10], reproduced as Table I. Noting a spectral peak of 1.5μ, we obtain DQE = .012 or 1.2 percent using

$N_{O\rightarrow\lambda} = 1.57 \times 10^{13}$ photons/cm^{2}sec

$R_{O\rightarrow\lambda} = 2.187 \times 10^{-6}$ watts/cm^2

$H_W = 7.7 \times 10^{-6}$ watts/cm^2 (RMS)

$NEP = \sqrt{5} \times 10^{-10}$ watts (RMS)

$A = 2.25 \times 10^{-2}$ cm^2

$\tau = 8.1 \times 10^{-5}$ sec

Detectivity Star (D*) is defined according to:

$$D^* = \frac{\sqrt{A \cdot \Delta f}}{NEP} = \frac{\sqrt{A \cdot \Delta f}}{HA \Big/ \frac{V_{S_{P-P}}}{V_{N_{RMS}}}} \qquad (22)$$

CELL SENSITIVITY	
500°K blackbody response	
H_N (watts/cps$^{1/2}$ · cm^2)	
(500, 90, 1)	4.5×10^{-9}
(500, , 1)	·····
P_N (watts/cps$^{1/2}$)	
(500, 90, 1)	1.0×10^{-10}
(500, , 1)	·····
Jones S (watts/cm)	
(500, 90, 1)	6.5×10^{-9}
(500, , 1)	·····
D^* (cm · cps$^{1/2}$/watt)	
(500, 90, 1)	1.5×10^{9}
(500, , 1)	·····
Spectral peak (μ)	1.5
Response at spectral peak	
H_N (watts/cps$^{1/2}$ · cm^2)	
(λ, 90, 1)	4.1×10^{-11}
(λ, , 1)	·····
P_N (watts/cps$^{1/2}$)	
(λ, 90, 1)	9.4×10^{-13}
(λ, , 1)	·····
Jones S (watts/cm)	
(λ, 90, 1)	5.8×10^{-11}
(λ, , 1)	·····
D^* (cm · cps$^{1/2}$/watt)	
(λ, 90, 1)	1.6×10^{11}
(λ, , 1)	·····
Effective time constant (μ sec)	8.1×10^{1}
DATA SHEET NO. 675	

CONDITIONS OF MEASUREMENT	
Chopping frequency (cps)	90
Bandwidth (cps)	5
Humidity (%)	23.5
Cell temperature (°C)	−195
Dark resistance (ohms)	5.2×10^{6}
Dynamic resistance (ohms)	···
Load resistance (ohms)	5.5×10^{6}
Transformer	···
Cell current (μ amps)	1.5
Cell noise (μ volts)	47
Blackbody flux density (μ watts/cm^2, rms)	7.7

CELL DESCRIPTION
Type: Ge (AuSb doped)
Angular field of view: approx. 110°
Window: sapphire
Method of preparation: crystal
Area (cm^2): 2.25×10^{-2}

PHILCO CORP., CELL NO. 1207

Table 1 **Detector data sheet** (*by permission of W. L. Eisenman and R. F. Potter, NOL, Corona, California, from NOLC Report 525, and the Philco Corporation*).

Therefore:

$$\frac{V_{S_{P-P}}}{V_{N_{RMS}}} = \frac{D^* H_{watt} \sqrt{A}}{.707 \times \sqrt{\Delta f}} \tag{23}$$

and

$$DQE = 2 \times \frac{R_{O\to\lambda}}{N_{O\to\lambda}} \frac{H_W}{\tau \Delta f} \times D^{*2}$$

$$= 2 \times \frac{1.39 \times 10^{-19} \times 7.7 \times 10^{-6}}{8.1 \times 10^{-5} \times 5} \times (1.5 \times 10^{9})^2$$

$$= \frac{2 \times 1.39 \times 7.7 \times 9}{8.1 \times 5 \times 4} \times 10^{-8}$$

$$= .012 \tag{24}$$

Note again that the device time constant has been used for the integration time in the definition of DQE, as in Equations 21 and 24.

III. Theoretical Models

A. Apertures, Windows and Mirrors

Consider the case of a circular hole cut in the face of a mask, illuminated by a photon test pattern described by the stationary sinusoid shown in Figure 2:

$$J_S = J_{SO}\, e^{2\pi i (x/\lambda)} + J_{21}/2 \tag{25a}$$

The total flux from this stationary pattern passing through the hole can better be expressed as:

$$J_S' = \int_0^A \left(J_{SO}\, e^{2\pi i \frac{x}{\lambda}} + \frac{J_{21}}{2}\right) da \tag{25b}$$

where $J_{21} = J_2 + J_1$. For a circular aperture of area A, this reduces to:

$$J_S' = J_{SO}\,AS + \frac{J_{21}A}{2} = J_{SO}\,AS + J_B\,A \qquad (26)$$

where S is the Bessel function given by:

$$S = J_0(Z) + J_2(Z) = \frac{2J_1(Z)}{Z} \qquad (27)$$

and $J_0(Z)$, $J_1(Z)$ and $J_2(Z)$ are zero, first order and second order Bessel functions respectively of argument Z. Accordingly, the magnitude of transmitted flux comprising signal at any particular spatial frequency depends upon the area of the aperture and the Bessel function at that frequency. This function, of course, is what one would expect from diffraction theory for a circular aperture, and is different for apertures of other shapes.

Supposing now that the circular hole is replaced by a circular disc of glass with a transmittance $T(\lambda)$. The flux that now passes through the glass is

$$J'' = TJ_S = TJ_{SO}AS + \frac{TJ_{21}A}{2} \qquad (28)$$

Assuming that the background is defined by the constant term, the signal (p-p) to noise (RMS) is given by:

$$\left(\frac{S_{P-P}}{N_{RMS}}\right)_{ORD} = \frac{TJ_{SO}AS}{\sqrt{T\frac{J_{21}A}{2}}} = \sqrt{TA}\;\frac{J_{SO}S}{\sqrt{J_B}}$$

Substituting in Equation 8 for the Detective Quantum Efficiency:

$$DQE = \frac{\frac{TA\ J_{SO}{}^{2}S^{2}}{J_{21}/2}}{\frac{(J_{SO}A)^{2}}{J_{21}\ A/2}} = TS^{2} \qquad (29)$$

Thus DQE for a circular plate of glass is its transmittance multiplied by its aperture function squared.

The case of a circular flat mirror dealt with as above results in:

$$DQE = \mathcal{R}\ S^{2} \qquad (30)$$

where $\mathcal{R}$ is the reflectance of the mirror.

Comparison of Equations 29 and 30 with 14 and 16 reveals that:

a. the transmittance and reflectance respectively are the equivalent of quantum efficiency.

b. the aperture function is equivalent to MTF.

c. the constant is equal to unity.

Lenses and mirrors will not be given any treatment here since their MTF's have been well established and appear in many good texts[9].

This treatment assumes that the limiting aperture does not affect the output noise spectrum. In effect, this is the equivalent of assuming that the mean value of the output J_B is constant, while peak to peak signal diminishes with increasing spatial frequency. The same assumption will be made for the analysis of photoelectronic imaging devices.

B. The Elemental Photoconductive Detector

The photoconductive detector is the simplest photoelectronic device that can be used to illustrate the relationship between DQE and η. Signal and noise relationship for the background and electronic noise limiting cases have been examined for this device using a simple model comprising an intrinsic detector[4,5,10], in which:

(1) Electron and hole mobilities were taken as being equal,

(2) Noise photons cause a fluctuation in the electronic carrier density through the generation and recombination process,

(3) Each photon absorbed created two carriers, that is, an electron and a hole.

The detector is shown schematically in Figure 1 with a transparent electrode, to be compatible with the practice for image tubes. Analysis of its signal and noise is carried out in Appendix A (See Equations 10, 24, 25).

The peak to peak signal current is given by:

$$I_{S_{P-P}} = I_b \frac{2\eta J_{SO} \tau}{nd \sqrt{(1+\omega\tau)^2}} \qquad (31)$$

where:

J_{SO} is the peak to peak photon flux (see Figure 2)

I_b is the bias current

η is the photosensor's intrinsic quantum efficiency

τ is the photoconductive time constant taken equal to the recombination lifetime for electrons and holes

n is the equilibrium density of electrons in the detector

d is the thickness of the detector

ω is equal to $2\pi f$

f is the video frequency

1) Case of the Photon (Background) Noise Limited Detector

The peak to peak signal to RMS noise ratio reduces to

$$\frac{I_{S_{P-P}}}{I_{BN}} = \left(\frac{\eta A}{\Delta f}\right)^{\frac{1}{2}} \cdot \frac{J_{SO}}{J_B^{\frac{1}{2}}} \qquad (32)$$

where:

J_B is the mean value of the background flux (see Fig. 2)

I_{BN} is the output noise current due to background flux

A is the detector area

Δf is the bandwidth

Substituting this into the numerator of Equation 7 gives:

$$DQE_{BL} = \frac{\eta}{T\ \Delta f} \qquad (33)$$

The integration time T can be related to detector time constant τ by $T = K\tau$, where K is a constant of proportionality. Accordingly,

$$DQE = \frac{\eta}{K\tau\Delta f} \qquad (34)$$

2) Electronic-Shot Noise Limited Condition

Normally photoconductive detectors are not limited by

shot noise, but by Johnson or excess noise. It can, however, appear as a limiting noise for a back-biased junction photodetector, operated in the photoconductive mode, or from non-ohmic contacts applied to a photoconductor. Expressions for the signal to noise ratio and DQE for this limiting case will be given here because first, it serves as an example of noise independent of frequency, and secondly, can be compared later with the expressions for return beam image tubes (which can be shot noise limited).

Shot noise is current dependent, such that:

$$\overline{\Delta I_b^2} = 2\, q\, I_b \Delta f \qquad (35)$$

where:

I_b is the bias current

$\overline{\Delta I_b^2}$ is the mean square fluctuation in the current

q is the charge of the electron.

The peak to peak signal to RMS noise ratio is:

$$\frac{I_{S_{P-P}}}{I_{ShN}} = \frac{\eta J_{SO}}{nd} \frac{\sqrt{2\vartheta_b A}}{\sqrt{q\Delta f}} \cdot E \qquad (36)$$

where:

$$I_{ShN} = \sqrt{\overline{\Delta I_b^2}}$$

$\vartheta_b = I_b/A$ is the current density

$E = 1/\sqrt{1+(\omega\tau)^2}$ is an electronic roll-off function

n = equilibrium density of carriers in the crystal.

The Detective Quantum Efficiency is derived by inserting Equation 36 into Equation 7 to get:

$$DQE_{ShL} = \frac{\eta}{K\tau\Delta f} [\eta\eta'] E^2 \qquad (37)$$

$$\text{and } \eta' = \frac{n^2 d^2 q}{2\tau^2 \vartheta_b J_B} \qquad (38)$$

3. Conclusions

DQE in Equation 34 and DQE_{ShL} in Equation 37 are both proportional to η.

DQE_{BL} is equal to η when $K\tau\Delta f = 1$. Thus, when DQE_{BL} is measured for a photodetector, its maximum value will be η for $K\tau\Delta f = 1$. The latter can be assured by adjusting the bandwidth of the measurement. K is a constant for any one detector which depends on the electronic mechanisms involved in photoresponse. For example, a single carrier photoconductor, or the omission of recombination in back-biased photodetectors, or more than one τ, would affect the value of K. Since η can be obtained from an independent measurement, the constant K could be evaluated after measuring DQE_{BL} and τ for some selected Δf. This might well help identify electronic processes responsible for device performance.

For our intrinsic model, $DQE_{BL} = 2\eta$, if $K = 1$ and $2\tau\Delta f = 1$. This results from our assuming that two countable carriers (an electron and a hole) were generated per absorbed photon. Unfortunately, practice is far less fortunate.

A comparison between the background and shot noise limited condition can be made most easily at low frequencies where E = 1. In order for the shot noise limit to reduce to the background limited case, the factor $[\eta\eta']$ must equal unity. An idea of the magnitude of η' can be found by using as representative numbers $J_B = 10^{13}$ photons/cm^2, $I_b = 10^{-5}$ amps, $n = 10^{14}$ electrons/cc, $d = 10^{-3}$cm, $A = 10^{-2}$cm^2, $\mathcal{J}_b = 10^{-3}$ amps/cm^2 and $q = 1.6 \times 10^{-19}$ coulombs. Substituting in (38) gives $\eta' = 1/8$. Assuming an η of unity, then η' would have to be improved by a factor of 8 to achieve the background limited condition. This could be done by any combination of increasing τ, $\mathcal{J}_b$ and/or J_B, or decreasing n and/or d.

DQE_{BL} is thus principally dependent on the quantum efficiency of the photosensor, and is equal to η when the bandwidth of the measurement is set so that $K\tau\Delta f = 1$. When white electronic noise such as shot noise exceeds photon induced noise, the electronic factor E appears. This roll off function has a maximum value of unity, decreasing with increasing frequency and reduces the effective bandwidth of device usefulness.

C. Intensifiers

The intensifier is an imaging device which provides a signal in the form of light output, rather than an electrical signal as from the photoconductor. Further, the light output is generated during the recombination of carriers in the phosphor, and is characterized by the luminescence decay time τ. In an early paper a model of the phosphor was assumed to be intrinsic for carrier generation and recombination[6]. This

permitted close comparison with the photoconductive detector discussed in Section IIIB. The analysis is given in Appendix B (see Equations 11, 15, 16). It led to the peak to peak signal given by:

$$L_{S_{PP}} = (h\nu)_{ave} \{ \eta SAJ_{SO} / [1 + (\omega\tau)^2] \} \qquad (39)$$

where $(h\nu)_{ave}$ is the average photon energy in light emission and all other factors are the same as for Equations 26 and 31.

Noise appears in the light output, and can be the result of background photons or dark current. In either event, it is manifested in the light output as a fluctuation in the recombination process and given by:

$$L_{BN} = (h\nu)_{ave} \{ \eta 2AJ_B \Delta f / [1 + (\omega\tau)^2] \}^{\frac{1}{2}} \qquad (40)$$

for the background noise limiting case.

The peak to peak signal to RMS noise ratio was then found to be:

$$L_{S_{P-P}} = \sqrt{\eta}\, S \cdot \sqrt{\frac{A}{2\Delta f}} \cdot \frac{J_{SO}}{\sqrt{J_B}} \qquad (41)$$

where S is the aperture function noted earlier in Equation 27, which for a circle is given by the sum of the two Bessel functions,

$$S = J_0(Z) + J_2(Z)$$

A = intensifier surface area

Substituting in Equation 7 gives:

$$DQE = \frac{\eta S^2}{2\tau\Delta f} \tag{42}$$

For the case where $2\tau\Delta f = 1$:

$$DQE = \eta S^2 \tag{43}$$

The factor S distinguishes the areal device from the elemental detector. Thus DQE is at best given by the quantum efficiency of the combined photosensor-phosphor layer. However, it rolls off with increasing frequency in a manner associated with the shape of the limiting aperture. For simplicity, this treatment has not included the roll off factor caused by electron-optics, which could be included easily when treated as an ideal lens.

Reference to Equations 14 and 16 reveals that the function S is nothing more than the device MTF, and the constant is given by $1/2\tau\Delta f$. S and S^2 are plotted in Figures 3a, 3b, 4. For intensifier areas other than circular, or for non-uniform electron flow, the function S will be different. For a real device, it would undoubtedly be modified by the MTF of the electron-optics.

D. Signal Generating "Pick-Up" Tubes

These tubes were examined for their dependence on factors governing device performance[7] and reviewed in Appendix C (see Equations 31, 34, 36 for signal to noise ratios below).

1. Background Limited

Theoretical analysis predicts that for the background

noise limited condition the signal to noise ratio is given by:

$$\frac{I_{S_{P-P}}}{I_{BN}} = \left(\frac{\eta_r T}{2\tau\Delta f}\right)^{\frac{1}{2}} \cdot \left(\frac{J_{SO}}{\sqrt{J_B}}\right)^{\gamma} \cdot S \qquad (44)$$

This expression applies when the test pattern is stationary, and is limited to its maximum value obtained at low spatial frequencies. Here:

r = area of a resolution element

T = integration time

τ = dwell time on a resolution element of the read-out beam

γ = slope of log/log plot I_S vs. photon flux irradiating photocathode

S = the aperture function, and depends on the distribution of electrons in the electrom beam at the storage surface. For a uniform distribution of electrons, through a focal circle area, S is given by the Bessel function found in Equation 27, that is $S=J_0(Z) + J_2(Z)$, and all other factors have been identified in Equation 31. The gain of a target does not appear here since it responds equally to photoelectrons generated by signal and noise photons. Clearly the signal to noise ratio improves as the square root of the area of a resolution element and of the integration time. This improvement with area is that commonly experienced with elemental photodetectors and denotes a principal advantage of large area devices. For a constant number of resolution elements, an

increasing value for r requires larger diameter pick-up tubes. The dwell time τ and bandwidth Δf are offsetting factors, in that small τ requires larger Δf and vice versa.

DQE can be evaluated for the background limited condition from Equations 44 and 7 to be:

$$DQE_{BL} = \frac{\eta S^2}{2\tau\Delta f} \cdot \frac{J_B^{(1-\gamma)}}{J_{SO}^{2(1-\gamma)}} = \eta S^2 \qquad (45)$$

for the case where $2\tau\Delta f = \gamma = 1$.

2. Johnson Noise Limited

An appraisal may be obtained for the Johnson noise limited condition imposed by the load resistor, the preamplifier or their combination. This signal to Johnson noise ratio thus is given by:

$$\frac{I_{S_{P-P}}}{I_{JN}} = \frac{\eta r T G q}{\sqrt{2\tau\Delta f}} \left(\frac{2}{\tau}\right)^{\frac{1}{2}} \frac{J_{SO}^{\gamma}}{\sqrt{\vartheta_{JN}}} SE \qquad (46)$$

Here:

G = target gain

I_{JN} = output noise current (RMS) caused by the Johnson noise sources

ϑ_{JN} = mean square fluctuation value of current flow per unit bandwidth induced by Johnson noise generated by the load resistor and preamplifier

$E = 1/(1 + \omega^2\tau^2)^{\frac{1}{2}}$ as defined in Equation 36

and all other quantities are the same as for Equation 44.

The signal to noise ratio now improves linearly with the target gain, area of a resolution element, and integration time. Further improvement results from using a shorter dwell time and better preamplifiers with reduced Johnson noise. Present limitations in these directions, however, are caused by bandwidth requirements and the state of the art of preamplifiers. In order for the Johnson noise limited condition to reduce to the background limited condition, it is necessary that:

$$G\sqrt{\eta J_B r T} = \frac{I_{JN}\tau}{q} \tag{47}$$

assuming for simplicity $2\tau\Delta f = 1$. This is simply a statement that the RMS number of electrons stored on the target during the integration time T must equal the number of electrons generated from Johnson noise sources during the dwell time τ.

DQE for the Johnson noise limiting case becomes (from Equations 46 and 7):

$$DQE_{JL} = \frac{\eta^2 J_B r T G^2}{2 I_{JN}^2 \tau^3 \Delta f / q^2} \cdot \frac{S^2 E^2}{J_{SO}^2 (1-\gamma)} \tag{48}$$

For simplicity, assume $\gamma = 2\tau\Delta f = 1$, so that in the Johnson noise limited condition, DQE becomes:

$$DQE_{JL} = \eta \left(\frac{\eta}{\eta''}\right) S^2 E^2 \tag{49}$$

where

$$\eta'' = \frac{I_{JN}^2 \tau^2 / q^2}{J_B r T G^2} \tag{50}$$

and

$$\eta'' = \frac{\text{noise electrons generated from Johnson sources during } \tau}{\text{background flux generating target charge in r during T}}$$

When the condition of Equation 47 is met, Johnson noise reduces to background noise and DQE increases to its maximum value, that is, DQE = ηS^2E^2 and DQE = η for frequencies sufficiently low such that $S \approx E \approx 1$. The functions E and E^2 are illustrated in Figures 3a, 3b and 5.

3. Beam Shot Noise Limited

Return beam tubes such as image orthicons and image isocons and SEC (when used with return beam) can be shot noise limited. The signal to noise ratio becomes:

$$\frac{I_{S_{P-P}}}{I_{ShN}} = \frac{G\eta rT}{\sqrt{2\tau\Delta f}} \cdot \left(\frac{q}{\tau}\right)^{\frac{1}{2}} \cdot \frac{J_{SO}^{\gamma}}{\sqrt{I_b}} \cdot \delta E \qquad (51)$$

Here the new factors are:

I_{ShN} = output shot noise current (RMS) caused by beam current

I_b = beam current (mean value)

and we note the linear improvement with target gain, resolution area and integration time. The gain of the multiplier does not appear since it acts equally on signal and noise. Similarly, as for the Johnson noise limited condition, improvement results from using smaller dwell time and reducing noise current, which is due to beam current. Limitations that prevail, however, are caused by the requirements of bandwidth and beam

current signal carrying capacity respectively. The shot noise limited condition reduces to the background limited condition when:

$$G\sqrt{\eta J_B r T} = \sqrt{I_b \tau q} \tag{52}$$

This is also nothing more than the statement that the RMS number of electrons replaced in a storage target during dwell time τ, is made equal to the RMS number of photoelectrons generated from the incident background photon flux irradiating the resolution area r during integration time T multiplied by the gain of the target. The multiplier gain follows and is sufficient to raise the shot noise to a level above that of the Johnson noise without significant degradation of the signal to noise ratio. We note again the importance of reducing I_b and τ while increasing η, T, G and r.

DQE can be derived for this condition from Equations 7 and 51 to be:

$$DQE_{ShL} = \frac{\eta^2 J_B r T G^2}{2\tau^2 \Delta f \; I_b/q} \cdot \frac{S^2 E^2}{J_{SO}{}^2 (1-\gamma)} \tag{53}$$

which can be expressed in the form:

$$DQE_{ShL} = \eta \left(\frac{\eta}{\eta'''}\right) S^2 E^2 \tag{54}$$

where $\eta''' \rangle \eta$, $2\tau\Delta f = \gamma = 1$.

$$\eta''' = \frac{I_b \tau / q}{J_B r T G^2} \tag{55}$$

and

$$\eta''' = \frac{\text{beam electrons on target during } \tau}{\text{background flux generating target charge in r during T}}$$

When the condition of Equation 52 is met, beam shot noise reduces to background noise and DQE increases to its maximum value, that is DQE = ηS^2E^2. This can be further maximized at low frequencies where $S \approx E \approx 1$, so that DQE = η.

For the case where the electron beam focused at the charge storage surface determines the area of a resolution element, then $I_b = \vartheta_b r$ and Equation 51 reduces to:

$$\frac{I_{S_{P-P}}}{I_{ShN}} = \frac{G\eta T}{\sqrt{2\tau\Delta f}} \cdot \left(\frac{qr}{\tau}\right)^{\frac{1}{2}} \cdot \frac{J_{SO}^{\gamma}}{\sqrt{\vartheta_b}} SE \qquad (56)$$

and Equation 54 reduces to:

$$DQE_{ShL} = \eta^2 \left(\frac{J_B T G^2}{I_b \tau / q}\right) S^2E^2 \frac{\eta^2}{\eta'''} S^2E^2 \qquad (57)$$

The result is that the signal to noise ratio is dependent on the square root of r, and DQE is independent of the size of the resolution element area.

4. Conclusions

a. Impact of aperture and electronic functions

For any imaging device, an aperture function defines the best performance that can be achieved as a function of spatial frequency. In all noise limiting cases, the signal to noise ratio is proportional to an aperture function, and DQE is

proportional to its value squared. Functions considered here in addition to S for a circular limiting aperture are R_o for an electron beam characterized by a Gaussian distribution, and S_1 for an electron beam characterized by a cosine squared distribution. The functions R_o and S_1 and their squares are shown in Figures 3a, 3b, 6 and 7.

All photoelectronic devices suffer a roll-off defined by the function E, when limited by any noise other than from photons. This function does not have a counterpart in optics, and has its origins in the generation, lifetime, storage and motion of electrons that are not associated with photon generated electrons. The factors E and E^2 appear in the signal to noise ratio and DQE respectively, for devices limited by Johnson and/or shot electronic noise. This type function is well known for elemental photodetectors. However, experiments have yet to be carried out to delineate aperture and electronic response curves, so that the existence of E for imaging devices has yet to be confirmed experimentally. E and E^2 are shown in Figures 3 and 5 respectively.

The effect of all these functions depends upon the size of a resolution element. A series of plots are shown in Figures 4, 5, 6 and 7, showing their squares as a function of spatial frequency for resolution elements of different diameters.

When a device is electronic noise limited then the function E exists and multiplies the appropriate aperture function

to get the theoretically limiting characteristic. Examples are shown in Figures 4, 6 and 7 for E^2S^2, $E^2R_o^2$ and $E^2S_1^2$.

b. Impact of quantum efficiency

One notes in background noise limited cases for all devices that the signal to noise ratios are all dependent on the square root of the quantum efficiency, and that DQE is linearly dependent on η. In the cases of Johnson and shot noises, it was noted that the signal to noise ratio was linearly dependent on η, and that DQE was proportional to η^2. It was also found, however, that DQE could be further expressed in the form DQE $\alpha\eta(\frac{\eta}{\eta''})$. Here η'' has a value greater than η and is a reflection of more noise electrons being generated during read-out than photogenerated and stored electrons. When η'' can be reduced to η, then DQE$\alpha\eta$.

Stress will be made here on the impact of the photosensor's quantum efficiency on imaging device efficiency at higher spatial frequencies. In recent years there has been considerable improvement in high gain targets, to the extent that the zeal for continuing to strive for improvement in the photosensor's quantum efficiency has waned. Examination of Equation 45 reveals that DQE improves linearly with the photosensor's quantum efficiency and does not include the factor of gain. Once enough gain is included in the device to have background noise predominate over shot or preamplifier noise, additional gain provides little or no benefit, and is no longer a factor in improving device performance. The impact of further improvement in η, however, continues to be most significant.

Reference to Figure 8a, which is a plot of Equation 45 for three different efficiencies, illustrates that there is not only a linear increase of DQE at low spatial frequencies, but that there is a tremendous improvement throughout the spectrum, with limiting resolution determined by the aperture function S. One normally does not think of DQE in these terms. However, if there is a full realization that this function can present the fraction of incident photons that is transmitting useful information at all spatial frequencies, then its application becomes far more useful. For example, with $\eta = 50^{o}/o$, DQE at low spatial frequencies has the same value; it rolls off to half as many photons being recorded at $\ell/\lambda = .5$; only one quarter of the incident photons are transmitting information at $\ell/\lambda = .7$. For a resolution element of diameter $\ell = 10$ microns, this corresponds to spatial frequencies of 50 and 70 ℓp/mm, respectively. Comparison between the background limited curves clearly reveals the advantage gained from improvement in η out to the limiting resolution defined by the aperture function.

When beam shot or preamplifier Johnson noise limited, the impact is more dramatic. As shown in Figures 8a and 8b, roll off occurs more rapidly because of the effect of the electronic function E. Clearly, increased η provides significantly improved performance with spatial frequency.

c. Impact on DQE and MTF of efficiency and frequency

The relationship between MTF and DQE was first illustrated by Equation 14. Subsequent analysis revealed that various

functions (aperture and electronic) could be derived to predict the roll-off of DQE with frequency. These functions then proved to be the equivalent of theoretical MTF's that would prevail for ideal models. Thus MTF is identified with the roll off functions, that is S, R_o, S_1 and their products with E.

Next most important is to examine the predictions of system performance based in MTF and DQE. It is well known that evaluations based on MTF have deteriorating value when the system is noise limited. It is hoped that using DQE in the manner customary for MTF will eliminate the limitations of MTF and provide an improved technique for predicting system performance.

Consider an optical system comprising three glass discs: the first had a transmittance of 100°/o, the second 50°/o and the third 25°/o. The MTF of each glass disc is S, and the system MTF is S^3. DQE, however, involves efficiency, and thus for each disc is S^2, $.5S^2$ and $.25S^2$ respectively. The system DQE is their product, given by $.125(S^2)^3$, which is shown in Fig. 9a. The system $(MTF)^3$ and $(MTF^2)^3$ is also shown for comparison. Clearly the presentations are markedly different. MTF would lead to very bright predictions compared to DQE. Unmistakably, DQE runs out of useful spatial spectrum before MTF. The degree of usefulness for high spatial frequencies depends next on irradiance and the DQE of the photon receiver. The plot of DQE reveals that at best the glass system transmits only 12.5°/o of the incident radiation, with a decreasing value

for increasing frequency. These curves can be replotted as a function of spatial frequency, as in Fig. 9b. Here, assuming a value of ℓ = 10 microns, for illustration, gives the corresponding curves.

A more realistic appraisal might be obtained using an x-ray intensifier whose efficiency is assumed to be about 50°/o, coupled to an ideal lens, and to a TV tube with a photocathode efficiency of 25°/o. Assume further that the intensifier has a limiting aperture function given by S, that the lens can be represented by the MTF for an ideal lens, and that the TV tube is limited in resolution by its beam which has a Gaussian distribution. Thus plots obtained from Figures 4 and 6 can be shown with the MTF^2 for an ideal lens as in Fig. 10a. These curves assume that the intensifier has a resolution element of 50 microns, and the pick-up tube of 10 microns. Fig. 10b illustrates the resultant systems plots for MTF and DQE as a function of spatial frequency.

d. Impact of resolution area, integration and gain

The effect of increasing the area of a resolution element in all noise limiting cases is to improve the signal to noise ratio. This improvement, however, is traded off for frequency response because of the more rapid roll off in S, R and E. The signal to noise ratios are proportional to the $\sqrt{r}$ for all devices, when the noise source is from photons or generated electronically within the device. For external noise sources such as Johnson noise from coupling circuitry or preamplifiers,

This, when done with an appropriate test pattern, can give directly DQE vs. spatial frequency.

Equally valid, however, is a second approach making use of MTF. The task here is to evaluate DQE at its maximum value for zero frequency. This evaluation automatically provides the product $C\eta$ noted in Equation 16, which when multiplied by $(MTF)^2$ gives DQE vs. spatial frequency.

The test facility at URI is being set up to evaluate DQE versus spatial frequency for TV type tubes. The experimental program comprises the following measurements.

A. The Measurements Program

1. Signal and Noise Input

This involves using a blackbody or standard lamp to irradiate a bar pattern mask covering the face of the tube. The bar patterns provide a square wave test pattern whose frequency depends upon the width of the bars. Irradiance through the bars provides a precisely determined input photon flux, with input signal given by its mean value, and input noise by the square root of the mean value. Present technology for cutting bars in a mask suggests that masks giving spatial frequencies of at least 6 ℓp/mm are possible. Beyond these frequencies, it appears necessary to use a lens to image a test pattern on the face of the tube. This requires a lens whose MTF and DQE are precisely known, so that the irradiance on the face of the tube from an imaged bright bar can be precisely determined.

2. Signal and Noise Output

The peak to peak signal output is being measured in two ways, both a considerable improvement over conventional methods. The first is an analog method and uses a box car integrator. A digital technique has also been devised which was intended for a precise measurement of RMS noise. However, it has also proven to be an excellent device for making accurate measurements of peak to peak signal. Both techniques are described and their performance evaluated in Appendix D, which is a paper recently given at the Fifth International Symposium on Photoelectronic Imaging Devices[11]. Assuming that the noise spectrum is flat, the RMS value obtained above coupled to the peak to peak signal measurements, provides the most accurate method to date of getting the signal to noise ratio, under severe noise limiting conditions.

3. Determination of DQE, Signal and Noise as a Function of Spectral Wavelength

A spectrophotometric apparatus has been established at URI capable of providing a measurement of signal versus λ leading to a calculation of DQE(λ). This measurement will be undertaken immediately after the systems described in both 1 and 2 above are operational.

4. The Computerized Program

In addition to the measurements noted in 1 and 2 above, the test set is being coupled to a PDP-9 computer (see Appendix D). The purpose of this arrangement is to have a facility

which will accept data on signal to noise input, with signal and noise output, and provide a user with:

1. Signal vs. spatial frequency
2. Noise vs. spatial frequency
3. The output signal to noise ratio
4. DQE as a function of spatial frequency.

This information is to be provided generally in terms of input photon flux. However, the computer is being programmed to provide information converted to photometric or radiometric units when applicable and requested. The noise evaluation will have additional importance in that it provides an opportunity to determine if the noise spectrum is really flat.

REFERENCES

1. A. Rose, J. Soc. Mot. Pict. Engrs. 47, 273, 1947.
2. R. C. Jones, in Advances in Electronics and Electron Physics, Academic Press, Inc., New York, 1959, Vol. 11.
3. P. Pryor, Private Communication.
4. S. Nudelman, Appl. Opt. 1, 627 (1962).
5. R. L. Petritz, Proc. IRE, 47, 1458 (1959).
6. S. Nudelman, Appl. Opt. 5, 1925 (1966).
7. S. Nudelman, Appl. Opt. 6, 149 (1967).
8. P. Pryor. Concepts which arose during conversations with P. Pryor.
9. L. Levi, Applied Optics: A Guide to Modern Optical System Design (Wiley, New York, 1968), p. 135.
10. M. R. Holter, S. Nudelman, G. H. Suits, W. Wolfe, G.J. Zissis, Fundamentals of Infrared Technology (MacMillan Co., New York, 1962), p. 312.
11. D. Fisher, R. Lee, V. McCollough, S. Nudelman, D. Tufts, M. Wilkinson, Advances in Electronics and Electron Physics, ed. by J. D. McGee, Academic Press, New York, in press.

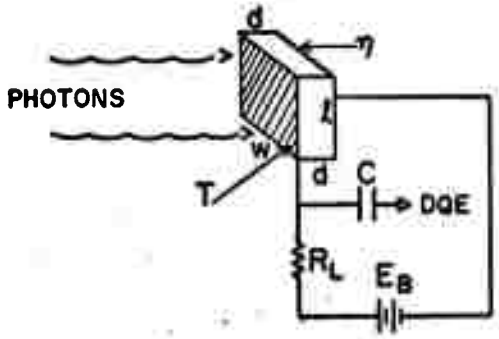

T – TRANSPARENT ELECTRODE ON FRONT SURFACE.
R_L – LOAD RESISTANCE
E_B – BIAS VOLTAGE
C – COUPLING CAPACITOR
η – SEMICONDUCTOR'S QUANTUM EFFICIENCY
DQE – DETECTORS DQE = $c_1\eta$ FOR $c_1 \leq 1$

(a) PHOTOCONDUCTIVE DETECTOR

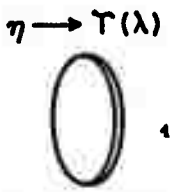

(b) GLASS DISC CIRCULAR MIRROR

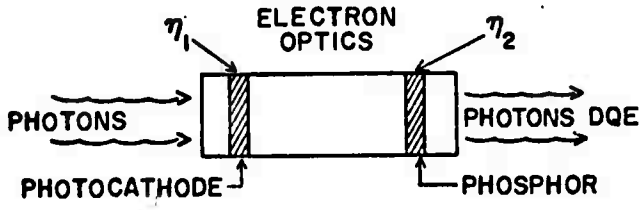

η_1 – PHOTOCATHODE QUANTUM EFFICIENCY
η_2 – PHOSPHOR QUANTUM EFFICIENCY
DQE – INTENSIFIER, DETECTIVE QUANTUM EFFICIENCY = $c_2\eta_1\eta_2$ FOR $c_2 \leq 1$

(c) INTENSIFIER

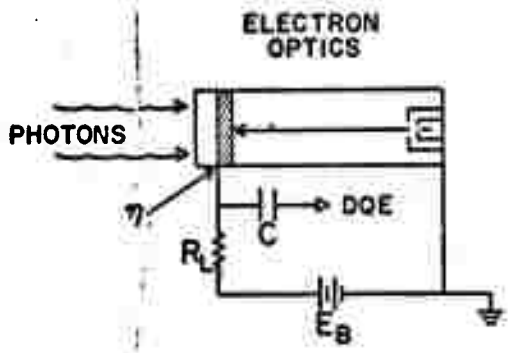

η – PHOTOCATHODE QUANTUM EFFICIENCY
DQE – TUBE DETECTIVE QUANTUM EFFICIENCY = $c_3\eta$ FOR $c_3 \leq 1$

(d) SIGNAL GENERATING TUBE

FIGURE 1

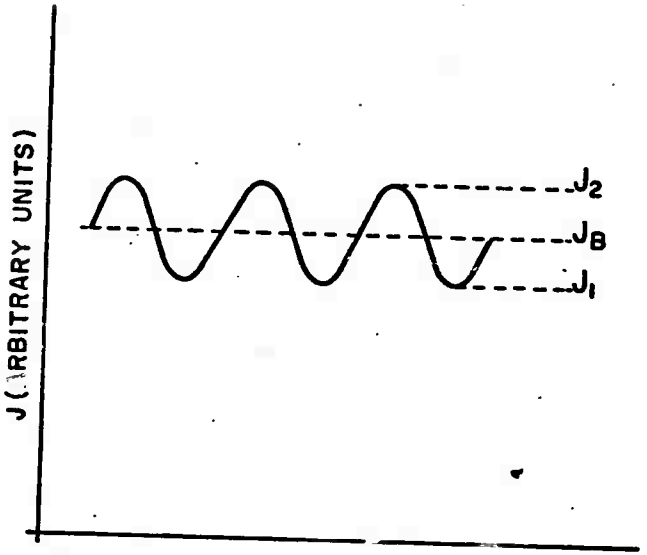

Figure a: Input in Photon Flux J;

$J_B = \frac{J_1 + J_2}{2} = J_{21}$; $J_{SO} = J_2 = J_1$

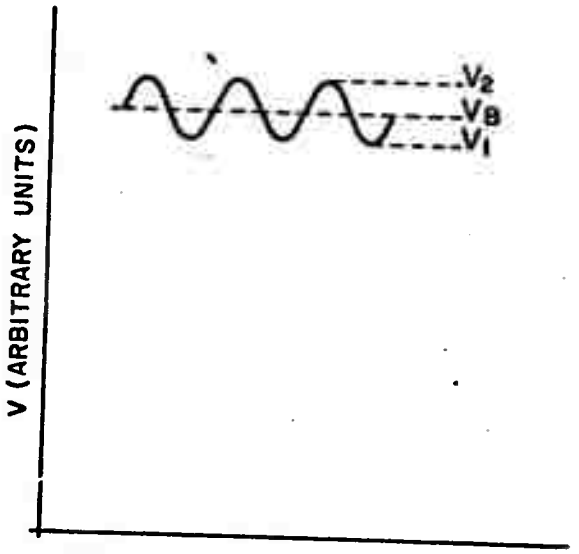

Figure b: Output in Light, Voltage or Current;

$V_B = \frac{V_2 + V_1}{2} = \frac{V_{21}}{2}$; $V_{SO} = V_2 - V_1$

FIGURE 2

TEST PATTERN FROM A SINUSOID PLUS A CONSTANT

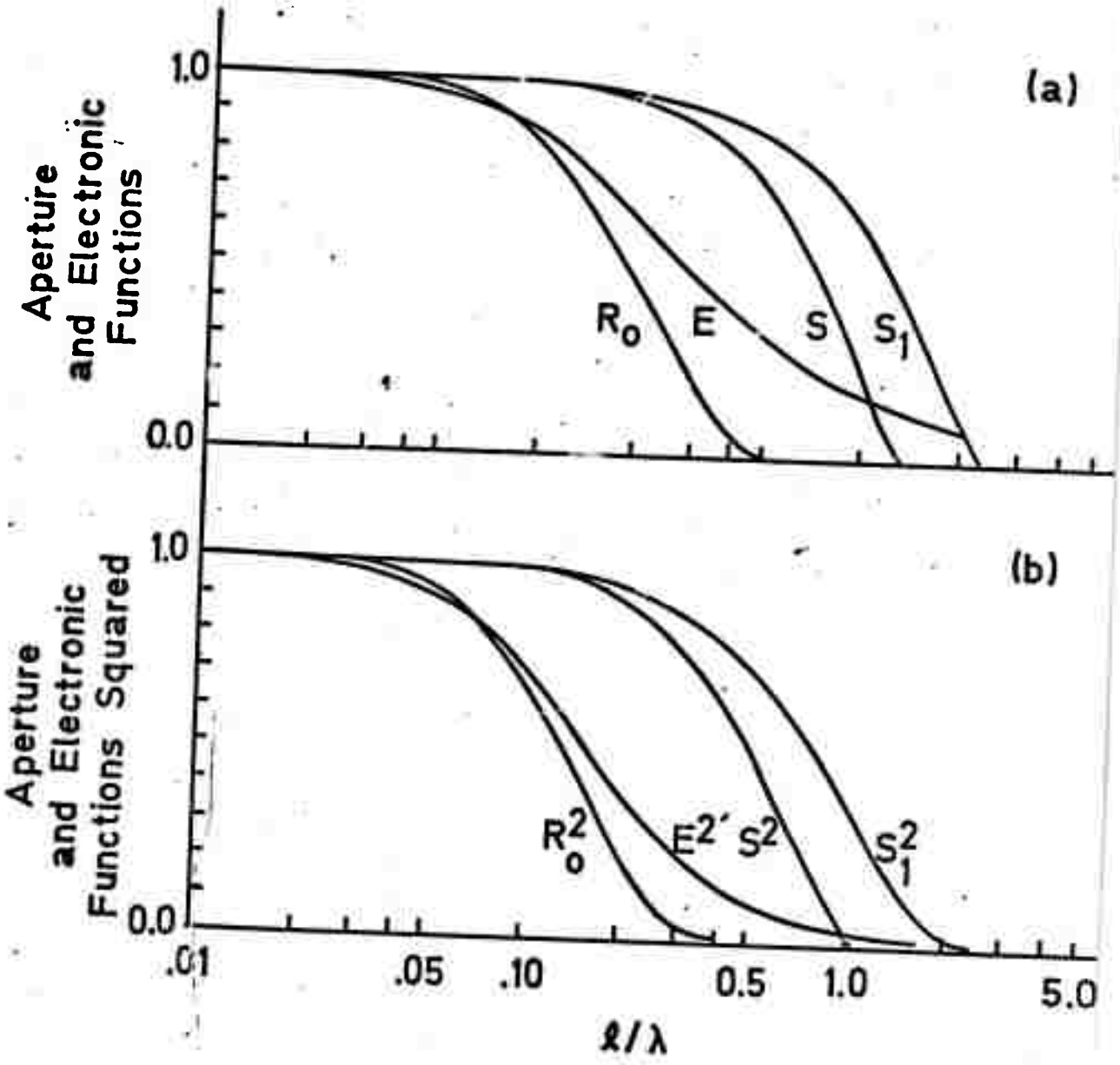
1.0
0.0
(a)
Aperture and Electronic Functions
R_o
E
S
S_1
1.0
0.0
(b)
Aperture and Electronic Functions Squared
R_o^2
E^2 S^2
S_1^2
.01
.05
.10
0.5
1.0
5.0
ℓ/λ

Fig. 3

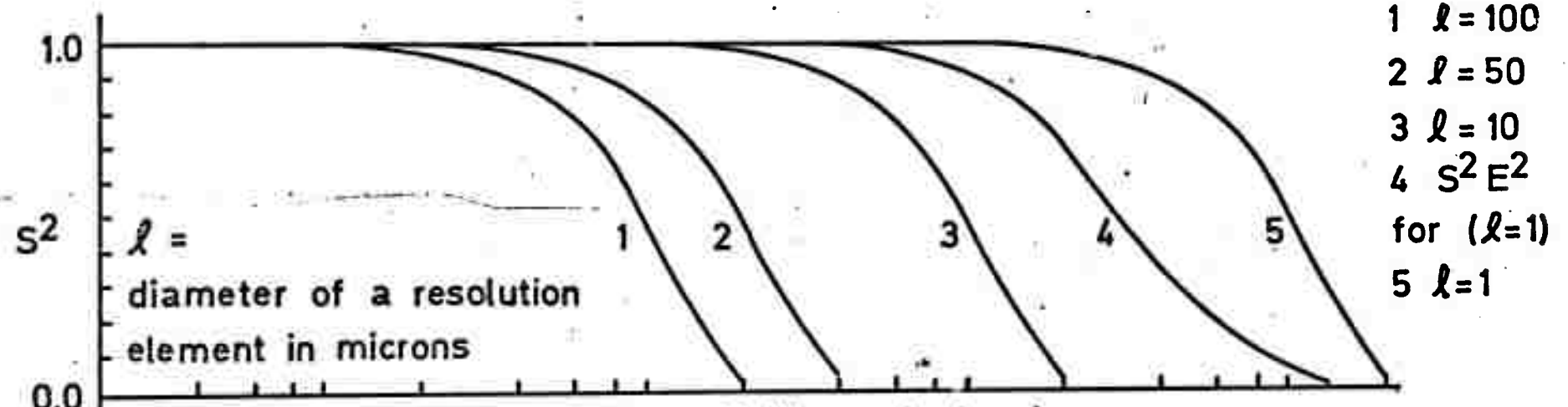
1.0
0.0
S^2
ℓ =
diameter of a resolution
element in microns
1
2
3
4
5
1 ℓ = 100
2 ℓ = 50
3 ℓ = 10
4 $S^2 E^2$
for (ℓ=1)
5 ℓ=1
Spatial Frequency N (line pairs/mm)

Fig. 4

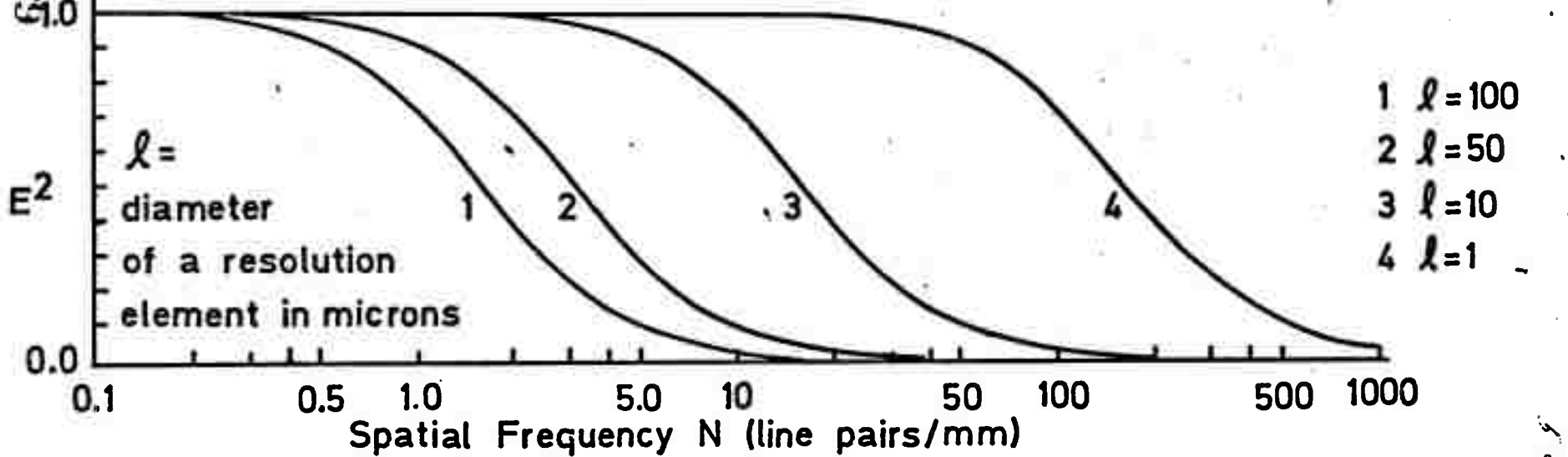
1.0
0.0
E^2
ℓ =
diameter
of a resolution
element in microns
1
2
3
4
1 ℓ = 100
2 ℓ = 50
3 ℓ = 10
4 ℓ = 1
0.1
0.5
1.0
5.0
10
50
100
500
1000
Spatial Frequency N (line pairs/mm)

Fig. 5

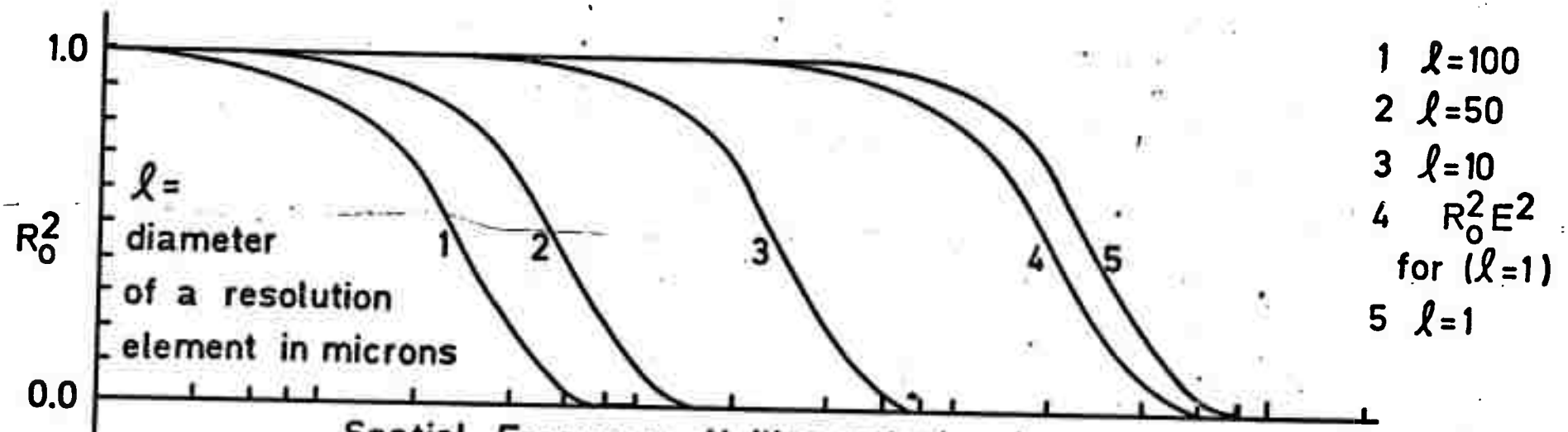
1.0
0.0
R_o^2
ℓ = diameter of a resolution element in microns
1
2
3
4
5
1 ℓ=100
2 ℓ=50
3 ℓ=10
4 $R_o^2 E^2$ for (ℓ=1)
5 ℓ=1
Spatial Frequency N (line pairs/mm)

Fig. 6

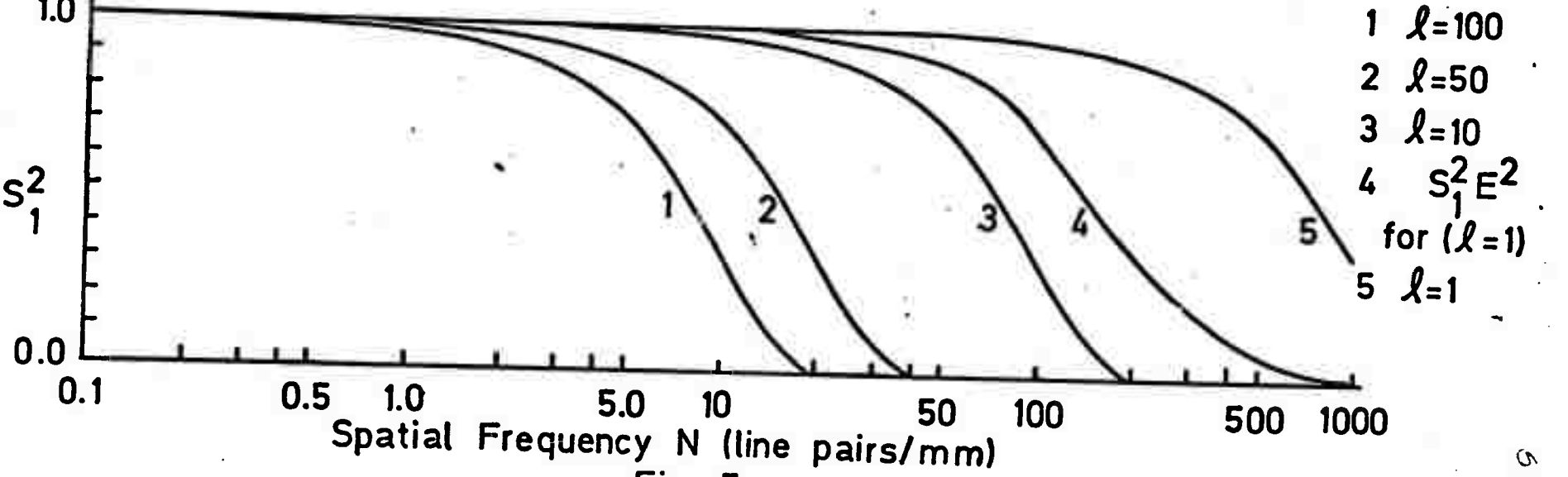
1.0
0.0
S_1^2
1
2
3
4
5
1 ℓ=100
2 ℓ=50
3 ℓ=10
4 $S_1^2 E^2$ for (ℓ=1)
5 ℓ=1
0.1
0.5
1.0
5.0
10
50
100
500
1000
Spatial Frequency N (line pairs/mm)

Fig. 7

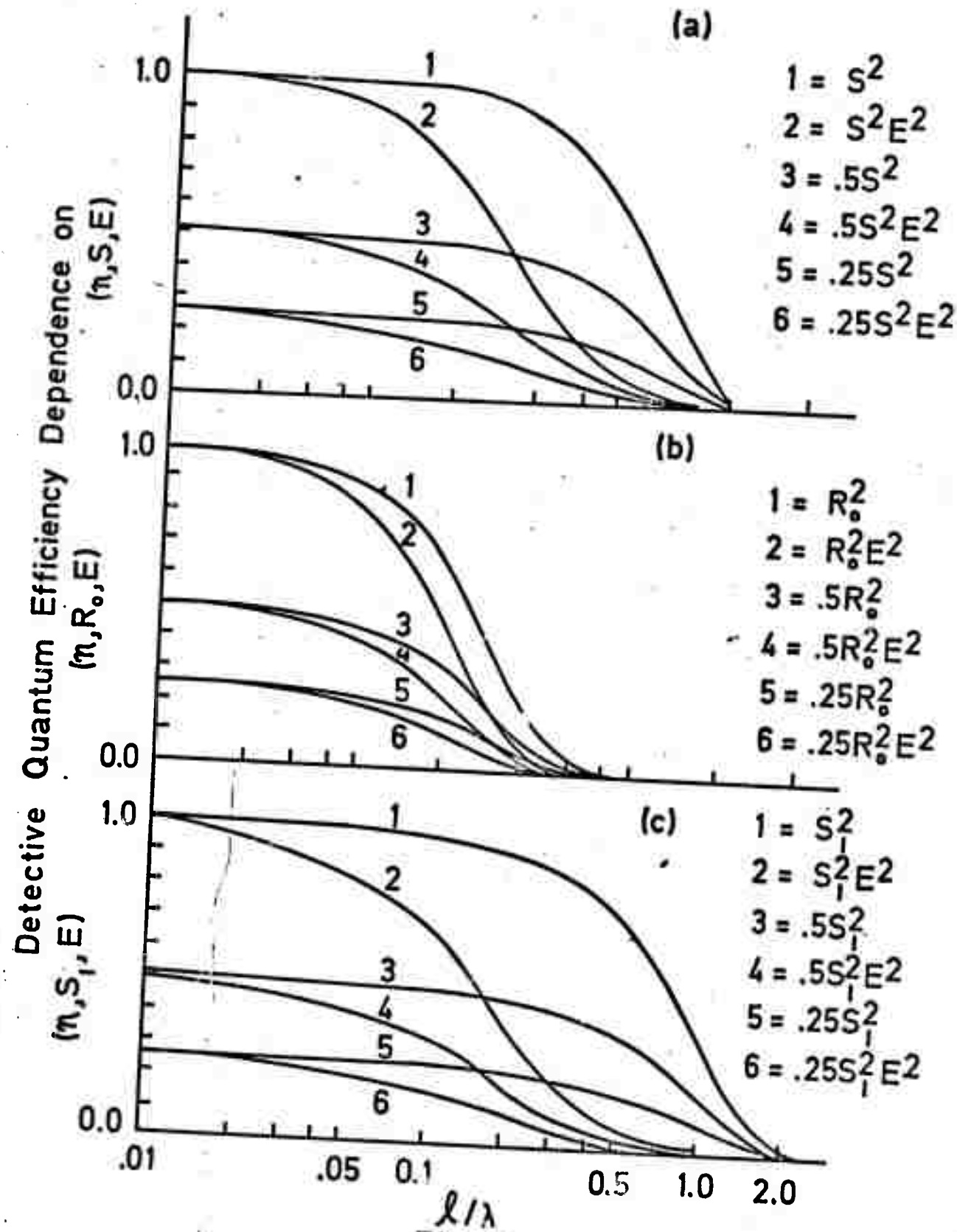
(a)
1.0
0.0
1
2
3
4
5
6
1 = S²
2 = S²E²
3 = .5S²
4 = .5S²E²
5 = .25S²
6 = .25S²E²
(b)
1.0
0.0
1 = R₀²
2 = R₀²E²
3 = .5R₀²
4 = .5R₀²E²
5 = .25R₀²
6 = .25R₀²E²
(c)
1.0
0.0
1 = S₁²
2 = S₁²E²
3 = .5S₁²
4 = .5S₁²E²
5 = .25S₁²
6 = .25S₁²E²
Detective Quantum Efficiency Dependence on
(n,S,E)
(n,R₀,E)
(n,S₁,E)
.01
.05
0.1
0.5
1.0
2.0
ℓ/λ

Fig. 8

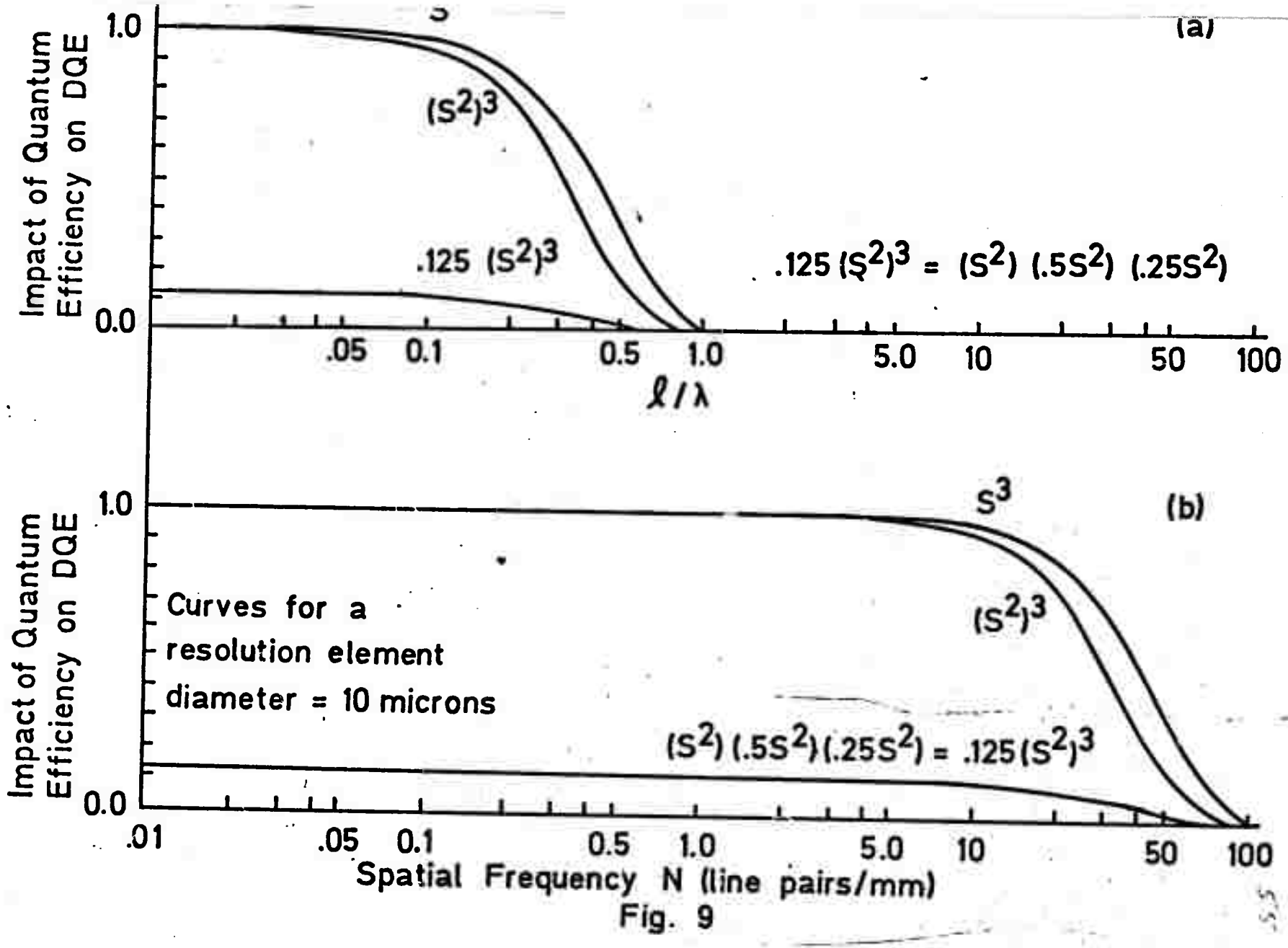
(a)
Impact of Quantum Efficiency on DQE
1.0
0.0
$(S^2)^3$
$.125\ (S^2)^3$
$.125\,(S^2)^3 = (S^2)\ (.5S^2)\ (.25S^2)$
.05
0.1
0.5
1.0
5.0
10
50
100
ℓ/λ
(b)
Impact of Quantum Efficiency on DQE
1.0
0.0
S^3
$(S^2)^3$
Curves for a
resolution element
diameter = 10 microns
$(S^2)\ (.5S^2)\ (.25S^2) = .125\,(S^2)^3$
.01
.05
0.1
0.5
1.0
5.0
10
50
100
Spatial Frequency N (line pairs/mm)

Fig. 9

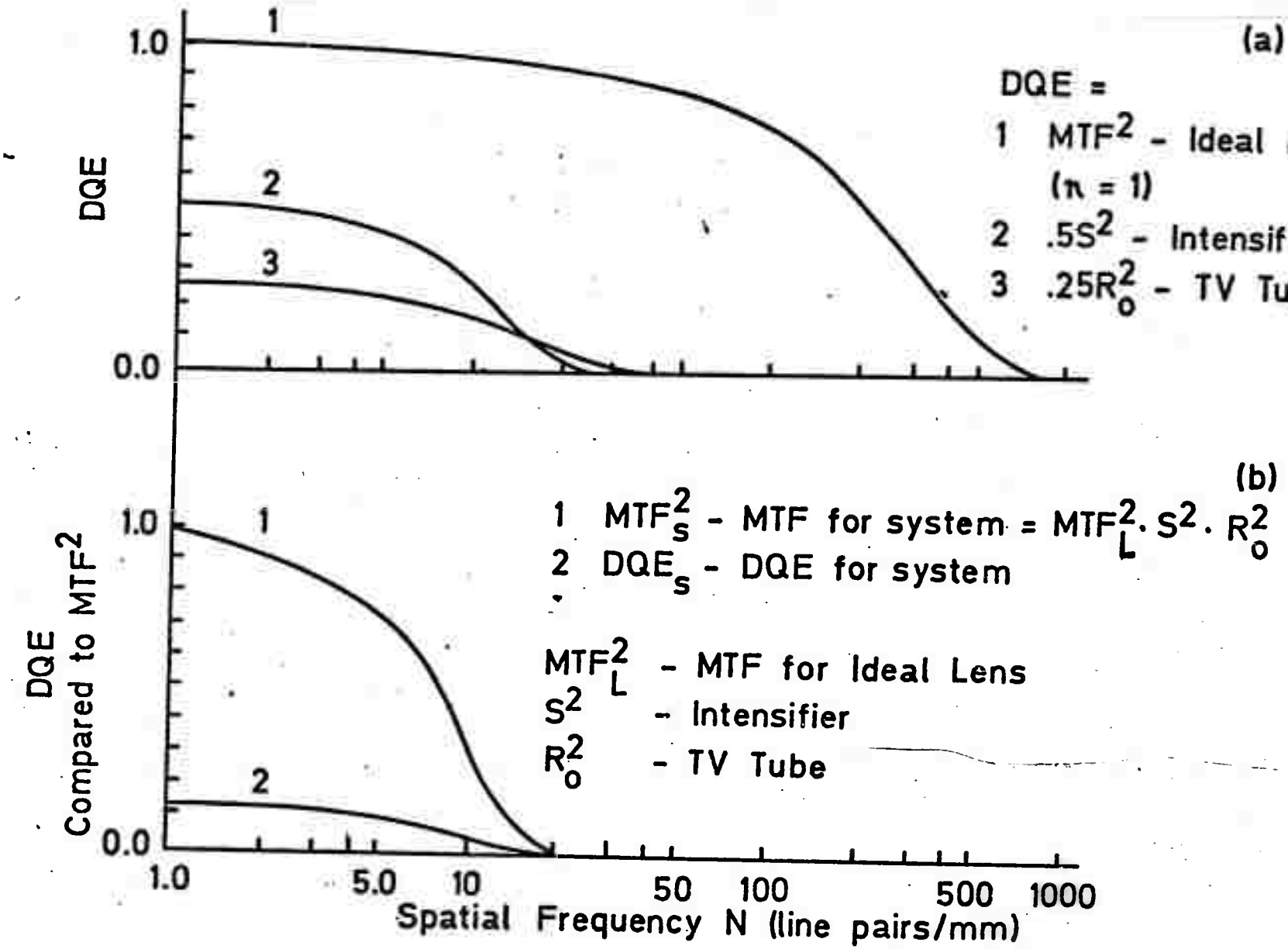
(a)
DQE =
1 MTF^2 - Ideal Lens
(π = 1)
2 .5S^2 - Intensifier
3 .25R$_o^2$ - TV Tube
DQE
1.0
0.0
1
2
3
(b)
1 MTF$_s^2$ - MTF for system = MTF$_L^2$. S^2. R$_o^2$
2 DQE$_s$ - DQE for system
MTF$_L^2$ - MTF for Ideal Lens
S^2 - Intensifier
R$_o^2$ - TV Tube
DQE Compared to MTF^2
1.0
0.0
1
2
1.0
5.0
10
50
100
500
1000
Spatial Frequency N (line pairs/mm)

Fig. 10

APPENDIX A

The Photoconductive Detector

This device was analyzed in a paper by S. Nudelman in Applied Optics 1, 627 (1962), of which Parts I and II are reproduced below. Changes in the reproduction have been made to accord with the notation and the model used throughout the paper. In particular, signal current is derived and used here rather than voltage. This is to conform with expressions derived for signal generating tubes in Appendices B and C.

I. Introduction

The purpose of this article is to present a review and an analysis of the factors involved in determining the capability of semiconducting photodetectors to detect radiation.

By 1953, considerable information on thermal detectors, photoemissive devices, and photographic film was available, to the extent that Jones[1] was able to present a detailed accounting of the "state of the art". In addition, he was able to ascertain consistent patterns of detector behavior, to formulate a system of detector classification, and to propose figures of merit. Semiconducting photodetectors were in the early stages of their development and it was possible to include only some of the preliminary information on lead-compound detectors in the report. Since that time, considerable effort has been expended toward the development of background-noise-limited infrared detectors, and to the understanding of the basic physical mechanisms responsible for

their performance. G-R (generation-recombination) noise was uncovered as a limiting fundamental process, while the role of shot noise in p-n junction detectors was ascertained. Excess or 1/f noise received intensive study, and significant reduction of this noise was achieved in the development of most photodetectors. However, its properties still remain to be organized and explained theoretically. The concept of detectivity-star (D*) was introduced by Jones[2] to provide a numerical rating for a detector. This concept has proven useful, and on the basis of recent measurements appears to be fully applicable to semiconducting photodetectors. With the accumulation of this wealth of new information, it is now fruitful to present a re-examination of the mechanisms involved in photodetection and to derive expressions for the noise currents appearing at the output of the detector for the various noise-limited conditions.

II. The Photoconductive Detector

The solid-state quantum detector absorbs electro-magnetic radiation (or photons) and generates from this absorption additional free charge carriers. The mechanisms of this process require that the quantum of energy associated with the photons ($E_{ph} = hc/\lambda$) be greater than some critical energy corresponding to allowed transitions between the conduction band, the valence band and/or a discrete energy level in the energy-gap region of the semiconducting detector. This process is carried out without any significant temperature change. The additional carriers that are generated appear in a form suitable for measurement as a voltage or a current.

A. Signal Generation

The photoconductive detector, which is the only device that will be discussed here, is generally operated with the simple circuitry of Fig. 1. The bias current (I_b) through the detector is given by:

$$I_b = \frac{V}{r_L + r_c} \tag{1}$$

where:

V = bias battery voltage

r_L = load resistor

r_c = resistance of the photoconductive detector

C = coupling capacitor

The signal current is the variation in current flow through the detector caused by changes in r_c, when the detector is exposed to radiation. Therefore, by taking the differential of Equation (1):

$$I_S = \Delta I_b = - \frac{V}{r_L + r_c} \cdot \frac{\Delta r_c}{r_L + r_c} \tag{2}$$

The change in resistance is due to the change in the number of carriers created by the absorption of signal photons. For the simplest kind of analysis, consider here the case of the intrinsic photoconductor whose hole and electron densities are equal, as are also their respective mobilities. The general case of unequal mobilities, and including the impurity photoconductive detector, results in an analysis requiring significantly extra arithmetic, and for the purposes of this paper, leads to the same conclusions. Let the detector shape be a parallelopiped, of length ℓ, width w, and thickness d. The quantity ℓw represents the surface

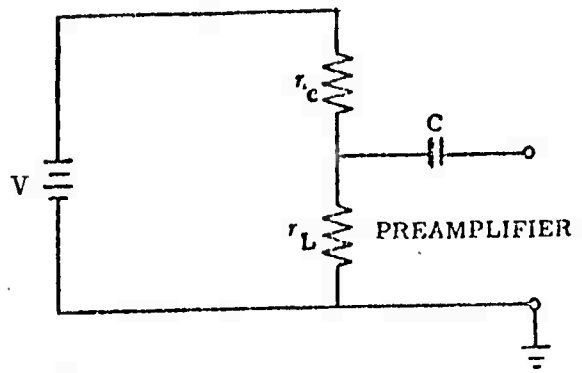

Fig. 1.

exposed to radiation and defines the detector area A, with the electrodes placed across the wd end faces. The cell resistance is given by:

$$r_c = \rho \frac{\ell}{wd} = \frac{\ell}{\sigma wd} = \frac{\ell}{2ne\mu wd} \qquad (3)$$

where:

ρ = electric resistivity = $1/\sigma$

σ = electric conductivity = $ne\mu_n + pe\mu_p = 2ne\mu$

μ = mobility ($\mu_n = \mu_p$)

n = density of electrons

p = n = density of holes

When radiation is absorbed by the detector, it causes a change in the density of carriers, and therefore a change in conductivity. The change in resistance due to electrons for example is given by:

$$\Delta r_c = \frac{dr_c}{dn} \cdot \Delta n = -\frac{\rho \ell}{wd} \cdot \frac{\Delta n_s}{n} \qquad (4)$$

The corresponding signal current is then derived from (2) and (3), and is given by:

$$I_S = \frac{V}{r_L + r_c} \left(\frac{r_c}{r_L + r_c} \right) \cdot \frac{\Delta n_S}{n} \tag{5}$$

or

$$I_S = I_b \cdot r_R \frac{\Delta N_S}{N} \tag{6}$$

where:

ΔN_s = total number of additional electrons given by $\Delta N_s w \ell d$, equal to $N(t)-N$

N = number of electrons in the absence of signal

$N(t)$ = instantaneous number of electrons

r_R = resistance ratio = $r_c/(r_L + r_c)$

In the work that follows we assume a small signal condition where $\Delta r_c \ll r_c$, so that the signal current is treated as linearly dependent on ΔN. The photodetector small signal properties are governed by (4):

$$\frac{d}{dt} \Delta N_s = A \eta_s J_s - \frac{\Delta N_s}{\tau} \tag{7}$$

where:

η_s = responsive quantum efficiency

τ = electron-hole lifetime

J_s = incident number of photons per unit area per second

The solution of this equation for a sinusoidal signal of modulation frequency $f = \omega/2\pi$ is:

$$|\Delta N_s(f)| = \frac{2A \eta_s |J_S| \tau}{\sqrt{1 + (\omega\tau)^2}} \tag{8}$$

The fractional change in the number of free electrons is:

$$\frac{|\Delta N_s(f)|}{N} = \frac{2\,\eta_s\,|J_S|\,\tau}{nd\sqrt{1+(\omega\tau)^2}} \qquad (9)$$

where the factor 2 is introduced to allow for two carriers generated (an electron and a hole) for each absorbed photon. The peak to peak signal current is derived by inserting Eq. (9) into (6) to get:

$$I_{S_{P-P}} = I_b \cdot r_R \cdot \frac{2\,\eta_s J_{SO}\,\tau}{nd\sqrt{1+(\omega\tau)^2}} \qquad (10)$$

where J_{SO} is the peak to peak value (amplitude) of the sinusoidally varying photon flux signal. It is clear that signal response improves with longer lifetimes, improved quantum efficiencies, and decreasing equilibrium density of carriers.

B. Noise

There are five kinds of electrical noise that appear in the output of semiconducting photodetectors. They will be described below, briefly.

1. Johnson Noise

This type of noise is often referred to as Nyquist noise, since both Nyquist and Johnson treated this noise problem in 1928 It can be expressed as:

$$\overline{v^2} = 4kTr\Delta f, \qquad (11)$$

where:

k = Boltzmann's constant,

T = absolute temperature,

Δf = electrical bandwidth,

r = resistance,

v = voltage, that is $[v(t) - v_{av}]$.

2. Generation-Recombination Noise

This type of noise is inherent in the electronic system of semiconducting materials. All atoms in a lattice vibrate in an organized manner to the extent that their vibrations are quantized and can be described in particle terminology as "phonons". Valence-band electrons are continually jostled by the vibrations of the lattice atoms. Every so often, the nature and phasing of vibrations between atoms is such that an electron in their midst is able to gain enough energy to be freed from its bound (valence-band) state, and to move about in the conduction band. The electron is said to have suffered a phonon collision, and to have absorbed energy in the process.

When electrons leave the valence band for the conduction band, charge carriers (electrons and holes) become available for the purposes of current flow. The equilibrium number of carriers created increases with a crystal's temperature, and for any one temperature will be greater for diminishing forbidden energy gap. The thermal (phonon) excitation process is statistical in nature, and the rate at which electrons are excited to the conduction band fluctuates.

In addition to the statistical pulses of generation, we find that a similar situation exists for the recombination of carriers. The electrons and holes wander about the crystal lattice with some thermal motion, and during a "lifetime" characteristic of the semiconductor material, get close enough together to recombine directly,

or through a recombination center. The lifetime is a statistically fluctuating quantity, as is the instantaneous number of electrons and holes. Current carrier fluctuations are therefore inherent in any semiconductor. When a sample is placed in an electric circuit, like Figure 1, one should expect, and in fact one does observe, conductivity fluctuations causing electrical noise completely described by the generation-recombination process.

This noise is a bulk property of the crystal and is due to conductivity fluctuations caused by carrier density changes. It was shown by Petritz that[7]:

$$\frac{\Delta N^2}{N} = \frac{2\tau}{1+\omega^2\tau^2}\,\Delta f \qquad (12)$$

Accordingly, assuming Poisson statistics apply, substitution in Equation (6) gives:

$$\overline{i^2} = I_b^2\, r_B^2\, \frac{2\tau}{N[1+(\omega\tau)^2]}\,\Delta f \qquad (13)$$

which is in a form first developed by Van Vliet(8).

3. Current, 1/f, Modulation, and Excess Noise

All of the names above have been used at various times as names for the same kind of noise. It is a noise that appears commonly in photodetectors in addition to the noise already discussed and is generally found to have characteristics that can be described by the expression (see ref. 9):

$$\overline{i^2} = C\,\frac{I^2}{fAd}\cdot\Delta f \qquad (14)$$

where:

I = total current through the sample,

f = frequency

C = constant.

Actually Eq. (17) is not universal in that cases have been cited where the current exponent has been found as small as 1.25 and as large as 4[9], while the frequency exponent has ranged from 1 to 3[10]. However, these extreme exponential variations are not particularly common, and can usually be associated with a specific material, or to some unique treatment and physical condition of a material[9].

The physical mechanism of this noise is the least understood of all the noise found to date. Petritz[11] introduced the name "modulation" noise to identify the mechanism as something quite different from simple carrier density fluctuations.

The modulation suggestion offered by Petritz, however, can still be only a part of the picture. Brophy and Rostoker[12], Brophy[13] and Bess[14] found with direct experimental evidence that the noise fluctuations in Hall voltage followed the same frequency dependence pattern as the noise from a conductivity measurement. It must be concluded, therefore, that, like conductivity, 1/f noise also follows the fluctuation in the density of the majority current carriers.

The location of a major source of 1/f noise (at least in the case of germanium filaments), has been found to be the surface of the crystal. Recent studies by MacRae[15] indicated that a surface inversion layer (a p-type surface on an n-type crystal or vice versa) is necessary to generate significant 1/f noise.

Although the surface provides 1/f noise, it is quite clear that this kind of noise can also be generated in the bulk material. Brophy[16] finds that, by plastic deformation, he can create noise sources and cause an increase of excess noise by orders of magnitude. These sources are uniformly distributed throughout the crystal, and also contribute an unusual I^4 dependence. Bess[17] assumed that the noise was due to edge dislocations with impurities diffusion along the edge. Such distributions throughout the bulk can provide noise spectra similar to that obtained by inversion surface layers[18]. Even when surfaces are treated so that their noise contribution is minimized, and bulk sources are removed, residual (1/f) noise may still exist. This noise has been associated with non-ohmic contact regions, probably due to minority carrier drift across the contacts. Thus the sources of 1/f noise can be found at the surface, in the bulk, and at the electrical contacts of a detector.

4. Shot Noise

This noise is usually associated with vacuum tubes; it is described as the electrical noise that appears in the output of a vacuum tube when the grid, if any, is held at a fixed potential. However, it is more precisely described in what is usually called the temperature-limited condition. By temperature limited it is meant that the anode voltage on the tube is sufficient to collect all of the electrons emitted from the cathode. Consider a temperature-limited diode connected to a resistance r. Because of the discreteness of the electronic charge, the number of electrons emitted at equal time intervals will fluctuate around an average value. The fluctuating current causes a fluctuating voltage

across r which can be amplified and measured. The mean square current fluctuation turns out to be constant up to frequencies of approximately the reciprocal of the transient time, and can be described by

$$\overline{I_b^2} = 2qI_b\Delta f \tag{15}$$

where q is the electronic charge and I_b is the bias current[19].

Semiconductor photovoltaic detectors and back-biased p-n junctions operating in a photoconductive circuit also exhibit shot noise. In a p-n junction diode, a space charge region and associated electric field is developed across the barrier. Electrons or holes created by phonons or the absorption of background photons, diffusing into the barrier region, are swept from the n-type material to the p-type material, or vice versa. This results in current pulses appearing across the diode with the same characteristics tha are observed for the vacuum tube.

Petritz (see r . 7) has developed a theory applicable to the lead chalcogenide (PbS, PbSe, PbTe) photoconductive films, which is suitable for use here. These films are composed of a system of tiny crystallites separated by intercrystalline barriers, where space charge regions exist. The barrier regions contribute both Johnson and shot noise, while the crystallites generate the usual Johnson noise. For thin barriers, compared to the carrier diffusion length, the barrier contribution to shot noise is given by

$$\overline{v^2} = \frac{2er_c^2 I_b}{n_i \ell} \cdot \Delta f \tag{16}$$

where n_i is the number of crystallites per unit length and r_c is the detector resistance.

5. Background-Radiation Noise

Background radiation can be thought of as a stream of photons originating from the detector environment. The cell walls surrounding the detector, its window, and the media viewed by the detector through the cell window all contribute to this radiation. The extent of the individual contributions is determined by their respective temperatures, emissivities and geometry.

Photons originating from the background and impinging on the detector arrive and are absorbed in a statistically fluctuating manner. This results in a well-defined type of electrical noise. When this is the predominant noise, the photodetector is said to be "background radiation-noise limited". The generation of carriers by this process follows the same statistical law as the G-R noise.

The complete expression that describes the fluctuation in carriers (electrons and holes) for the case of equilibrium when generation rates are equal to recombination rates is given by Petritz[4,7] as:

$$\overline{\Delta N^2}_{\text{noise}} = \frac{4\tau^2 \cdot \Delta f \cdot A(\eta_B J_B + \eta_\ell J_\ell)}{1 + (\omega\tau^2)} \qquad (17)$$

where:

$N_L = A\eta_L J_L \tau$ = equilibrium number of excess electrons from lattice phonons

$N_B = A\eta_B J_B \tau$ = equilibrium number of excess electrons from background photons

η_L, η_B = conversion efficiencies of phonons and photons to electrons respectively

J_L, J_B = lattice phonon flux and background photon flux respectively

Equation 17 includes a factor of 2 to include the effect of a number of excess holes equal to electrons.

III. Signal to Noise Ratios

a. Case of the Background Noise Limited Detector

The peak to peak signal can be expressed from Equation (6) in the form:

$$I_{S_{P-P}} = I_b r_R \frac{\Delta N_{SO}}{N} \tag{18}$$

where:

$I_{S_{P-P}}$ = Peak to peak signal current (see main text - Figure 2)

I_b = Bias Current

ΔN_{SO} = Number of signal carriers generated on absorbing peak to peak flux of J_{SO}.

Correspondingly, the rms background noise current (I_{BN}) can be expressed as:

$$I_{BN} = I_b r_R \frac{\sqrt{\overline{\Delta N^2}_{Noise}}}{N} \tag{19}$$

Accordingly, the peak to peak signal to RMS noise ratio is given by:

$$\frac{I_{S_{P-P}}}{I_{BN}} = \frac{\Delta N_{SO}}{\sqrt{\overline{\Delta N^2}_{Noise}}} \tag{20}$$

ΔN_S is given by Equation 8 while ΔN^2_{Noise} is given by Equation (2) in the background limited case, where $\eta_B J_B \rangle\rangle \eta_\ell J_\ell$. Accordingly, by substituting in Equation (20) the signal to noise ratio is given by:

$$\frac{I_{S_{P-P}}}{I_{BN}} = \left(\frac{\eta A}{\Delta f}\right)^{\frac{1}{2}} \cdot \frac{J_{SO}}{(J_B)^{\frac{1}{2}}} \qquad (21)$$

where $\eta_S = \eta_B$, that is the spectrum for signal and noise photons is treated as the same, so that they are absorbed and generate carriers with equal efficiency.

Note that this expression is independent of frequency because signal and noise photons generate the same response from the photoconductor, assuming that they are absorbed and generate carriers with equal efficiency. This is in accord with their being treated here as having the same spectrum (color).

b. Case of the Shot Noise Limited Detector

The peak to peak signal current was expressed in Equation (10) and shot noise in the form of Equation (15). Modifying (15) to Figure 1 leads to a signal to noise ratio given by:

$$\frac{I_{S_{P-P}}}{I_{ShN}} = \frac{\eta J_{SO} \tau}{nd} \times \frac{\sqrt{2 J_b A}}{\sqrt{f}} \cdot E \qquad (22)$$

where:

$$I_{ShN} = \sqrt{\overline{\Delta I_b^2}}$$

$$I_b = \vartheta_b A$$

$$E = 1 \Big/ \sqrt{1+(\omega\tau)^2}$$

ϑ_b = the bias current density

References for Appendix A

1. R. C. Jones, "Advances in Electronics", (Academic Press, Inc., New York, 1953).
2. R. C. Jones, J. Opt. Soc. Am. 50, 1058 (1960).
3. The photoconductive detector has also been treated in considerable detail by D. H. Roberts and B.L.H. Wilson, Brit. J. Appl. Phys. 9, 291 (1958).
4. R. L. Petritz, Proc. IRE 47, 1458 (1959).
5. J. B. Johnson, Phys. Rev. 32, 97 (1928).
6. H. Nyquist, Phys. Rev. 33, 110 (1928).
7. R. L. Petritz, Phys. Rev. 104, 1508 (1956). See also ref. 4.
8. K. M. Van Vliet, Proc. IRE 46, 1004 (1958).
9. J. J. Brophy, J. Appl. Phys. 27, 1383 (1957).
10. T. G. Maple, L. Bess and H. A. Gebbie, J. Appl. Phys. 26, 490 (1955).
11. R. L. Petritz, Proc. IRE 40, 1440 (1952).
12. J. J. Brophy and N. Rostoker, Phys. Rev. 100, 754 (1955).
13. J. J. Brophy, Phys. Rev. 106, 675 (1957).
14. L. Bess, J. Appl. Phys. 26, 1377 (1955).
15. A. U. MacRae and H. Levinstein, Phys. Rev. 119, 62 (1960).
16. J. J. Brophy, J. Appl. Phys. 27, 1383 (1956).
17. L. Bess, Phys. Rev. 103, 72 (1956).
18. J. R. Morrison, Phys. Rev. 104, 619 (1956).
19. A. Van der Ziel, Proc. IRE 46, 1019 (1958).

APPENDIX B

The Image Intensifier

This device was analyzed in reference (1), and then reappeared in a modified form in a report to ARPA. A part of the ARPA revision will be used here, with slightly modified notation for conformity with this report.

The intensifier provides a signal in the form of light output (L_s), rather than an electrical signal as from the photoconductor. Accordingly, its signal is derived from:

$$L_s = (h\nu)_{ave} \cdot \frac{\Delta N_s}{\tau} \qquad (1)$$

where:

$(h\nu)_{ave}$ is an average energy for the spectral distribution of emitted photons

L_s = light output emitted from some area A of the phosphor screen of the device

ΔN_s = number of excess electrons in the conduction band or other excited states in area A of the phosphor

τ = lifetime of electrons in that excited state

There remains the task of determining ΔN_s in a useable form, hopefully similar to that developed for the photoconductor in Appendix A.

Determination of tube performance requires that it be illuminated by some test pattern. The pattern used with the photoconductor was simply a sinusoidally modulated light source. When used with a scanner, dynamic performance would be governed by the detectors frequency response to the modulated light source. Intensifiers are areal display devices which not only are responsive to the strengths of object signals,

but also provide information on location and movement. Accordingly, although stationary test patterns are customary, more informative results can be obtained by using a traveling test pattern moving across the face of the tube, with some known velocity, v. The pattern used here will consist of light whose intensity is spatially modulated sinusoidally, since this facilitates mathematical analysis. It is described by the usual form:

$$J_s = \frac{J_{SO}}{2} e^{2\pi i \left(\frac{x}{\lambda} - \frac{t}{T_o}\right)} + \frac{J_{21}}{2} \qquad (2)$$

where λ is the wavelength of the test pattern, T_o is the period required to move a distance of one wavelength such that the wave velocity $v = \lambda/T_o$ (see Fig. 2 of the main text).

Phosphors of the simple type used here have electronic decay processes governed by a simple exponential law, such that for a quantum efficiency η,

$$\Delta N_s = \Delta N_{so} e^{-t/\tau} \qquad (3)$$

$$\text{with } \Delta N_{so} = \eta J_s$$

Therefore, the light output also decays exponentially, according to

$$L_s = L_{so} e^{-t/\tau} \qquad (4)$$

A detailed analysis of the variation in time constant when excitation and recombination occur simultaneously reveals that there is an apparent change in device time constant which can be expressed in the form:

$$\tau' = \tau/\left(1 - e^{\frac{-t_o}{\tau}}\right) \qquad (5)$$

where t_o is the time required for a wave to travel the distance across a resolution element, equal to ℓ'/v (where ℓ' is the diameter of a resolution element) (2).

Since the phosphor behavior is assumed to be governed by the same intrinsic excitation and recombination processes as the photoconductor, the equation for the photoconductor can now be modified for adaptation to the intensifier by substituting Equation (2) into Equation (7) of Appendix A and making use of Figure (2) in the main text, such that:

$$\frac{d}{dt}\Delta N_s t \frac{\Delta N_s}{\tau} = \eta G \left\{ \int_o^A \left(\frac{J_{so}}{2} \cdot e^{2\pi i\left(\frac{X}{\ell} - \frac{t}{T_o}\right)} + \frac{J_{21}}{2} \right) da \right\} \qquad (6)$$

This equation includes an integral which represents the number of carriers created by the incident flux per unit time within the area A, the efficiency of the photoemitter η and the gain of the phosphor G in creating excited carriers. This gain is a function of the accelerating potential applied to the intensifier tube and may be substantially greater than unity. Integration over a circular area leads to a solution in the form of a Bessel function, such that the equation simplifies to:

$$\frac{d}{dt}\Delta N_s + \frac{\Delta N_s}{\tau} = \frac{\eta G A}{2} \left\{ J_{so} S\, e^{\frac{-2\pi i t}{T_o}} + J_{21} \right. \qquad (7)$$

where:

$$S = J_o(z) + J_2(z); \qquad (8)$$

$z = \pi\ell/2$

ℓ = diameter of a resolution element

$J_o(z)$ and $J_2(z)$ are Bessel functions of zero and second order, respectively

as shown in Figure (1), using Schade's notation for z (3). This analysis does not include the effect of MTF from electron optics.

A point to be noted here is that the Bessel function S appears to reproduce Schade's response curve for the case of a circular aperture scanning a photon flux test bar pattern (making due allowance for our sinusoidal test pattern). His curve was developed while concerned with electron beam scanning types of image tubes and derived by other methods. It has general applicability, however, in so far as geometrical optical considerations provide limitations on the frequency response and resolution of image tubes. Nevertheless, it remains to be shown whether these optical limitations govern device performance to those to be associated with dynamic electronic processes through the time constant τ'.

The area A denoted in Equation (7) is not the area of the face of the tube, but is a small area that can be located over any region of the tubes's rear surface. In a test procedure, it can readily be defined by the size of a calibrated circular hole in a mask placed behind the intensifier's light emitting surface (Fig. 2). This permits examination of any localized region of the intensifier's surface and changing the area of the hole. The experimental apparatus needed to complete a test facility, comprises a photodetector to measure the intensifier's light output, followed by the same arrangement of equipment as used for elemental infrared photodetectors in measuring signal and noise. This type of experiment provides uniform data and allows localized determination of intensifier's performance. Information on frequency response, electro-optic distortions, granularity and constant response contours can be readily obtained. The solution to the differential Equation (7) is

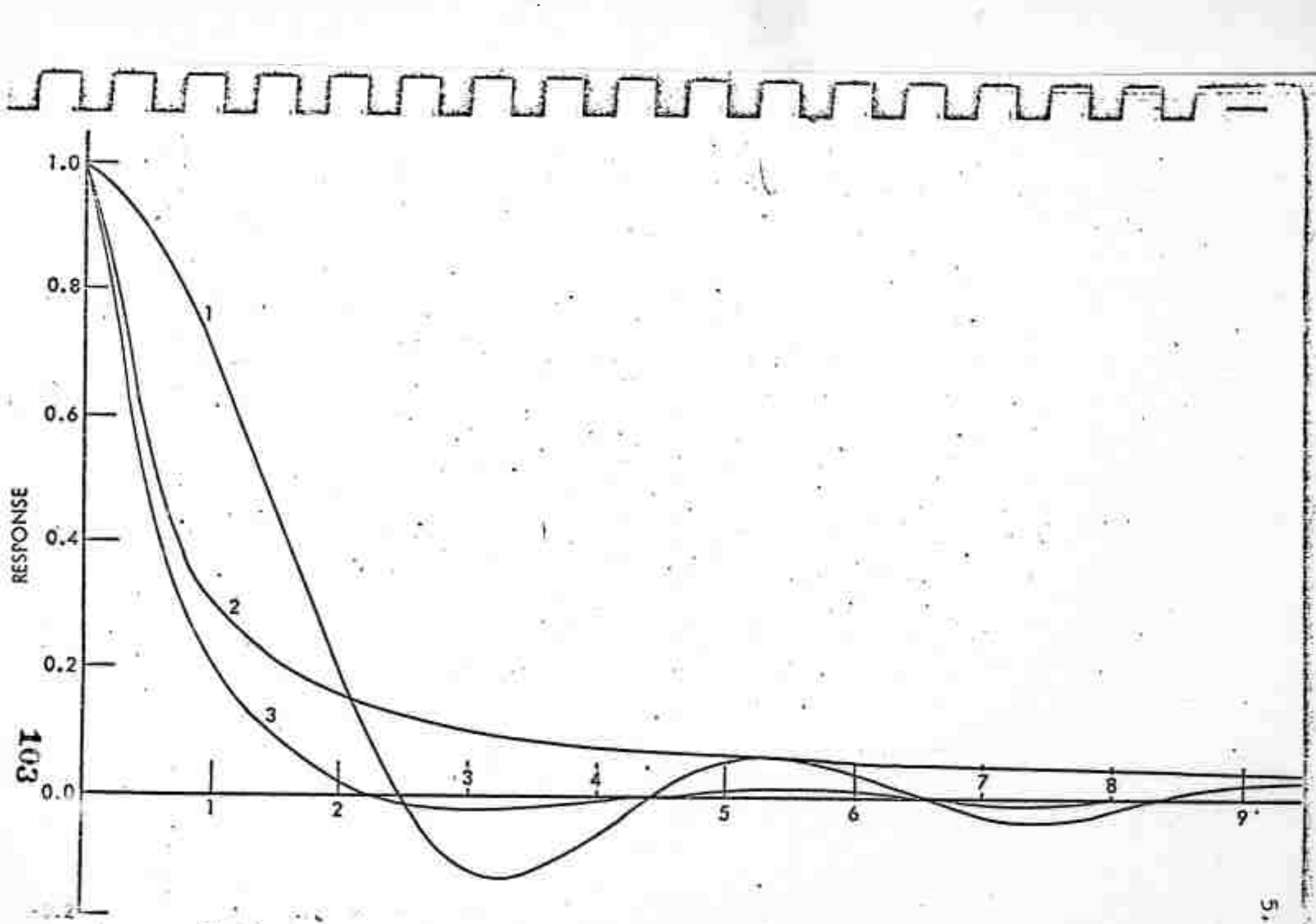

FIG. 2. Relative line number (N/N_0). (1) $S = J_0(x) + J_2(x)$. (2) $f = [1 + (2\pi l/\lambda)^2]^{-3/2}$. (3) $S \times f$. Note: N is the television line number (counting black and white). N_0 is the line number when a line width is equal to the diameter of a resolution element. $N/N_0 = (2/\pi)z = 2l/\lambda$.

$$\Delta N_s = \frac{\eta GA}{2} \left\{ J_{so} S \frac{\tau}{1-i\omega\tau} e^{-i\omega t} + \tau J_{21} + Ce^{-t/\tau} \right\} \quad (9)$$

At time t = o, we impose the condition that the total light output is maximum and given from Equ. 1 by:

$$L = (h\nu)_{ave} \cdot \frac{GA}{2} \left\{ J_{so} + J_{21} \right\} \quad (10)$$

Corresponding to the case of low spatial frequency where S = 1, $\omega\tau \ll 1$, and c = o.

The peak to peak signal light output ($L_{S_{P-P}}$) is frequency dependent, whose magnitude is given by the absolute value of the signal term, that is by:

$$L_{S_{PP}} = (h\nu)_{ave} \frac{\eta GSAJ_{so}}{\sqrt{1+(\omega\tau)^2}} \quad (11)$$

Noise Generation

Contributors to noise come from background photons, shot noise from the tube's internal electron current and generation - recombination noise from the phosphor. The tube's current can result from photoemission, thermionic emission, field emission, positive ion feedback in gassy tubes, light feedback to the photocathode from glass bombardment, corona and secondary electron emission at the phosphor surface.

Intensifiers designed for ultimate performance, sufficiently sensitive to respond to fluctuations in the incident photon stream, must first have their photoemissive current exceed the sum of all other contributors to tube current. This will ensure that the shot noise of the tube will be descriptive of the noise from the incident photon flux.

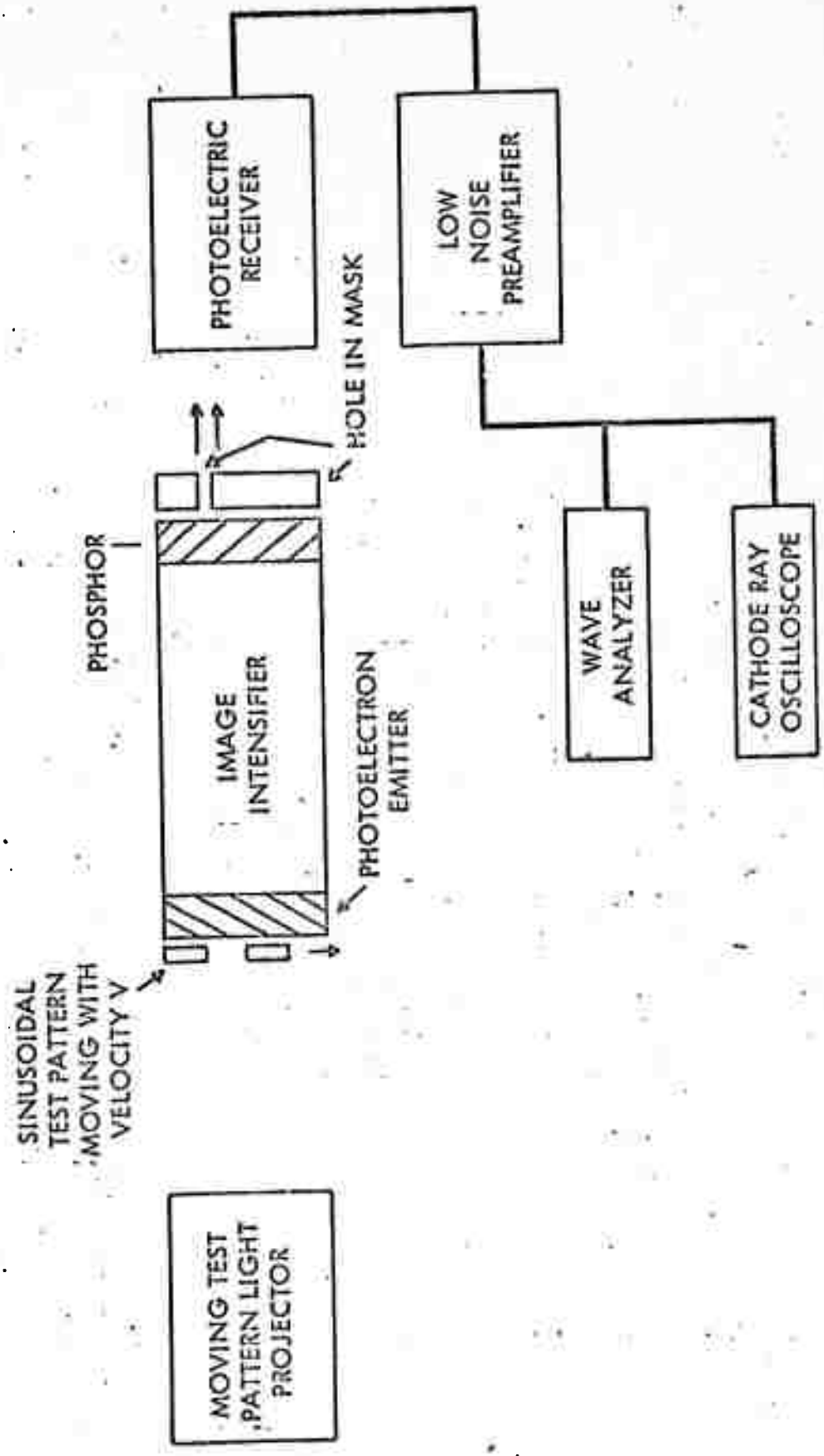

Fig. 2. Block diagram of a system to measure intensifier performance

Dark current caused by thermionic emission can be reduced by cooling the photocathode, while that resulting from field emission is lowered by reducing the acceleration voltage. Positive ion feedback is reduced by achieving a better tube vacuum, while light feedback is reduced by various forms of light shielding and proper application of absorbing black paint. Secondary electron emission noise can be appreciable, particularly in the past when transmission secondary emission electrodes are utilized between the photoemitter and the phosphor surfaces. These electrodes are designed to provide further gain by intermediate electron multiplication.

Internal secondary emission can also occur in the phosphor. Photoelectrons bombarding the phosphor target, are often given sufficient energy from the electric field to cause many more phosphor electrons to be excited to luminescence than are in the incident stream. Light amplification results, since many more photons are emitted from the phosphor layer than are absorbed at the photocathode. Due to the nature of the bombarding mechanism in the excitation process, each photoelectron will not excite exactly the same number of phosphor electrons. Rather, there will be a fluctuation about some average value which contributes to noise in the light output.

Tubes designed to be background limited must have their photoemissive shot noise dominant. They can then transform the background noise to the phosphor, where it can be measured as noise in the fluctuations from the phosphor's light output. The phosphor's light output is not likely to be influenced by any other type of current noise. It must only be kept sufficiently cool so that generation-recombination noise induced by a hot lattice does not dominate the noise from the background.

Noise in the light output when induced by background is given by:

$$L_N = (h\nu)_{ave} \sqrt{\frac{\overline{[\Delta N_N]^2}}{\tau'}} \qquad (12)$$

where $\overline{\Delta N_N^2}$ is the same quantity used for the photoconductor. The mean square fluctuation in the number of carriers has been discussed for the general case in considerable detail by Petritz[4], Van Vliet[5], Van der Ziel[6] and others. It is given by Petritz in the form

$$\overline{\Delta N^2} = \frac{4\tau^2 \cdot \Delta f \cdot A\,(\eta_B J_B + \eta_\ell J_\ell)}{1 + (\omega\tau)^2} \qquad (13)$$

where the subscript B refers to the effect of background photons. The subscript ℓ refers to lattice. $\eta_B J_B$ is meant to indicate the number of excess electrons generated in the conduction band caused by absorbing background photons flux (see Appendix A, Equation 17).

Luminescence occurs when an excited charge carrier returns to a lower energy state. The simple model utilized here involves only the recombination of an electron and a hole. Accordingly, noise in the light output is generated only during the recombination process. Equation (13) applies to the carrier fluctuation induced in the generation and recombination processes and is a factor of two larger than would prevail for luminescence. In the background limited case, the contribution from the lattice becomes negligible, and Equation (13), when applied to luminescence and now including the factor of gain reduces to

$$\overline{\Delta N^2} = \frac{2(\tau')^2 \cdot \Delta f \cdot A\eta_B G^2 J_B}{1 + (\omega\tau')^2} \qquad (14)$$

Accordingly, the noise in the light output when governed by background is obtained by substituting Equation (13) in (12) giving

$$L_{BN} = (h\nu)_{ave} G \sqrt{\frac{2A\eta_B J_B \Delta f}{1 + (\omega\tau')^2}} \qquad (15)$$

A signal to noise ratio can now be determined on dividing Equation (11) by (15), so that

$$\frac{L_S}{L_{BN}} = \frac{\Delta N_{SO}}{\sqrt{\overline{\Delta N_N^2}}} = \sqrt{\frac{\eta A}{2\Delta f}} \cdot \frac{S J_{SO}}{\sqrt{J_B}} \qquad (16)$$

assuming that $\eta = \eta_B$.

REFERENCES

1. S. Nudelman, Appl. Opt. 5, 1925 (1966).
2. Holter, Nudelman, Suits, Wolfe, Zissis, Fundamentals of Infrared Technology, MacMillan, 1962, p. 251.
3. O. H. Schade, RCA Review, Vol. 9, part II, (1948).
4. R. L. Petritz, Photoconductivity Conference, New York, Wiley, (1956).
5. K. M. van Vliet, Proc. Inst. Radio Engrs. 46, 1004 (1958).
6. A. van der Ziel, Fluctuation Phenomenon in Semiconductors, London, Butterworths, 1959.

APPENDIX C

Electron Beam - Signal Generating Scanning Devices

This device was analyzed in a paper by S. Nudelman in Applied Optics, 1, 627 (1962), and then reappeared in an extended form in an ARPA report. A part of the ARPA report will be used here with slightly modified notation for conformity with this report.

All scanning electron beam types of image tubes have two common features, that is, a surface in which an electronic image is formed and a scanning electron beam to generate the video signal. The film supporting the electronic image must have several important properties for successful signal generation. It must be highly resistive between its surface to provide storage times longer than a frame time and be sufficiently rapid in response to create an electronic surface image within a frame time. The film should be even more highly resistive in the plane of the surface to avoid lateral leakage and loss of resolution. An ideal electron beam will have a spot size less than the resolution element size inherent in the film, with all of its electrons having identical velocities and striking the surface normally. The real situation, however, presents a spot size affecting resolution and signal quality, with an inherent distribution in electron velocities which contributes to signal degradation and electrical noise. Studies of camera tube signal and noise properties have been carried out by various investigators[1,2]. The treatment here offered extends such work toward compatibility with NEP, D* and Q_D.

The vidicon will be examined here in considerable detail, since the electronic mechanisms governing its operation seem to be more complicated than for other electron beam scanning types of tubes. Results obtained for the vidicon, however, are then easily extended to other tubes. Discussions of basic mechanisms presented below are oriented toward a theoretical analysis of device performance, characterization and evaluation.

A. Device Operation - The Photoconductor

Signal and noise properties can be derived by treating a resolution element of the vidicons photosensitive surface as a simple photodetector. Reference to Figure 1 shows a schematic of this element as the capacitor C in the vidicon preamplifier circuit. Switch S is included to indicate that during the time the beam dwells on a resolution element, it charges that element to cathode potential. Thus the beam behaves like a switch which is closed during the time that the electron beam traverses the element, and is open during the remainder of a sweep period. Assume that the element has just been charged, that the switch is opened, and discharge begins. This discharge results from thermally generated carriers, photoexcited carriers and dielectric relaxation. During the open switch time, this discharging affects only the voltage drop across C, and does not affect that drop across R_L. As a result, the preamplifier does not respond to the discharging process.

Assume now that the condenser C has been discharged to some extent during the frame time T', whereupon the electron

beam reappears and replaces the lost electrons during the resolution element dwell time τ. This deposition constitutes an instantaneous current (i) through C (via capacitive coupling), resulting in a voltage drop iR_L, which is subsequently enhanced by the preamplifier-amplifier electronics that follow C_c. This voltage drop (iR_L) is made up then basically of three components; namely, signal resulting from photo-absorption, electrical noise from various sources, and some small discharge associated with the properties discussed above. Our theoretical treatment will deal with signal and noise generation in considerable detail. It will not be concerned, however, with the small discharge, and essentially assumes that this effect can be minimized from the vidicon's output through a properly designed electronic system.

Various models exist that help explain transfer characteristics of vidicons. A model is proposed below which depends on the exponential manner of photon absorption, recombination rate of carriers through the film. It attempts to help our understanding of factors contributing to the device "gamma" and to lead into device theory that follows.

Reference to Figure 1 shows an element assumed to be an intrinsic p type semiconductor ($\mu_p \rangle\rangle \mu_n$) supporting an electron charge across its back surface (sprayed on by the electron beam) and arranged so that its front surface is illuminated by incident radiation. Photons absorbed create electron-hole pairs, which separate under the influence of the field and drift toward the front and rear surfaces respectively. Holes generated within the surface layer rather than at the front surface will

require less time to reach the rear. Once the holes arrive at the rear, recombination with surface electrons occurs leaving an equivalent positive surface charge.

Three efficiency factors govern the success of the process described above. They are the following:

1. Efficiency of hole generation through photon absorption.

The number of carriers generated is taken proportional to the number of photons illuminating the device, or

$$P = \eta J_o \qquad (1)$$

where J_o = the number of photons illuminating the photoconductor per second per unit area (after reflection losses).

P = the number of holes generated per second per unit area by the absorption of J_o photons

η = the efficiency factor for photon to hole carrier conversion.

2. Loss of holes through bulk recombination

Vidicons exhibit a power law relationship between their output signal and irradiance. Thus

$$I_s = BH^{\gamma} \qquad (2)$$

or

$$\ell_n I_s = \gamma \ \ell nH + \ell nB$$

where B is a constant.

The dynamic range of the device is that range over which the slope (γ) of the log plot of I_s vs. H remains essentially constant. Maximum signal is derived for a gamma of unity. Orthicons often show gammas approaching one, while vidicons have always been considerably less than one.

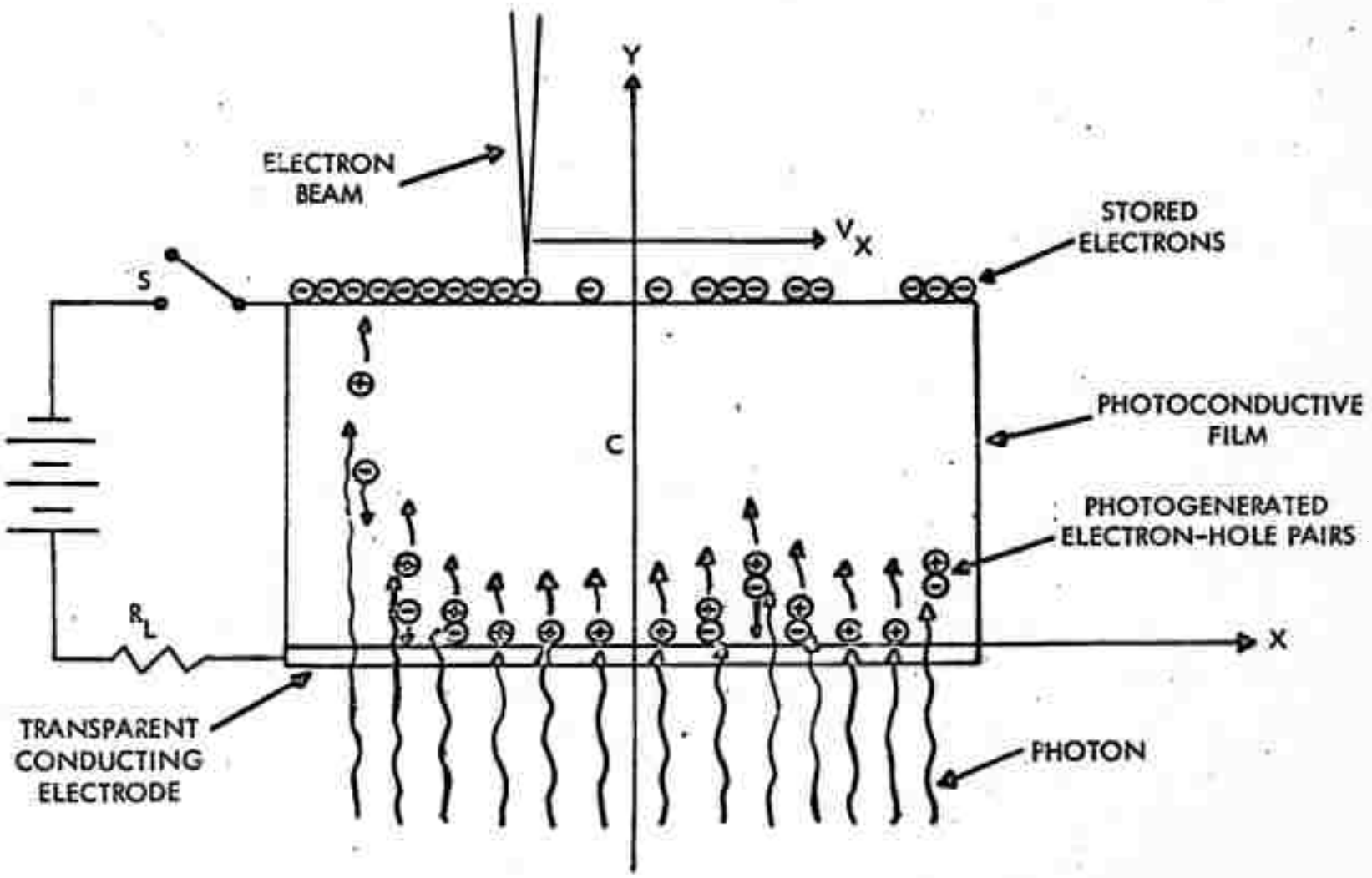

Fig. 1. Schematic of photoconductor film exhibiting carrier model for signal generation

Signal current will be shown in a later section to be directly proportional to hole generation, while the photon flux density can be linearly related to the irradiance by $H = (h\nu)_{ave} J_o$, where $(h\nu)_{ave}$ is an averaged photon energy. Equation (2), when compared with (1), indicates that some photogenerated holes must be lost before they are able to reach the rear surface and recombine with stored electrons. The exact mechanism responsible for this loss has yet to be precisely established. However, it seems reasonably safe to associate this loss with electron-hole recombinations that occur rapidly (compared to bulk recombination rate), most frequenctly at the front surface, and to a decreasing extent with distance from the front surface.

Two recombination mechanisms will be described here that appear applicable to vidicon photoconductors. There undoubtedly are others. The first makes use of the exponential manner in which light is absorbed by a medium, that is

$$J = J_o e^{-\alpha y} \qquad (3)$$

where α is the absorption coefficient.

From Equation (2) it is clear that the concentration of holes would follow a similar exponential behavior, being greatest at the front surface. When dealing with near intrinsic material, and for hole densities appreciable compared to intrinsic carrier densities, a recombination lifetime exists which is considerably less than that for the base material. Thus the shortest recombination lifetime would exist at the front surface, increasing with distance into the film until the normal lifetime for the

basic material prevails. Another means for achieving shorter lifetimes is through surface states. Such states are commonly described in semiconductor devices, and are associated with impurities, crystallographic flaws and surface layers of various kinds. These states provide recombination centers, which permit a more rapid recombination rate than characteristic of the bulk material, and can result in significant losses of holes.

A meaningful association between holes and photon flux can be developed from the differential form of Equation (3):

$$\frac{dJ}{J} = \alpha dy$$

which is the statement that layers of equal thickness absorb equal fractions of the incident photons. The hole distribution can be taken proportional to the photon distribution, so that

$$\frac{dP}{p} = \gamma \frac{dJ}{J} - \alpha\gamma dy \qquad (4)$$

Integration Equation

$$\ell n\, P = \ell n\, J^{\gamma} + D$$

and

$$P = cJ^{\gamma} \qquad (5)$$

where D is an arbitrary constant. In view of Equation (1) prevailing when $\gamma = 1$, clearly $c = \eta$. Assuming the vidicon film sufficiently thick to absorb all photons, J can be taken as the incident photon flux J_o and P becomes the number of holes per unit area that survive and reach the rear surface of the film. The distribution of holes from Equation (4) is given by

$$P = P_o\, e^{-\alpha\gamma y}$$

The effect of $\gamma < 1$ is to flatten the exponential distribution, which is consistent with the mechanisms proposed above, whereby most holes are lost at the front surface.

3. Loss of holes associated with carrier transport

Holes must be able to move from the front to the rear surface within a time less than a frame period. Any longer time will cause what is referred to as photoconductive lag, wherein smearing of an image results. Thus, information carried by holes appears at the rear surface more than one frame period after its receipt, resulting in loss of information, particularly in regard to moving objects. This effect is denoted by the factor η_T.

4. Summary

The number of holes per unit area reaching the rear surface is given by

$$P = \eta\eta_T J_o^{\gamma} = \eta' J_o^{\gamma} \qquad (6)$$

where $\eta' = \eta\eta_T$ is a combined efficiency factor.

B. Signal Generation

The signal is from pick-up tubes is developed when electrons discharged during a raster period are replaced by the electron beam, in the time that the beam takes to pass over a resolution element. Accordingly,,

$$I_s = q \frac{N_o - N}{\tau} \qquad (7)$$

where N_o is the full number of electronic charges stored on the rear surface within a resolution element.

N is the number remaining after discharge of holes, during a frame time period.

τ is the dwell time of the beam on a resolution element. Determination of tube performance requires that it be illuminated by some test pattern. The photoconductor required simply a sinusoidally modulated light source. For an areal device such as the intensifier tube, we used a traveling test pattern moving across the face of the tube with velocity v (see Appendix B). It consisted of light whose intensity was modulated sinusoidally rather than the bar patterns of TV. An identical test pattern will be used for the vidicon as for the intensifier, excepting that it will remain motionless, in accordance with the suggestion of Coltman[8].

The electron beam has the dual function of scanning the charged surface and of replacing missing electrons. Accordingly, it must be described by a function which is dependent on position and time. The rate at which such a function changes with time is given by

$$\frac{dF}{dt} = \frac{\partial F}{\partial x} \cdot \frac{dx}{dt} + \frac{\partial F}{\partial t} \qquad (8)$$

The beams value as a function of position depends upon the test pattern, given as

$$J = \frac{Jso}{2} e^{2\pi ix/\lambda} + \frac{J_{12}}{2} \qquad (9)$$

where λ is the spatial wavelength, in accordance with Fig. 2 of the main text. Electrons discharged during a frame time T' within

a circular resolution element of area r, are then evaluated from

$$\eta T' \int_o^r \left\{ \left(\frac{J_{SO}}{2} \right)^\gamma e^{2\pi i \frac{x}{\lambda}} + \left(\frac{J_{21}}{2} \right)^\gamma \right\} da \qquad (10)$$

However, the electron beam scanning across the sinusoidal charge distribution responds in signal generation as though it sees a sinusoidal traveling wave of electrons moving past with a velocity. Accordingly, relative to the charge distribution, the electron beam should be characterized by the traveling wave form, such that

$$F' = \eta T' \int_o^r \left\{ \left(\frac{J_{SO}}{2} \right)^\gamma e^{2\pi i \left(\frac{x}{\lambda} - \frac{t}{T_o} \right)} + \left(\frac{J_{21}}{2} \right)^\gamma \right\} da \qquad (11)$$

Integration of Equation (11) has already been carried out for the intensifier,

$$F' = \frac{\eta r T'}{2^\gamma} \left\{ J_{SO}^\gamma S e^{-\frac{2\pi i t}{T_o}} + J_{21}^\gamma \right\} \qquad (12)$$

where S is the sum of two Bessel functions

$$= J_o(z) + J_2(z) \qquad (13)$$

and $z = r\ell'/\lambda$

ℓ' = diameter of resolution element.

For $\ell' \ll \lambda$, S = ; while for ℓ' in the order of or larger than λ, the factor S becomes smaller and then oscillates in the manner typical of Bessel functions.

This analysis can be treated as applicable to a circular resolution element whose cross section is that of the electron beam focused at the photoconductor's rear surface. Actually,

the electrons streaming through this cross section are generally assumed not to be uniform in their distribution, and the current density is peaked at the center, and falls off radially. This effect has been approximated by a cosine square factor having rotational symmetry[4]. Its effect can be included in this analysis by introducing it as a factor in the signal term of Equation (11). That is

$$\eta T' \left(\frac{J_{S0}}{2}\right)^{\gamma} \left[\int_0^r e^{2\pi i \left(\frac{x}{\lambda} - \frac{t}{T_o}\right)} \cos^2\phi \, da + \int_0^r \cos^2\phi \, da \right] \qquad (14)$$

Integration of this expression results in the solution

$$F'' = \eta' \left(\frac{J_{S0}}{2}\right)^{\gamma} T' r \left[\frac{S_1 e^{-2\pi i t/T_o}}{2} + 0.2\right] \qquad (15)$$

where S_1 is the sum of four Bessel functions

$$= \frac{1}{2} \left[J_o(z_1) + J_o(z_2) + J_2(z_1) + J_2(z_2)\right]$$

$$z_1 = \pi \ell'/\lambda$$
$$z_2 = \pi \left[\frac{\ell'}{\lambda} - 1\right] \qquad (16)$$

Plots of S and $S_1/2$ are shown Figure 2 of this appendix using Schade's notation for z. Our curves essentially reproduce his results for the circular and cosine square apertures which he obtained by different methods (making proper allowance for the sinusoidal test pattern used here). Clearly there is a distinct improvement in frequency response brought on by introducing the cosine square factor.

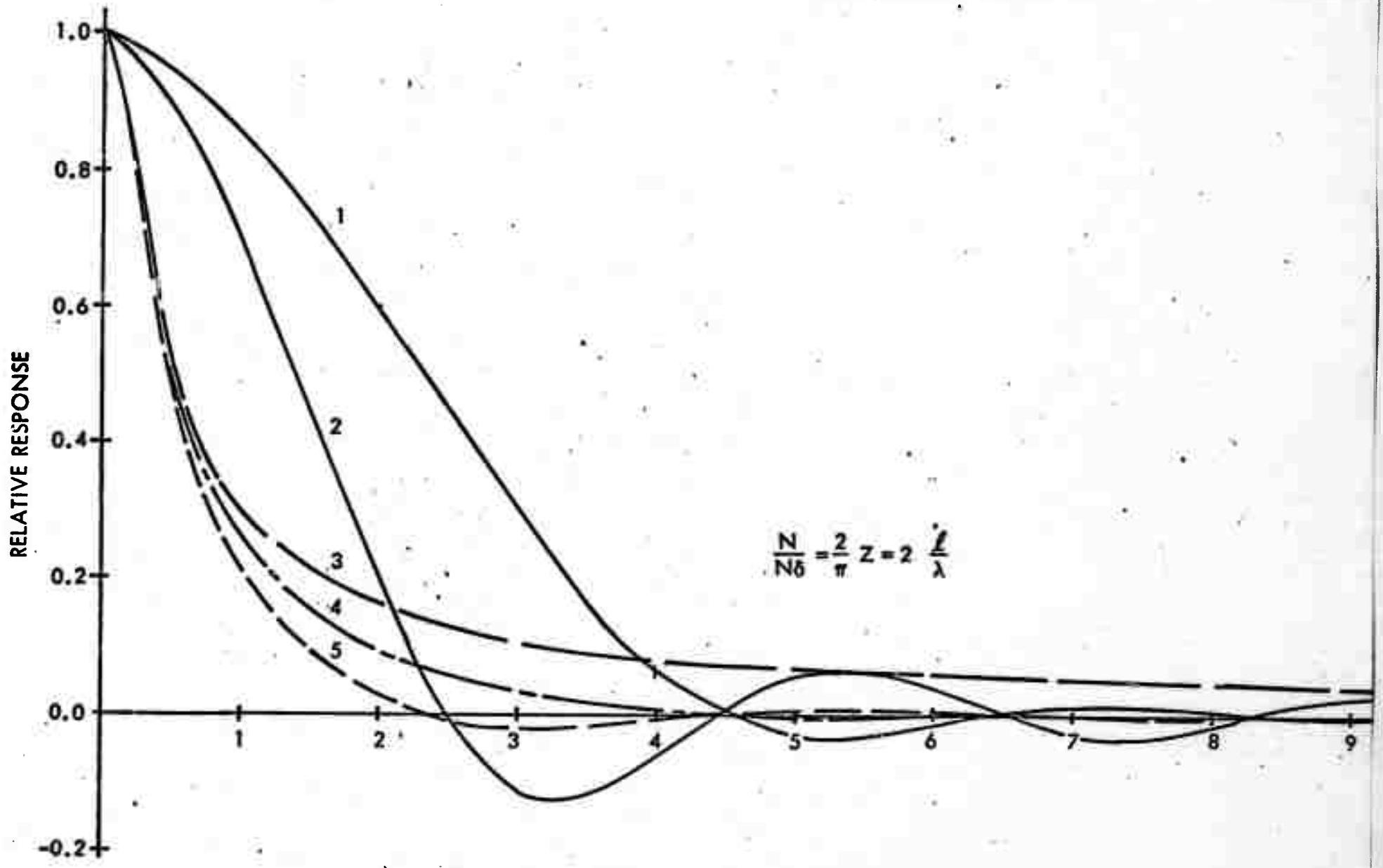

Fig. 2. Relative line number ($N/N\delta$). 1. $S_1 = \frac{1}{2}[J_0(z_1) + J_2(z_1) + J_0(z_2) - J_2(z_2)]$. 2. $S = J_0(z) + J_1(z)$. 3. $E = [1 + (\pi N/N\delta)^2]^{-1/2}$. 4. $S_1 \times E$. 5. $S \times E$. Note: N is the television line number (counting black and white). $N\delta$ is the line number when a line width is equal to the diameter of a resolution element.

In the case of the circular aperture, the number of missing electrons returned by the beam per unit length is given by

$$\frac{\partial F}{\partial x} = \frac{F'}{\ell'} \tag{17}$$

and the velocity of scan $v_o = \frac{dx}{dt}$ (18)

Furthermore, since electrons are replaced within a time τ.

$$\frac{\partial F}{\partial t} = \frac{N_o - N}{\tau} \tag{19}$$

Substituting Equations (17), (18) and (19) into Equation (8), and rearranging, gives:

$$\frac{d}{dt}(N_o - N) + \frac{N_o - N}{\tau} = \frac{\eta' r T' v}{2^{\gamma} \ell'} \left[J_{SO}^{\gamma} e^{-\frac{2\pi i t}{T_o}} + J_{21}^{\gamma} \right] \tag{20}$$

which is an equation identical in form to those derived for the photoconductor and the intensifier. It has the solution:

$$N_o - N = \eta' \left(\frac{J_{SO}}{2}\right)^{\gamma} r T' \left\{ \frac{S e^{-\frac{2\pi i t}{T_o}}}{1 - i\omega\tau} \right\} + \eta' r \left(\frac{J_{21}}{2}\right)^{\gamma} T' + C' \eta' Y \left(\frac{J_{SO}}{2}\right)^{\gamma} T' e^{-t/\tau} \tag{21}$$

At time t=o, we assume the condition that the total charge generated is maximum and given from Equation (21) by:

$$N_o - N = \eta' \left(\frac{J_{SO}}{2}\right)^{\gamma} r T' + \eta' \left(\frac{J_{21}}{2}\right)^{\gamma} r T' \tag{22}$$

corresponding to the case of low spatial frequency where S = 1, $\omega\tau \ll 1$, and c' = o. Consequently, the peak to peak signal is developed from the real part of the periodic term and found to be:

$$I_{S_{PP}} = q\,\frac{N_o - N}{\tau} = \eta' q\, J_{SO}^{\gamma}\, r\,\frac{T'}{\tau}\cdot\frac{S}{\sqrt{1+\omega^2\tau^2}} \qquad (23)$$

The area of the vidicon surface is given by:

$$A = r\,\frac{T'}{\tau} = r\,M \qquad (24)$$

where M is the number of resolution elements. Accordingly,

$$I_{S_{PP}} = \frac{\eta' q J_{SO}^{\gamma}\cdot rMS}{\sqrt{1+(\omega\tau)^2}} = \frac{i_s MS}{\sqrt{1+(\omega\tau)^2}} \qquad (25)$$

Note that J_{SO} represents the peak to peak value of incident signal flux as used in DQE, whereas $J_{SO}/2$ is the peak value as used in MTF. The quantity $\eta' q(\frac{J_{SO}}{2})^{\gamma}r = i_s$ represents the normal peak current flow expected from a resolution element without storage. The factor $\frac{T'}{\tau}$ provides enhanced signal through charge storage.

Signal response expressed in the form

$$I_{S_{P-P}} = \frac{\eta' q\, J_{SO}^{\gamma}\, rMS}{\sqrt{1+(2\pi\,\frac{\ell'}{\lambda})^2}} \qquad (26)$$

is useful for delineating the influence of aperture from electronic effects. It is obtained from Equation (25) making use of

$$\omega = 2\pi f = 2\pi n v = \frac{2\pi}{\lambda}\,v \qquad (27)$$

where n = the number of test waves per unit length

λ = the wavelength = 1/n

v = scan velocity = ℓ'/τ

In the case of the cosine squared aperture the corresponding signal expression is:

$$I_{S_{P-P}} = \frac{\eta' q \, J_{SO}^{\gamma} \, rMS_1}{\sqrt{1+(2\pi \frac{\ell'}{\lambda})^2}} \qquad (28)$$

Notice that this case not only contains the factor S_1 rather than S, but that the effective resolution element area is reduced by one half, as a factor governing signal.

C. Gain is another factor which needs discussion. It appears through:

1. The addition of an intensifier before the signal generating tube.
2. The introduction of a suitable target in tubes such as the image orthicon and isocon, SEC and most recently high gain silicon (SEBIR) tubes.
3. Electron multipliers in return beam tubes.

The first two devices provide gain with a minimum of bandwidth, corresponding usually to matching the response time of the human and TV raster periods, respectively, while the third is wide band matching the video requirements imposed by the readout beam in the signal generating process.

Selection of the type of gain device needed depends upon the nature of the requirement. For example, a low light level device needing to be background light limited could use an intensifier, followed by a silicon target. Sufficient gain here would ensure that the noise associated with background photons

would predominate over any noise introduced by the coupling network and/or the preamplifier.

The vidicon used heretofore as our model does not normally provide any device for gain. Gain can and has been introduced however by addition of the return beam multiplier[4]. When gain is included, the signal is simply enhanced by that factor, so that Equation (25) can be rewritten in the form:

$$I_{S_{PP}} = \eta' q \, J_{SO}^{\gamma} \, GrMSE \qquad (29)$$

where:

G = gain

E = $1/\sqrt{1+(\omega\tau)^2}$ and is called the electronic function

$I_{S_{PP}}$ = peak to peak value of signal

= $2 I_{S_P}$

Noise and Signal to Noise Ratios

We shall examine analytically the effects of noise from the background, beam current (shot) and Johnson sources on signal to noise ratios. They serve to illustrate properties in common as well as their different effects particularly on frequency dependence. Noise from the environment for infrared sensitive tubes and from the lattice (generation-recombination) affect device output similar to background noise. Further, if noise in signal followed Poissonian statistics, it too could be treated in a manner similar to background.

Gain was discussed briefly with respect to Equation (29). Its importance can be appreciated more fully when one examines its impact on noise. In the background noise limiting case where photon induced noise predominates, gain is applied equally to the signal and background (noise) photons, so that it cancels and does not appear in the signal to noise ratio. The opposite occurs when the noise limiting device performance arises in the coupling network, or the preamplifier, and gain only affects signal. There is also an intermediate case, when one wants to improve on device performance by making use of a return beam multiplier. This device adds additional gain not only to signal, but also to the shot noise from the scanning electron beam. It is a profitable procedure up to the point where beam shot noise exceeds preamplifier or coupling network noise (Johnson). These comments are pertinent to the signal to noise ratios derived below.

1. Background Noise current (I_{BN}) can be obtained from Equations (14) and (21) of Appendix B. One should note that Equation (14) was used for the recombination process necessary for luminescence. Here it applies to the generation process responsible for hole production and associated conductivity. Making use of Equation 14 in Appendix A, in conjunction with Equations 23, 25 and 29, it is possible to arrive at the RMS value of the background noise, as:

$$I_{BN} = qG \frac{\sqrt{2\eta A \Delta f \, J_B^{\gamma}}}{\sqrt{1+(\omega\tau)^2}} \qquad (30)$$

Accordingly, using the peak to peak signal obtained from Equation (29) and the RMS noise from Equation (29), the signal to noise ratio becomes:

$$\frac{I_{S_{PP}}}{I_{BN}} = \left(\frac{\eta r T}{2\tau \Delta f} \right)^{\frac{1}{2}} \cdot \left(\frac{J_{SO}^{\gamma}}{\sqrt{J_B}} \right) \cdot S \qquad (31)$$

where I_{BN} = RMS value of noise current induced by background photons.

2. Johnson Noise limited photoelectronic imaging devices is generated in either the load resistor, coupling network and/or the preamplifier. When purely resistive, it can be expressed in the form:

$$I_{JN} = \sqrt{\frac{4kT\Delta f}{R}} \qquad (32)$$

where R is the effective resistance. However, because of the various sources possible for generating Johnson noise, it will be sufficient to express it here in the general form:

$$I_{JN} = \sqrt{\mathcal{J}_{jn} \cdot \Delta f} \tag{33}$$

where $\mathcal{J}_{JN}$ = the mean square fluctuation in current per unit bandwidth caused by the Johnson noise.

Gain from intensifiers, target or return beam multipliers does not apply here, so that the signal to noise ratio derived from Equation (29) and (33) becomes:

$$\frac{I_{S_{PP}}}{I_{JN}} = \frac{\eta r T G q}{\sqrt{2\tau\Delta f}} \left(\frac{2}{\tau}\right)^{\frac{1}{2}} \frac{J_{SO}^{\gamma}}{\sqrt{\mathcal{J}_{JN}}} \cdot \mathcal{E} \tag{34}$$

3. Beam Shot Noise Limited - This source of noise is inherent in electron current flow, and denoted by:

$$I_{ShN} = \sqrt{2qI_b\Delta f} \tag{35}$$

where I_b = beam current (mean value). Most often this type of noise limiting condition prevails when a return beam multiplier is incorporated in the tube providing sufficient gain to ensure that shot noise predominates over Johnson noise. Once this condition is met, the maximum signal to noise ratio is achieved. Further gain raises signal and shot noise to the same extent,

so that there is no further improvement in their ratio. Accordingly, we will use Equation (29) for signal and (35) for noise to calculate:

$$\frac{I_{S_{PP}}}{I_{ShN}} = \frac{\eta r T G}{\sqrt{2\tau\Delta f}} \cdot \left(\frac{q}{\tau}\right)^{\frac{1}{2}} \cdot \frac{J_{SO}^{\gamma}}{\sqrt{I_b}} \cdot gE \qquad (36)$$

References - Appendix C

1. R. Thiele, Advances in Electronics and Electron Physics, New York, Academic Press, Vol. 12, 1960, p. 263.
2. E. F. DeHaan, Reference 1, p. 277.
3. J. W. Coltman, J. Opt. Soc. Amer. 44, 468, 1954.
4. O. H. Schade, RCA Review, Vol. 9, part II, 1948.

APPENDIX D

I. Introduction

Of considerable concern is a determination of how best to evaluate and specify the performance of image tubes. In particular, examination of current procedures reveals serious problems related to the accuracy of measuring output video signal and noise, as well as that imposed by intermediate optics for measuring input photon flux from signal and noise sources. For high light level conditions, accuracy in measurements tends not to be a serious matter. However, for low light level conditions where one wishes to know how much useful information is transmitted by the device, regardless of the source of limiting noise, the accuracy of measurements and the manner of presenting information relevant to device performance becomes increasingly important.

The current procedure used in industry is described by Miller[1]. The essence of the procedure is to generate a video square wave signal from a bar test pattern which is displayed on a line selector A-scope. "The output signal voltage is measured between the average voltage fluctuations of the video base line and the average voltage fluctuations at the top of the pulse. The noise voltage is measured without an input signal on the camera tube". It is accomplished by judging the width of the grass envelope displayed and dividing this value by six to obtain an estimate of the RMS value. The purpose of our program is to improve on

these measurements. In general, the following ideals comprise our goals:

1. Precise measurements of RMS noise, particularly noise in signal under noise limited conditions
2. Precise measurements of peak to peak signals (square wave) as a function of spatial frequency
3. Signal and noise spectra in terms of sinusoidal response
4. Calculate signal to noise ratios from steps 1 and 2 above, and similarly in step 3
5. Calculate the detective quantum efficiency as a function of spatial frequency.

The instrumentation for steps 1 and 2 can be relatively simple and inexpensive and suited to the small laboratory. Our approach to step 3 utilizes a computer and represents a much more substantial experimental effort. The approaches used in steps 1 and 2 are described in II below, while that to be used for steps 3 to 5 will be summarized in III.

The core of the test system is a Westinghouse tube test facility which uses a line selector A-scope type of presentation. Sampling instrumentation has been added for the determination of signal and noise as described in steps 1 and 2 above, in particular a box car integrator and sampling oscilloscope. To meet the requirements of steps 3, 4 and 5, the test facility has been interfaced to a PDP-9 computer graphics facility by a PEP storage terminal for line scan conversion and an HS-703 Computer Labs A/D (analog to digital) converter.

II. Analog P-P Signal and RMS Noise Measurements

The device used for measuring peak to peak signal is a box car

integrator (2,3). It is comparable to a lock-in-amplifier, but operates in the time rather than the frequency domain. The purpose of this instrument is to provide a noise free recorder trace of the signal waveform, particularly in noise limiting conditions where the A-scope measurement becomes inaccurate. Its operation is described in Section 1 below. Corresponding to this improvement in measuring signal however, is a loss of ability to measure the reduced noise. Measurement of noise requires a different repetitive sampling and integration technique which is the subject of Section 2.

1. Signal Recovery with a Box Car Integrator

A simplified block diagram is shown in Fig. 1a. A repetitive input signal is required, which need not necessarily be periodic. The input waveform is sampled at the repetition frequency. A trigger is provided to the "box car" in the "same manner that would be required for good high speed oscillographic reproduction, while the noise is random in nature. The gate interval Δt represents an (on time) of an electronic switch, during which the signal and noise voltage is fed directly into an integrator. By sampling successive intervals and averaging, it is possible to reduce the noise-voltage fluctuation observed at the integrator output without affecting the signal level. Quantitatively, the noise-voltage fluctuations are reduced by $1/\sqrt{N}$, where N is the number of observations made during an average measurement. The signal to noise voltage ratio is then improved by the square root of N. If Δt is made small compared to the signal transient time, and is slowly and uniformly retarded in time with respect to signal onset,

an accurate chart record of the signal wave shape may be produced".[3]

The box car integrator used was a PAR Model 160, manufactured by Princeton Applied Research. This instrument provides an adjustable sampling gate width and a capability of positioning the sampling gate anywhere on the signal waveform. In addition, it provides considerable flexibility for regulating the rate at which the gate scans across the signal waveform.

The Model 160 utilizes RC type circuits to achieve integration and time constants which are adjustable in steps from 3 nanoseconds to 100 seconds. The time constant used is important because it will, along with the sampling gate aperture, determine the improvement in signal to noise obtainable and also experiment time required to recover a point or waveform.

The system utilizing the "box car integrator" is shown in Fig. 1b. In practice, the user views the test pattern displayed on the "test set" monitor. He positions a horizontal strobe line on the monitor, so that it crosses the part of the test pattern to be measured. The strobe line is obtained by delaying the vertical sync scan pulse with a continuously variable delay circuit. The video signal in the raster line selected by the positioning of the strobe line is then viewed on the A-scope.

The strobe trigger is also used to trigger the time base and sampling gate of the box car integrator. The trigger to the sampling gate is, of course, delayed again by the box car to allow positioning anywhere on the line being viewed on the A-scope.

This method for measurement of P-P signal, which is illustrated

in Fig. 2, was compared to that using the "box car" approach. Fig. 2 shows an A-scope presentation taken with a typical Polaroid exposure. This exposure is then used by making a visual measurement between the centers of the average noise envelopes at the minimum-maximum levels.

Fig. 3 shows the results obtainable with the box car for comparison with signal on the A-scope in Fig. 2 at 300 and 400 TV lines.

Measurements made using the box car integrator at high signal levels and low spatial frequency differed only slightly from those made using the conventional technique under the same conditions. However, the box car integrator does show remarkable improvement over the conventional method at high spatial frequency and low light levels where noise limiting conditions dominate.

Because the box car integrator is capable of extracting waveforms at spatial frequencies approaching resolution limits (corresponding to small signals buried in noise), it will also be useful as a tool for analysis of signal shapes leading to a better understanding of the electronic mechanisms involved in signal generation.

2a. RMS Noise Measuring Technique (Analog)

The discussion that follows describes a precise, non-subjective method for measuring the RMS magnitude of a non-synchronous waveform (noise) added to a synchronous input waveform (video signal). Its successful operation requires only that the input waveform be stationary and repetitive. Sampling techniques are used which provide wide bandwidth (12.4 GHz), good accuracy, a maximum data accumulation rate of 3600 samples/minute and which make no requirements on the type of statistics governing noise or of the shape of the sampled waveform.

The principal method currently used for measuring noise is that standardized by the IRE and described in the introduction[1]. An improvement on the above, developed by Jensen and Fawcett[4] at Westinghouse, made use of a clamping circuit to remove blanking pulses from the video signal. Then, assuming uniform target and input irradiance, this signal was fed to a standard RMS voltmeter, the output of which was corrected for duty factor.

We have attempted to improve on the above methods by developing a technique in which the only requirement is that the test pattern be stationary for one half of a minute. The sampling technique used here is directly analogous to the familiar stroboscopic technique used with rotating machinery where a dynamic phenomenon is made to apparently stand still by looking at it only when it is in the same position each time. The signal portion of the video output which is synchronized with the sampling strobe corresponds to a rotating shaft in the above analogy, while bearing chatter would be an analogous example of noise. Since the signal appears in the same position each time, it will appear as a constant level superimposed on which are added the fluctuations caused by noise. Sampling gate time is very short ($\approx 10^{-11}$ sec) compared to the highest frequencies encountered ($\approx$ 12 MHz), so that we can consider the sampled voltage as the instantaneous value of signal plus noise at that time. From these samples we can construct an ensemble of voltages, the RMS value of which is given by:

$$\sigma = \left[\frac{1}{N} \sum_{i=1}^{N} (X_i - \overline{X}) \right]^{\frac{1}{2}} \qquad (1)$$

where X_i equals signal s(t) plus noise n(t) at each sample time and $\overline{X}$ is the signal s(t).

By instrumental design the signal level can become the reference level and adjusted to a zero voltage level (discussed below). Thus, the noise expression becomes:

$$\sigma = \left[\frac{1}{N} \sum_{i=1}^{N} n_i(t)^2 \right]^{\frac{1}{2}} \qquad (2)$$

where $n_i(t)$ is the sample $X_i - \overline{X}$ from frame i.
The solution of the above equation was first accomplished with analog and then digital computer type circuitry, which are described below.

The analog circuitry is depicted by the steady state block diagram of Fig. 4. The heart of this noise measuring system is a Hewlett Packard 1400 series sampling oscilloscope. It is a dual trace 12.4 GHz scope with delayed sweep time base, chart recorder output and manual positioning of the sampling point which makes the oscilloscope very attractive for this application.

The scope acts as the sample and hold circuit shown in Fig. 4, providing an output voltage which is held for one sixtieth of a second (one field period). Since the gain of the oscilloscope from input to output is one half, an amplifier was required to obtain an overall gain of unity. The amplifier output is then fed to a squaring device (PAR 230) every time a sample is taken. Since statistical variations about the video signal are sought, the signal level is adjusted to zero. This is accomplished by positioning the trace on the scope so that the average variation of the waveform about the zero volt level is zero. Circuitry for this purpose is described below.

A trigger signal corresponding to a selected raster line is obtained from the camera tube test set and is used to trigger simultaneously the oscilloscope and a counting circuit. This counting circuit controls a gate which controls the input to an integrator. Through the gate is fed the output of the squaring device. The time constant of the integrator is chosen so that if the integrator gate is enabled for 2000 one-sixtieth of a second samples, the output of the integrator will correspond to the mean sum of its input waveform. Since the input waveform was the instantaneous noise levels squared, we now have the mean squared value at the integrator output.

The RMS value is obtained by applying the output from the integrator to a device which takes the square root and then displaying the results on a digital voltmeter.

To remove the uncertainty in positioning the trace on the scope and to compensate for slow DC drift of the pedestal, a circuit was added which generates an error signal proportional to the mean of the input waveform by summing the output of the oscilloscope. Since any DC level which appears represents a shift of the trace from zero mean, this error voltage is subtracted from the video input voltage. This is easily accomplished by feeding the video signal into Channel A of the scope, the offset into Channel B and subtracting the two in the scope.

The limiting accuracy of this analog system is about 4°/o. Thus the smallest signal detectable through 6.5 nanoamperes of noise is about 2.4 nA.

2b. RMS Noise Measurement Technique (Digital)

To measure RMS noise by digital means, the sampling oscilloscope has been interfaced with the University's PDP-9 Computer Graphic Facility which is equipped with an A/D converter. This system is much simpler in hardware, the only components being the scope, computer and a low frequency buffer amplifier to match the scope output to the A/D input. Equation (1) can be rewritten as:

$$\sigma^2 = \overline{X^2} - \overline{X}^2 \qquad (3)$$

by expanding the parenthetical expression and combining terms. The computer A/D converts 2000 samples and stores them in successive locations in memory. Then $\overline{X^2}$, $\overline{X}^2$ and finally σ are calculated and the RMS value is printed out. There are several advantages to this method.

a) The A to D converter is very accurate (.025%).

b) There is no necessity for positioning the trace to zero on the scope screen or being concerned about D.C. levels or slow drifts which were a problem in the analog system, since any D.C. level appears in $\overline{X}$ and its effects are eliminated mathematically.

c) Fewer demands are made upon the sampling oscilloscope perhaps permitting use of one that would be less expensive.

d) The sampling rate is variable giving a choice of sampling every frame or every field, as is N, the number of samples taken.

e) The calculated $\overline{X}$ represents the signal level plus a constant at a point on the waveform. A measurement is first made at a point on the waveform (S_I+C) and then at a point on a bar (S_D+C),

where S_I is the signal at an illuminated portion of the photocathode, S_D is the signal from a dark portion and C is a constant. When the difference is formed, the constant falls out and we are left with the peak to peak signal.

f) The amplitude distribution of the noise can be obtained by comparing each input sample with an array of bins, each one representing a ΔI, and incrementing the level of the bin in which the input falls. The bins are then displayed on the graphics terminal.

An absolute accuracy of a measurement of this type is difficult if not impossible to specify, due to the statistics involved. What is usually done is to define a probable error, r, such that the probability is 1/2 that a measurement would lie within the interval $\sigma \pm r$. Figure 5 shows the distribution of errors for a series of measurements, each one of 2000 samples. Reference to this curve indicates that the probable error is $\approx 1.5^{o}/o$ (or the measurement will be within $1.5^{o}/o$ fifty percent of the time).

The D.C. accuracy of the digital system is $\approx 1^{o}/o$ down to 2.5 mv which corresponds to a .5nA noise current. The uncertainty of the RMS measurement is the sum of the uncertainties due to this error plus those due to sampling discussed above. The sum of the system error and the statistical error indicates that $50^{o}/o$ of the measurements will be within $2.5^{o}/o$. This figure can be improved upon by taking more samples, which will decrease the size of r discussed above. A trade-off exists between experiment time and tolerable error.

With a 6.5 nA noise current in the preamp-amp combination the smallest input or tube noise current that could be detected would be about 1nA.

Calculation of the noise for the first stage of our tube type preamplifier indicates that the noise to be expected with a 15MHz bandwidth would be 10.9 nA and at 10 MHz would be 6.0 nA. The measured noise at 15 MHz was 12 nA and at 10 MHz was 6.5 nA.

Peak to peak signal levels can also be measured readily with this digital technique and compared with those obtained from "box cars", as shown in Table I.

	Box Car	Sampling Oscilloscope
300 TV Lines	23.2 nA	23.7
400 TV Lines	15.8 nA	15.2

The accuracy of the last decimal point using the sampling oscilloscope is uncertain. However, it offers tremendous advantage in the time required to make a measurement compared to the "box car". The latter, however, can readily provide an accurate measurement, and detailed waveform without the requirement of a digital computer. On the other hand, the need of a digital computer with the sampling oscilloscope need not be a severe drawback, since a new acceptable TI mini-computer has appeared on the market for $2,800.

III. Digital System for Detailed Evaluation of Image Tubes

This portion of the paper will describe a system which is being developed to measure the performance of signal generating tubes using a digital computer. The motivation for developing such a digital system

is that a more detailed and flexible analysis of the data can be performed than is possible with analog methods. It will provide initially detailed computation of the devices signal and noise characteristics in terms of sinusoidal spatial frequencies, as derived from bar type test patterns. Further, its output will include a calculation of signal to noise ratio (SNR), Detective Quantum Efficiency, and be referenced to input signal based on photon flux. In addition, the computer will be programmed to provide a user with information referenced to photometric or radiometric units where applicable and requested.

The status of this system is that all components have been installed for interfacing the tube test set and computer, and are undergoing evaluation tests for optimization. This work is described below.

1. System Operation

Fig. 6 is a block diagram of the system which consists of the tube and its associated test set (see introduction), a digital computer and the interface between them. The interface is necessary to reduce the rate at which the video signal is sent (hence its bandwidth) compatible with the input capabilities of the computer. The computer, a Digital Equipment Corporation PDP-9, has a maximum input rate of 1 million data words per second via its direct memory access (DMA) channel.

A TV rate video signal obviously cannot be adequately sampled at a 1 MHz rate because of its much larger bandwidth. By using a storage terminal, here a Princeton Electronic Products Model 400, the video can be stored and subsequently read out at the desired slower rate. Storage and read out are governed by the control unit. In typical operation the

storage terminal is first erased and then one raster written at the TV rate with the unit synchronized to the camera tube. External drives are then applied to the storage terminal at a slower rate for read out. Vertical drive is a 10 bit D/A converter which can be set to either scan, producing a sawtooth-like waveform, or stay and reread at the same line. Horizontal drive is a sawtooth whose amplitude, DC offset level and frequency are independently adjustable. During read out, by adjusting these drive controls, several lines, one line or parts of a line in the stored image can be read out and sent to the computer. Note that since the sampling rate is constant (1 MHz), the sampling density is controlled by the amplitude and frequency of the horizontal drive.

The selected portion of the stored raster image is read out, A/D converted into a 7 bit integer and sent, via the DMA channel, to the computer memory. Control of the DMA channel is shared by the control unit and the program which is processing the data. The number of data words desired and their storage location in memory are set at the control unit, and when the program requests data, the control unit initiates the transfer. The program then goes to the proper location and stores the data on magnetic tape in FORTRAN compatible records, after presenting it on the display terminal. The display terminal is a special purpose computer driving a CRT with 1024 x 1024 addressable points. It is an especially powerful and convenient feature. Data can be displayed here for evaluation as soon as it is taken and permit immediate modification of the experiment, if necessary. Similarly, results of calculations on the data or the processing programs themselves can be displayed and edited.

The transfer function of the interface is not unity for all frequencies of interest and requires compensation. The transfer function of the storage terminal (as furnished by its manufacturer) is shown in Figure 7. Also shown is the product of storage terminal and the video amplifier response curve. Comparison of actual data and data generated using a low pass filter model of this video channel indicate that at present the response of the terminal is considerably worse than this curve predicts. This is attributed to misadjustments made during the installation of the interface and is correctable by realigning the unit.

In preliminary measurements signal currents of approximately 15 nA could be resolved. This should improve when the PEP-400 is properly aligned, and adjusted to use the full range of the A/D converter instead of the present reduced range (only 1/8 to 1/4 of full scale).

2. Signal Processing

This section indicates how the sine wave response of the tube is calculated from the collected data and is representative of the type of calculations which are performed. The video waveform out of the storage terminal is represented as $v(t) = s(t) + n(t)$, where $s(t)$ is the signal component and $n(t)$ the noise.

The noise is assumed Gaussian and can be represented by its mean m and variance σ^2. The mean is assumed to be zero, since it is indistinguishable from the pedestal. Now with the tube looking at a Limansky test chart, we take N samples of a video line, then M scans of this line (on successive rasters) and store them to generate an array of data which can be represented by:

$$v_j(k) = s(k) + n_j(k)$$

where $k = 1,2,3,.....N$

$j = 1,2,3,.....M$

By averaging the data from successive lines $\bar{v}(k)$, an estimate of $s(k)$ can be formed as shown below:

$$\bar{v}(k) = \frac{1}{M}\sum_{j=1}^{M} v_j(k) = \frac{1}{M}\sum_{j=1}^{M}[s(k) + n_j(k)]$$

$$= \frac{1}{M}\sum_{j=1}^{M} s(k) + \frac{1}{M}\sum_{j=1}^{M} n_j(k) = s(k) + n'(k) \qquad (4)$$

The $n'(k)$ themselves are Gaussian distributed but have RMS value $= \sigma/\sqrt{M}$ (assuming that noise on successive lines is statistically independent). Clearly as $M \to \infty$, $\bar{v}(k) \to s(k)$. The value of M depends on how good an estimate of $s(k)$ is desired and σ of the original noise.

Assuming a suitable value of M has been used to get a good approximation $\bar{v}(k)$ to $s(k)$, this can now be used as follows to compute sine wave response of the tube. The Fourier transform $V(f)$ can be found using the FFT algorithm on $\bar{v}(k)$[5].

Assuming linearity, it can be seen from Fig. 6 that the sine wave response of the tube $S(f)$ is given by

$$S(f) = \frac{V(f)}{C(f)\ H(f)} \qquad (5)$$

where $H(f)$ is the curve of Fig. 7 and $C(f)$ of the frequency spectrum of the bar chart if read by an ideal tube at the TV rate. The denominator can be calculated analytically, but is more conveniently done on the computer by simulating the bar chart.

It should be mentioned that $V(f)$ will have errors in it because

of the noise which still was present in $\bar{v}(k)$. To minimize the effect of these errors, the amplitude C(f) should be high for all f and relatively constant. This is not the case with the present bar chart. Under investigation is a new chart based on pseudo random sequences which is better suited to our system.

In Figs. 8a and 8b are shown the results of some data collection experiments. These photographs taken from the display terminal show a pulse and 300 KHz sine wave which were injected at the video amplifier input. At the input to the storage terminal both had peak to peak amplitudes of 200 nA. Note that in the photographs both signal and noise are clearly visible. Considerable improvement in the quality of data is expected when the storage terminal is realigned and as the system is fully developed.

References

1. Miller, L.D., in "Photo-Electronic Imaging Devices", ed. by L. M. Biberman and S. Nudelman, Vol. I, p. 267, Plenum Press, New York, 1971.

2. Nudelman, S. and Hickmott, J.T., Bull. Am. Phys. Soc., 4, 153 (1959).

3. Holter, M.R., Nudelman, S., Suits, G.H., Wolfe, W. L. and Zissis, G.J., "Fundamentals of Infrared Technology", p. 299, MacMillan, New York (1962).

4. Jensen, A.S. and Fawcett, J.M., in "Advances in Electronics and Electron Physics", ed. by J. D. McGee, D. McMullan, E. Kahan and B. L. Morgan, Vol. 28A, p. 289, Academic Press (1969).

5. Bergland, G. D., IEEE Spectrum, p. 41, July, 1969.

6. Lamb, J. D., IEEE Transactions on Automatic Control, p. 478, August, 1970.

Figure Captions

Figure 1a - Box Car Integrator Simplified Block Diagram

Figure 1b - System Block Diagram

Figure 2 - Typical A Scope Presentation with a Vidicon

Figure 3 - Box Car Integrator Output for 300 and 400 TVL/PH

Figure 4 - Block Diagram RMS Noise Measuring Circuit

Figure 5 - Distribution of Errors for 53 Measurements

Figure 6 - Block Diagram of Interface System

Figure 7 - Frequency Response Characteristics of Interface

Figure 8a - 8b - Examples of Video Data Collected Using System

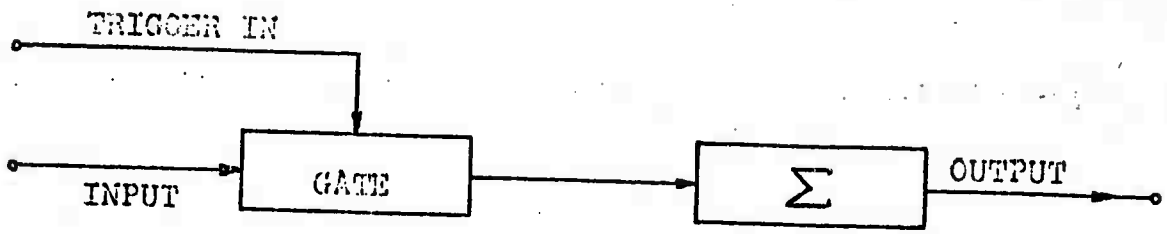

Fig. 1a.

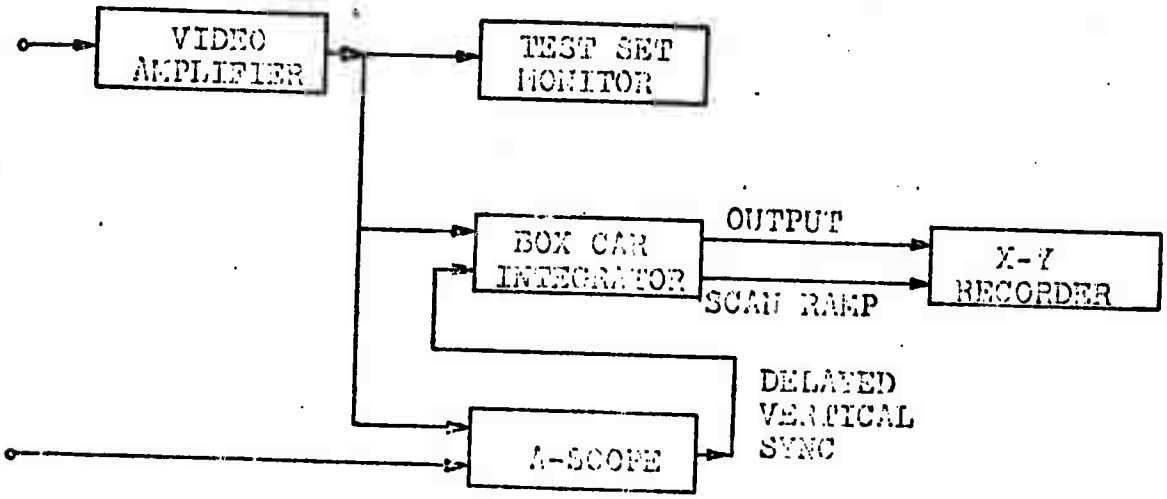

Fig. 1b.

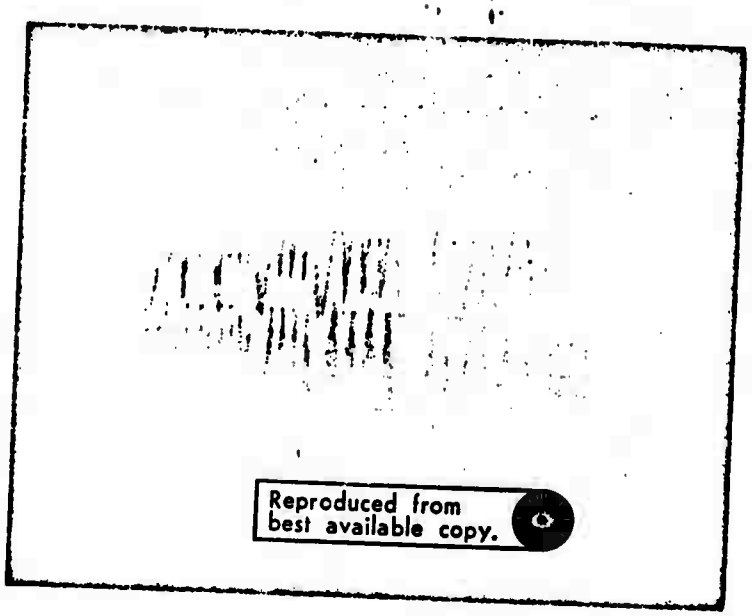

Figure 2

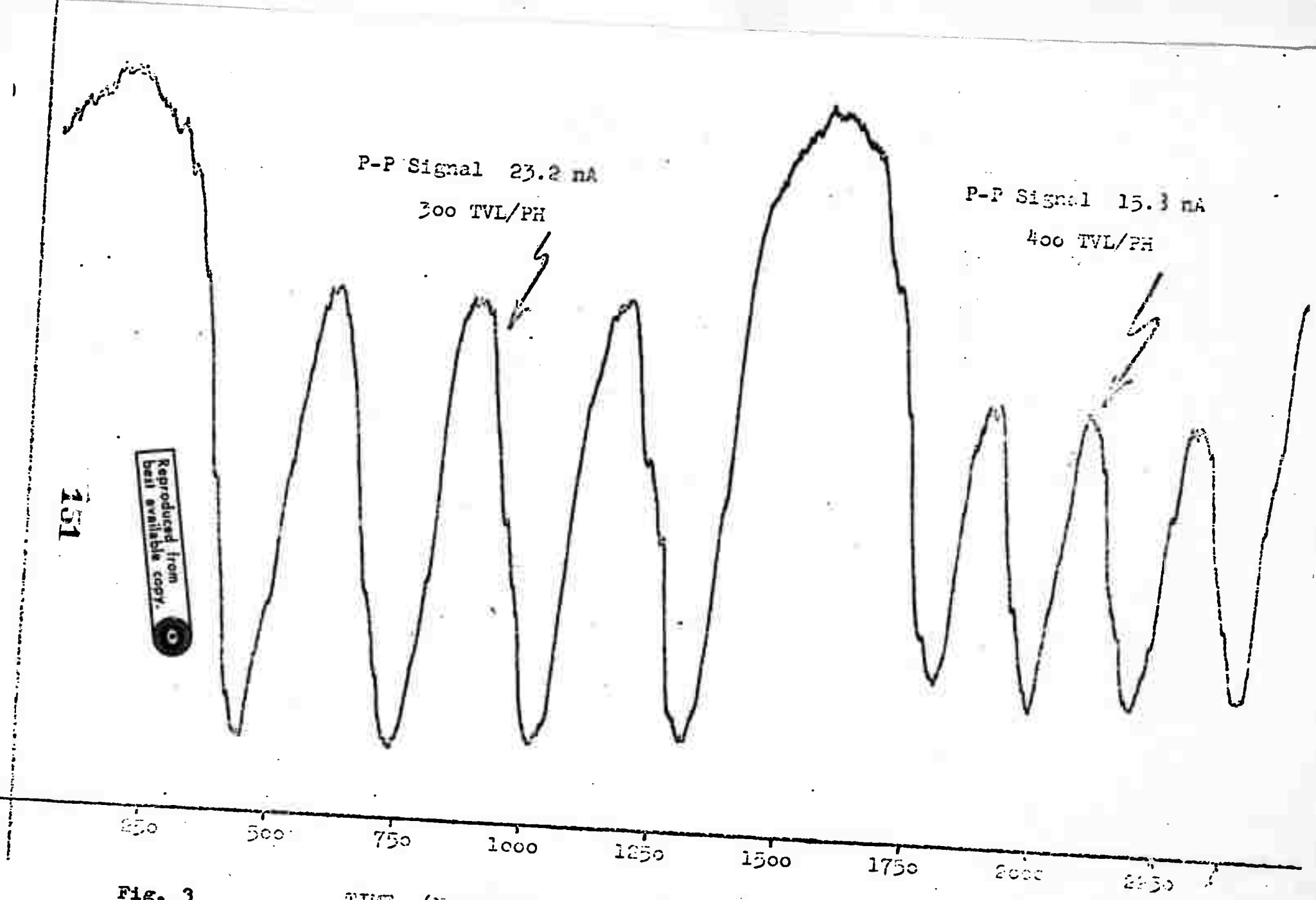

Fig. 3

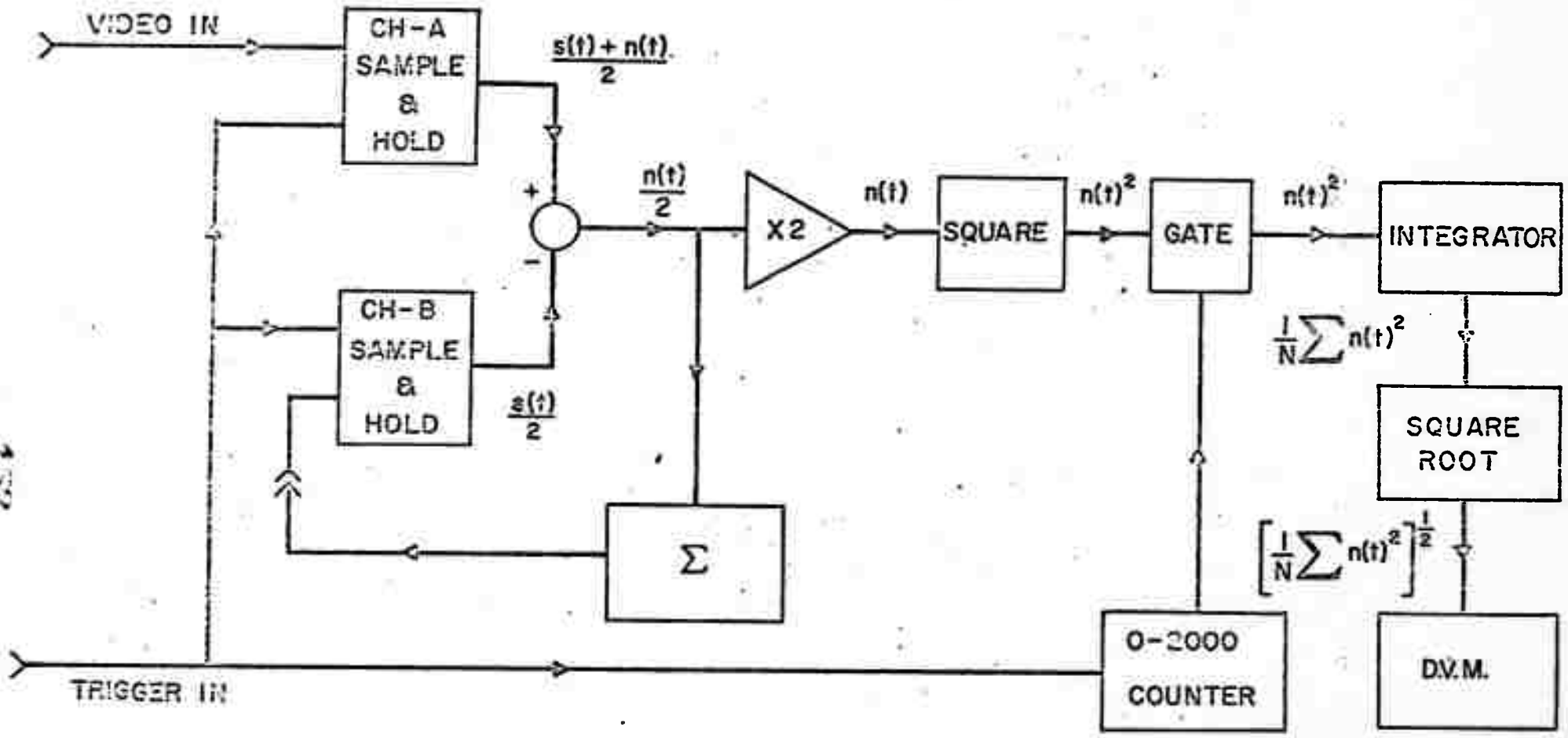

BLOCK DIAGRAM, RMS NOISE MEASURING CIRCUIT

FIGURE 4

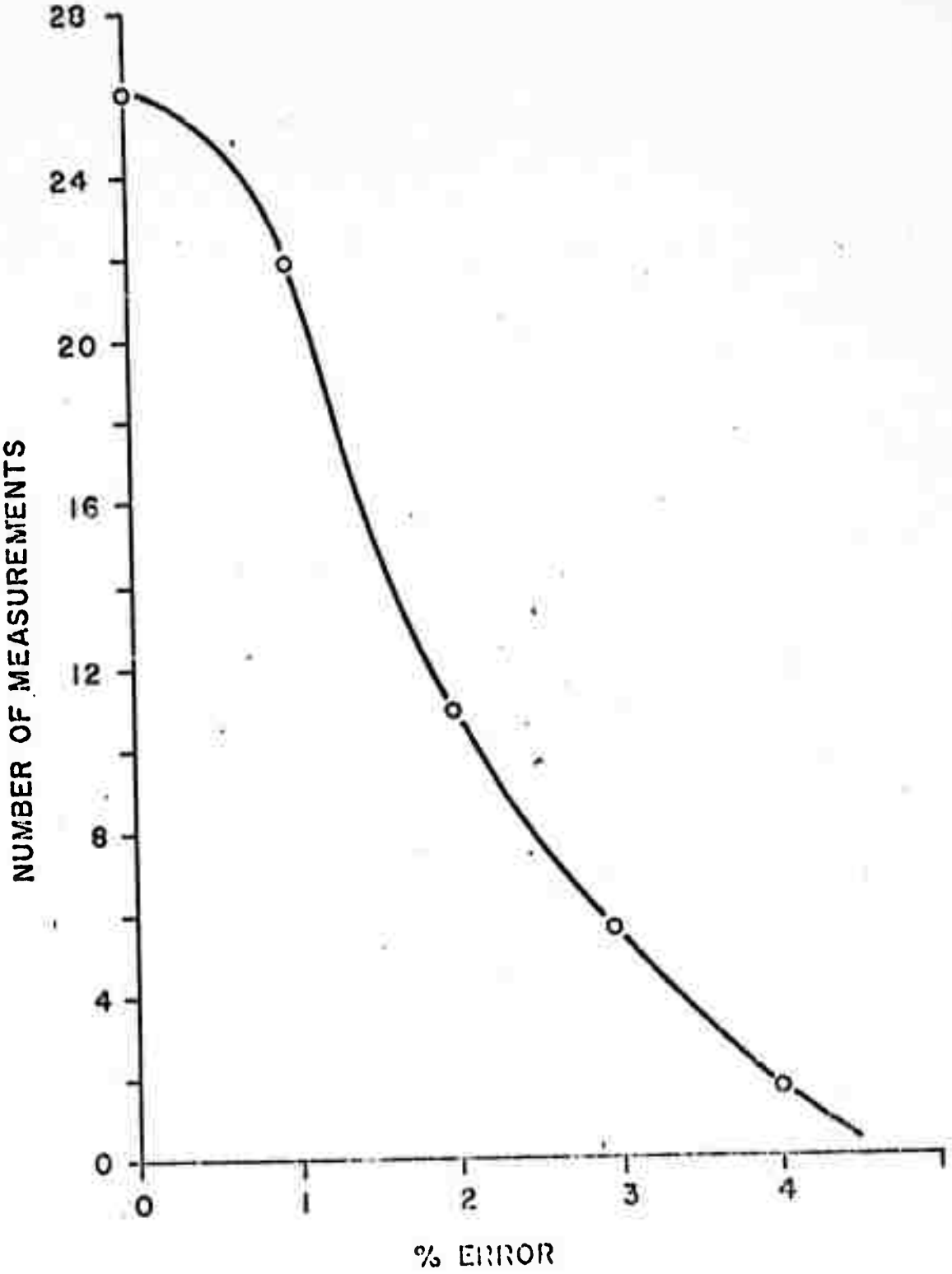

FIGURE 5

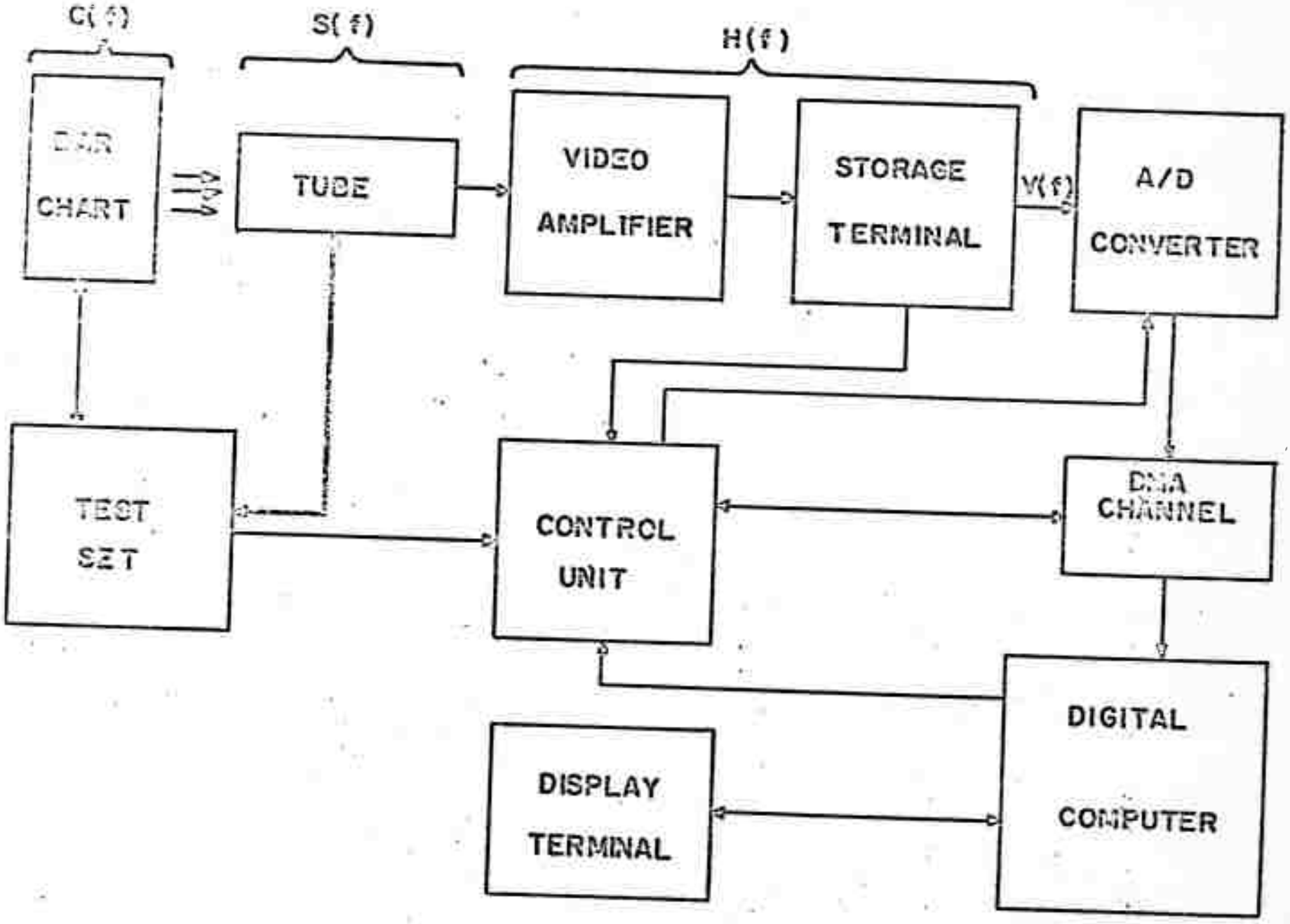
C(f)
S(f)
H(f)
BAR CHART
TUBE
VIDEO AMPLIFIER
STORAGE TERMINAL
V(f)
A/D CONVERTER
TEST SET
CONTROL UNIT
DMA CHANNEL
DISPLAY TERMINAL
DIGITAL COMPUTER

FIGURE 6

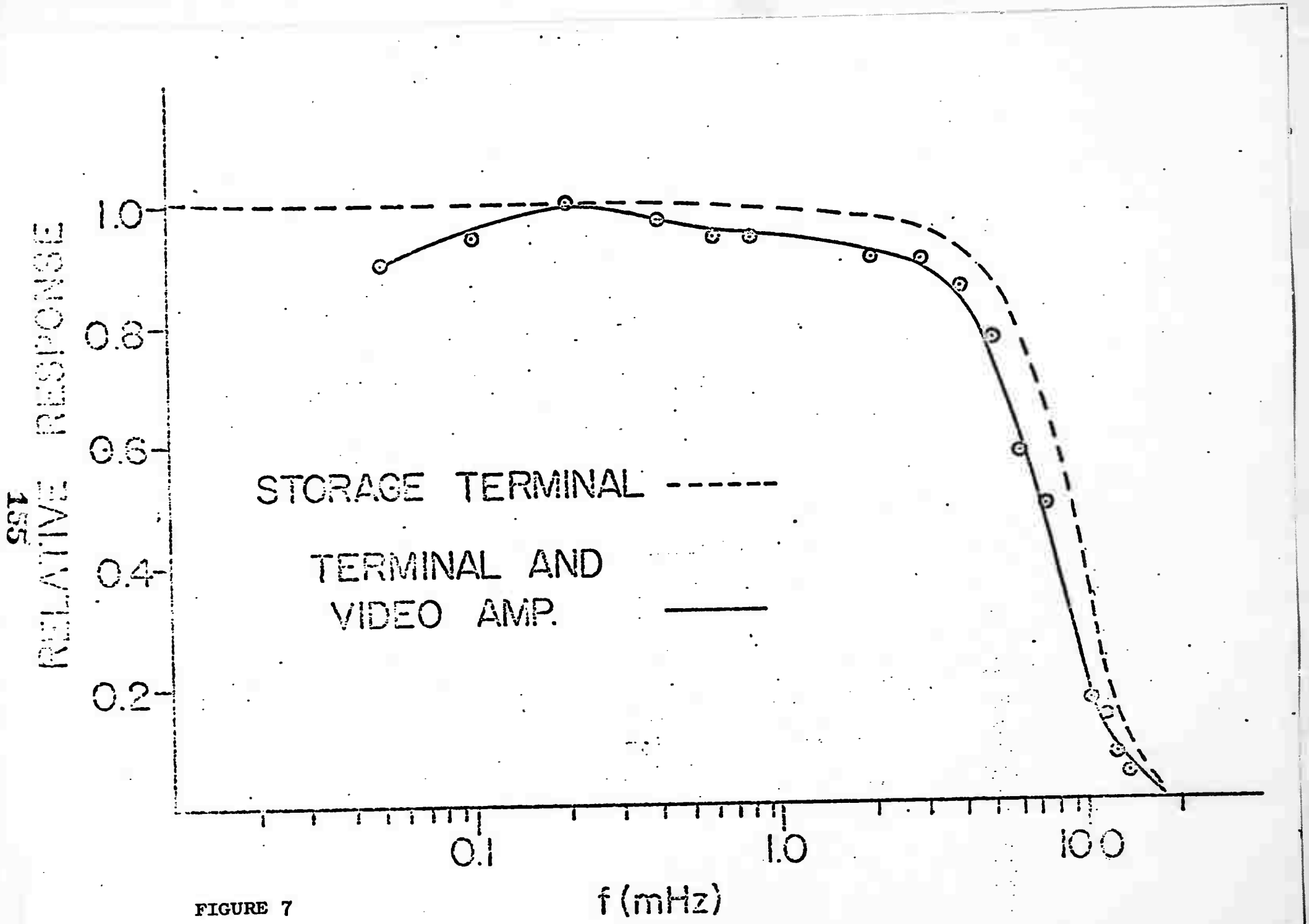
RELATIVE RESPONSE
1.0
0.8
0.6
0.4
0.2
STORAGE TERMINAL -----
TERMINAL AND
VIDEO AMP. ——
0.1
1.0
10.0
f (mHz)

FIGURE 7

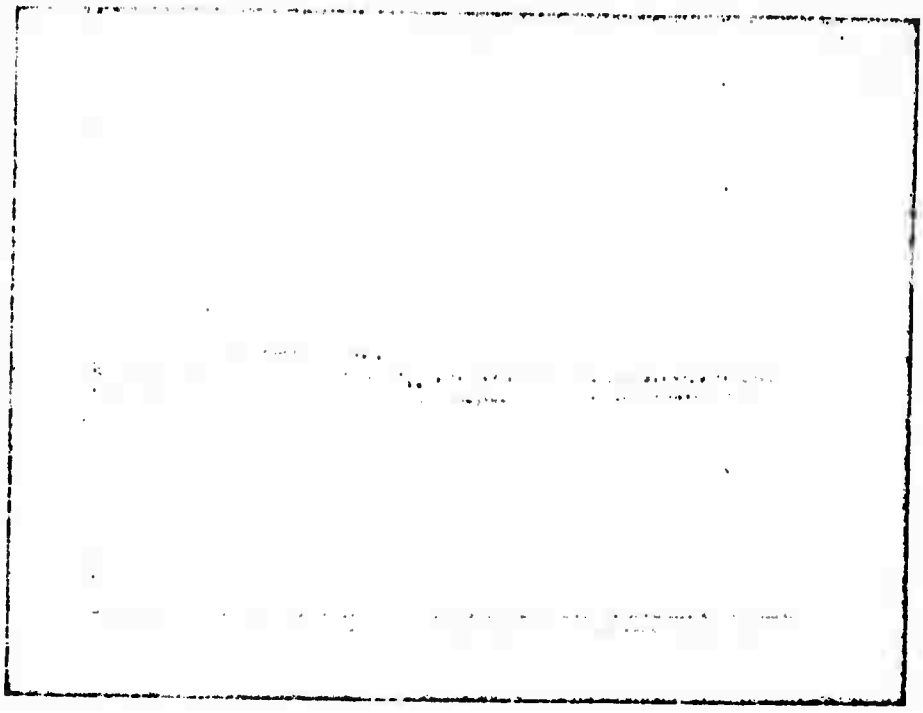

FIGURE 8a

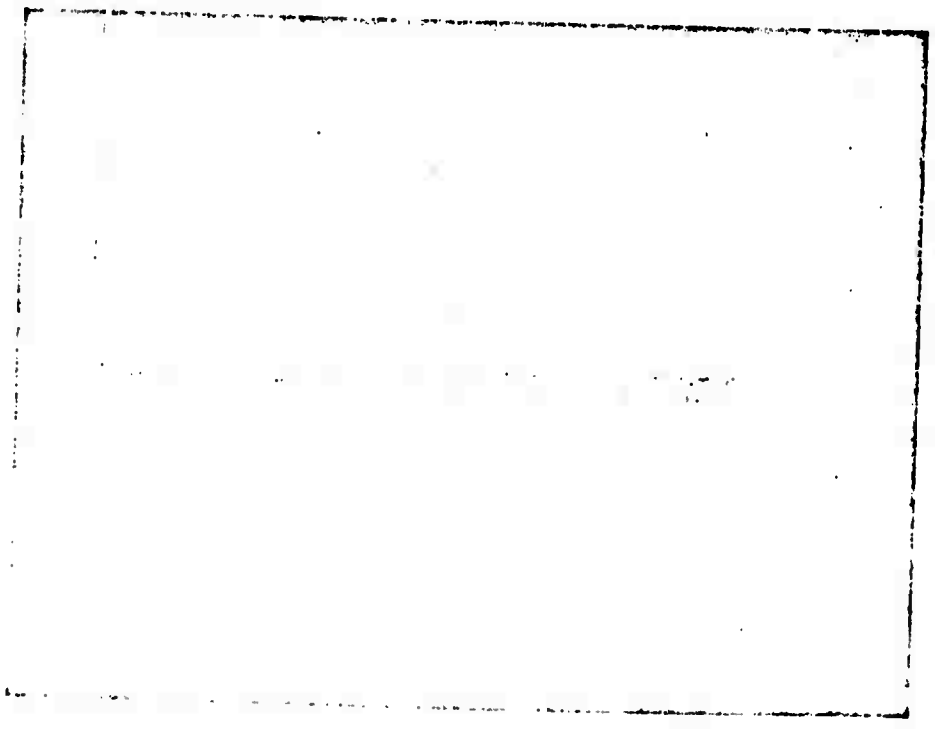

FIGURE 8b

The following, Appendix II, was published as a separate paper. Its page numbers are not consistent with the rest of the report.

Appendix II

METHODS FOR EVALUATING CAMERA TUBES

D. Fisher, R. Lee, V. McCollough, S. Nudelman

D. Tufts, M. Wilkinson

University of Rhode Island

A paper presented at the Fifth International Conference on Photo-Electronic Imaging Devices, September 17, 1971, Imperial College, University of London.

I. Introduction

Of considerable concern is a determination of how best to evaluate and specify the performance of image tubes. In particular, examination of current procedures reveals serious problems related to the accuracy of measuring output video signal and noise, as well as in accurately measuring input photon flux from signal and noise sources. For high light level conditions, accuracy in measurements tends not to be a serious matter. However, for low light level conditions where one wishes to know how much useful information is transmitted by the device, regardless of the source of limiting noise, the accuracy of measurements and the manner of presenting information relevant to device performance becomes increasingly important.

The current procedure used in industry is described by Miller[1]. The essence of the procedure is to generate a video square wave signal from a bar test pattern which is displayed on a line selector A-scope. "The output signal voltage is measured between the average voltage fluctuations of the video base line and the average voltage fluctuations at the top of the pulse. The noise voltage is measured without an input signal on the camera tube". It is accomplished by judging the width of the grass envelope displayed and dividing this value by six to obtain an estimate of the RMS value. The purpose of our program is to improve on

these measurements. In general, the following ideals comprise our goals:

1. Precise measurements of RMS noise, particularly noise in signal under noise limited conditions
2. Precise measurements of peak to peak signals (square wave) as a function of spatial frequency
3. Signal and noise spectra in terms of sinusoidal response
4. Calculate signal to noise ratios from steps 1 and 2 above, and similarly in step 3
5. Calculate the detective quantum efficiency as a function of spatial frequency.

The instrumentation for steps 1 and 2 can be relatively simple and inexpensive and suited to the small laboratory. Our approach to step 3 utilizes a computer and represents a much more substantial experimental effort. The approaches used in steps 1 and 2 are described in II below, while that to be used for steps 3 to 5 will be summarized in III.

The core of the test system is a Westinghouse tube test facility which uses a line selector A-scope type of presentation. Sampling instrumentation has been added for the determination of signal and noise as described in steps 1 and 2 above, in particular a box car integrator and sampling oscilloscope. To meet the requirements of steps 3, 4 and 5, the test facility has been interfaced to a PDP-9 computer graphics facility by a PEP storage terminal for line scan conversion and an HS-703 Computer Labs A/D (analog to digital) converter.

II. Analog P-P Signal and RMS Noise Measurements

The device used for measuring peak to peak signal is a box car

integrator (2,3). It is comparable to a lock-in-amplifier, but operates in the time rather than the frequency domain. The purpose of this instrument is to provide a noise free recorder trace of the signal waveform, particularly in noise limiting conditions where the A-scope measurement becomes inaccurate. Its operation is described in Section 1 below. Corresponding to this improvement in measuring signal however, is a loss of ability to measure the reduced noise. Measurement of noise requires a different repetitive sampling and integration technique which is the subject of Section 2.

1. Signal Recovery with a Box Car Integrator

A simplified block diagram is shown in Fig. 1a. A repetitive input signal is required, which need not necessarily be periodic. The input waveform is sampled at the repetition frequency. A trigger is provided to the "box car" in the same manner that would be required for good high speed oscillographic reproduction. The gate interval Δt represents an "on time" of an electronic switch, during which the signal and noise voltage is fed directly into an integrator. By sampling successive intervals and averaging, it is possible to reduce the noise-voltage fluctuation observed at the integrator output without affecting the signal level. Quantitatively, the noise-voltage fluctuations are reduced by $1/\sqrt{N}$, where N is the number of observations made during an average measurement. The signal to noise voltage ratio is then improved by the square root of N. If Δt is made small compared to the signal transient time, and is slowly and uniformly retarded in time with respect to signal onset,

an accurate chart record of the signal wave shape may be produced .[3]

The box car integrator used was a PAR Model 160, manufactured by Princeton Applied Research. This instrument provides an adjustable sampling gate width and a capability of positioning the sampling gate anywhere on the signal waveform. In addition, it provides considerable flexibility for regulating the rate at which the gate scans across the signal waveform.

The Model 160 utilizes RC type circuits to achieve integration and time constants which are adjustable in steps from 3 nanoseconds to 100 seconds. The time constant used is important because it will, along with the sampling gate aperture, determine the improvement in signal to noise obtainable and also the experiment time required to recover a point or waveform.

The system utilizing the "box car integrator" is shown in Fig. 1b. In practice, the user views the test pattern displayed on the "test set" monitor. He positions a horizontal strobe line on the monitor, so that it crosses the part of the test pattern to be measured. The strobe line is obtained by a pulse delayed from the vertical sync scan pulse with a continuously variable delay circuit. The video signal in the raster line selected by the positioning of the strobe line is then viewed on the A-scope.

The strobe trigger is also used to trigger the time base and sampling gate of the box car integrator. The trigger to the sampling gate is, of course, delayed again by the box car integrator to allow positioning anywhere on the line being viewed on the A-scope.

The conventional "A-scope" method for measurement of P-P signal which is illustrated in Fig. 2, was compared to that using the "box car"

approach. Fig. 2 shows an A-scope presentation taken with a typical Polaroid exposure. This exposure is then used by making a visual measurement between the centers of the average noise envelopes at the minimum and maximum levels.

Fig. 3 shows the results obtainable with the box car integrator for comparison with signal on the A-scope in Fig. 2 at 300 and 400 TV lines.

Measurements made using the box car integrator at high signal levels and low spatial frequency differed only slightly in apparent accuracy from those made using the conventional technique under the same conditions. However, the box car integrator does show remarkable improvement in readability over the conventional method at high spatial frequency and low light levels where noise limiting conditions dominate.

Because the box car integrator is capable of extracting waveforms at spatial frequencies approaching resolution limits (corresponding to small signals buried in noise), it will also be useful as a tool for analysis of signal shapes, leading to a better understanding of the electronic mechanisms involved in signal generation.

2a. RMS Noise Measuring Technique (Analog)

The discussion that follows describes a precise, non-subjective method for measuring the RMS magnitude of a non-synchronous waveform (noise) added to a synchronous input waveform (video signal). Its successful operation requires only that the input waveform be stationary and repetitive. Sampling techniques are used which provide wide bandwidth (12.4 GHz), good accuracy, a maximum data accumulation rate of 3600 samples/minute and which make no assumptions about the type of statistics governing noise or of the shape of the sampled waveform.

The principal method currently used for measuring noise is that described in the introduction[1]. An improvement on the above, developed by Jensen and Fawcett[4] at Westinghouse, made use of a clamping circuit to remove blanking pulses from the video signal. Then, assuming uniform target and input irradiance, this signal was fed to a standard RMS voltmeter, the output of which was corrected for duty factor.

We have attempted to improve on the above methods by developing a technique in which the only requirement is that the test pattern be stationary for a minute. The sampling technique used here is directly analogous to the familiar stroboscopic technique used with rotating machinery where a dynamic phenomenon is made to appear stationary by looking at it only when it is in the same position each time. The signal portion of the video output which is synchronized with the sampling strobe corresponds to a rotating shaft in the above analogy, while bearing chatter would be an analogous example of noise. Since the signal appears in the same position each time, it will appear as a constant level superimposed on which are added the fluctuations caused by noise. Sampling gate time is very short ($\approx 10^{-11}$ sec) compared to the highest frequencies encountered ($\approx$ 12 MHz), so that we can consider the sampled voltage as the instantaneous value of signal plus noise at that time. From these samples we can construct an ensemble of voltages, the RMS value of whose fluctuation is given by:

$$\sigma = \left[\frac{1}{N}\sum_{i=1}^{N}(X_i-\bar{X})^2\right]^{\frac{1}{2}} \qquad \text{where } \bar{X} = \frac{1}{N}\sum_{i=1}^{N} X_i \qquad (1)$$

where X_i equals the "instantaneous" value of signal s(t) plus noise n(t) at each sample time and $\overline{X}$ is the "stationary" signal s(t).

By instrumental design the signal level can become the reference level and adjusted to a zero voltage level (discussed below). Thus, the noise expression becomes:

$$\sigma = \left[\frac{1}{N_i} \sum_{i=1}^{N} n_i(t)^2 \right]^{\frac{1}{2}} \qquad (2)$$

where $n_i(t)$ is the sample $X_i - \overline{X}$ from frame i.
The solution of the above equation was first accomplished with analog and then digital computer type circuitry, which are described below.

The analog circuitry is depicted by the steady state block diagram of Fig. 4. The heart of this noise measuring system is a Hewlett Packard 1400 series sampling oscilloscope. It is a dual trace 12.4 GHz scope with delayed sweep time base, chart recorder output and manual positioning of the sampling point which makes the oscilloscope very attractive for this application.

The scope acts as the sample and hold circuit shown in Fig. 4, providing an output voltage which is held for one sixtieth of a second (one field period). Since the gain of the oscilloscope from input to output is one half, an amplifier was required to obtain an overall gain of unity. The amplifier output is then fed to a squaring device (PAR 230) every time a sample is taken. Since statistical variations about the video signal are sought, the signal level is adjusted to zero. This is accomplished by positioning the trace on the scope so that the average variation of the waveform about the zero volt level is zero. Circuitry for this purpose is described below.

A trigger signal corresponding to a selected raster line is obtained from the camera tube test set and is used to trigger simultaneously the oscilloscope and a counting circuit. This counting circuit controls a gate which controls the input to an integrator. Through the gate is fed the output of the squaring device. The time constant of the integrator is chosen so that if the integrator gate is enabled for 2000 one-sixtieth of a second samples, the output of the integrator will correspond to the mean sum of its input waveform. Since the input waveform was the instantaneous noise levels squared, we now have the mean squared value at the integrator output.

The RMS value is obtained by applying the output from the integrator to a device which takes the square root and then displaying the results on a digital voltmeter.

To remove the uncertainty in positioning the trace on the scope and to compensate for slow DC drift of the pedestal circuit in the test set video amplifier, a circuit was added which generates an error signal proportional to the mean of the input waveform by summing the output of the oscilloscope. Since any DC level which appears represents a shift of the trace from zero mean, this error voltage is subtracted from the video input voltage. This is easily accomplished by feeding the video signal into Channel A of the scope, the offset into Channel B and subtracting the two in the scope.

The limiting accuracy of this analog system is about 4°/o. This accuracy is far superior to that obtained by the visual estimation of the noise envelope on an A-scope, but further improvement is strongly desired. Since noise powers from independent sources add, RMS noise amplitudes add in quadrature, and thus the smallest added noise from, e.g. the tube under test, detectable through 6.5 nanoamperes of system preamplifier noise is about 1.9 nA.

2b, RMS Noise Measurement Technique (Digital)

To measure RMS noise by digital means, the sampling oscilloscope has been interfaced with the University's PDP-9 Computer Graphic Facility which is equipped with an A/D converter. This system is much simpler in hardware, the only components being the scope, computer and a low frequency buffer amplifier to match the scope output to the A/D input. Equation (1) can be rewritten as:

$$\sigma^2 = \overline{X^2} - \overline{X}^2 \qquad (3)$$

by expanding the parenthetical expression and combining terms. The computer A/D converts 2000 samples and stores them in successive locations in memory. Then $\overline{X^2}$, $\overline{X}^2$ and finally σ are calculated and the RMS value is printed out. There are several advantages to this method.

a) The A to D converter is very accurate (.025%).

b) There is no necessity for positioning the trace to zero on the scope screen, which was a problem in the analog system, since any D.C. level appears in $\overline{X}$ and its effects are eliminated mathematically.

c) Fewer demands are made upon the sampling oscilloscope, perhaps permitting use of one that would be less expensive.

d) The sampling rate is variable giving a choice of sampling every frame or every field, as is N, the number of samples taken.

e) The video signal amplitude can be determined accurately from the same experimental arrangement, since the calculated $\overline{X}$ represents the signal level plus a constant representing some arbitrary "zero level" at a point on the waveform. A measurement is first made at a maximum point on the waveform where $X = (S_I+C)$ and then at a minimum point where $X = (S_D+C)$,

where S_I is the signal at an illuminated portion of the photocathode, S_D is the signal from a dark portion and C is the "zero" constant. When the difference is formed, the constant falls out and we are left with an accurate determination of the peak to peak signal.

f) The amplitude distribution of the noise can be obtained by comparing each input sample with an array of bins, each one representing a ΔI, and incrementing the level of the bin in which the input falls. The bins are then displayed on the graphics terminal.

The absolute accuracy of a measurement of this type is difficult if not impossible to specify, due to the statistics involved. What is usually done is to define a probable error, r, such that the probability is 1/2 that a measurement would lie within the interval $\sigma \pm r$. Figure 5 shows the distribution of errors for a series of measurements, each one of 2000 samples. Reference to this curve indicates that the probable error is $\approx 1.5^{o}/o$ (or the measurement will be within $1.5^{o}/o$ fifty percent of the time), for any single measurement.

The D.C. accuracy of the digital system is $\approx 1^{o}/o$ down to 2.5 mv which corresponds to a .5nA noise current. The uncertainty of the RMS measurement is the sum of the uncertainties due to this error plus those due to sampling discussed above. The sum of the system error and the statistical error indicates that $50^{o}/o$ of the measurements will be within $2.5^{o}/o$. This figure can be improved upon by taking more samples, which will decrease the size of r discussed above. A trade-off exists between experiment time and tolerable error.

With a 6.5 nA noise current in the preamp-amp combination the smallest input or tube noise current that could be detected would be about 1nA.

Calculation of the noise for the first stage of our tube type preamplifier used for testing SEC camera tubes indicates that the noise to be expected with a 12MHz bandwidth would be 10.9 nA and at 10 MHz would be 6.0 nA. The measured noise at 12 MHz was 12nA and at 10 MHz was 6.5 nA, using the digital method just described.

Peak to peak signal levels measured with digital technique were compared with those obtained from a "box car" integrator, shown in Table I.

	Box Car Integrator	Sampling Oscilloscope with Computer Averaging
300 TV Lines	23.2 nA	23.7
400 TV Lines	15.8 nA	15.2

The accuracy of the last decimal point using the sampling oscilloscope is uncertain. However, it offers a tremendous advantage in the time required to make a measurement compared to the "box car" method. The latter, however, can readily provide an accurate measurement of signal amplitude plus a detailed record of the complete waveform without the requirement of a digital computer. On the other hand, the need for a digital computer with the sampling oscilloscope need not be a severe drawback, since an apparently acceptable and reasonably cheap computer has just appeared on the market.

III. Digital System for Detailed Evaluation of Image Tubes

This portion of the paper will describe a system which is being developed to measure the performance of signal generating tubes using a digital computer. The motivation for developing such a digital system

is that a more detailed and flexible analysis of the data can be performed than is possible with analog methods. Initially it will provide detailed computation of the devices signal and noise characteristics in terms of sinusoidal spatial frequencies, as derived from bar type test patterns. Further, its output will include a calculation of signal to noise ratio (SNR), Detective Quantum Efficiency, and be referenced to input signal based on photon flux. In addition, the computer will be programmed to provide a user with information referenced to photometric or radiometric units where applicable and requested.

The status of this system is that all components have been installed for interfacing the tube test set and computer, and are undergoing evaluation tests for optimization. This work is described below.

1. System Operation

Fig. 6 is a block diagram of the system which consists of the tube and its associated test set (see introduction), a digital computer and the interface between them. The interface is necessary to reduce the rate at which the video signal is sent (hence its bandwidth) compatible with the input capabilities of the computer. The computer, a Digital Equipment Corporation PDP-9, has a maximum input rate of 1 million data words per second via its direct memory access (DMA) channel.

A TV rate video signal obviously cannot be adequately sampled at a 1 MHz rate because of its much larger bandwidth. By using a storage terminal, here a Princeton Electronic Products Model 400, the video signal for an entire frame can be stored and subsequently read out at the desired slower rate. Storage and readout are governed by the control unit. In typical operation the storage terminal is first erased and

then one raster written at the TV rate with the unit synchronized to the camera tube. External drives are then applied to the storage terminal at a slower rate for readout. Vertical drive is a 10 bit D/A converter which can be set either to scan, producing a sawtooth-like waveform, or to stay and reread at the same line. Horizontal drive is a sawtooth whose amplitude, DC offset level, and frequency are independently adjustable. During readout, by adjusting these drive controls, several lines, one line, or parts of a line in the stored image can be read out and sent to the computer. Note that since the sampling rate is constant (1 MHz), the sampling density is controlled by the amplitude and frequency of the horizontal drive.

The selected portion of the stored raster image is read out, A/D converted into a 7 bit integer and sent, via the DMA channel, to the computer memory. Control of the DMA channel is shared by the control unit and the program which is processing the data. The number of data words desired and their storage location in memory are set at the control unit, and when the program requests data, the control unit initiates the transfer. The program then goes to the proper location and stores the data on magnetic tape in FORTRAN compatible records, after presenting it on the display terminal. The display terminal is a special purpose computer driving a CRT with 1024 x 1024 addressable points. It is an especially powerful and convenient feature. Data can be displayed here for evaluation as soon as it is taken to permit immediate modification of the experiment, if necessary. Similarly, results of calculations on the data or the processing programs themselves can be displayed and edited.

2. Signal Processing

This section indicates how the sine wave response of the tube is calculated from the collected data and is representative of the type of calculations which are performed. The video waveform out of the storage terminal is represented as $v(t) = s(t) + n(t)$, where $s(t)$ is the signal component and $n(t)$ the noise.

The noise is assumed Gaussian and can be represented by its mean m and variance σ^2. The mean is assumed to be zero, since it is indistinguishable from the pedestal. Now with the tube looking at a Limansky test chart, we take N samples along a video line, then M scans of this line (on successive rasters) and store them to generate an array of data which can be represented by:

$$v_j(k) = s(k) + n_j(k)$$

where $k = 1,2,3,\ldots\ldots N$

$j = 1,2,3,\ldots\ldots M$

By averaging the data from successive lines $\bar{v}(k)$, an estimate of $s(k)$ can be formed as shown below:

$$\bar{v}(k) = \frac{1}{M}\sum_{j=1}^{M} v_j(k) = \frac{1}{M}\sum_{j=1}^{M}[s(k) + n_j(k)]$$

$$= \frac{1}{M}\sum_{j=1}^{M} s(k) + \frac{1}{M}\sum_{j=1}^{M} n_j(k) = s(k) + n'(k) \qquad (4)$$

The $n'(k)$ themselves are Gaussian distributed but have RMS value $= \sigma/\sqrt{M}$ (assuming that noise on successive lines is statistically independent). Clearly as $M\to\infty$, $\bar{v}(k) \to s(k)$. The value of M depends on how good an estimate of $s(k)$ is desired and σ of the original noise.

Assuming a suitable value of M has been used to get a good approximation $\bar{v}(k)$ to $s(k)$, this can now be used as follows to compute sine

wave response of the tube. The Fourier transform V(f) can be found using the FFT algorithm on $\bar{v}(k)$[5].

Assuming linearity, it can be seen from Fig. 6 that the sine wave response of the tube S(f) is given by

$$S(f) = \frac{V(f)}{C(f)\ H(f)} \qquad (5)$$

where H(f) is the curve of Fig. 7 and C(f) is the frequency spectrum of the bar chart if read by an ideal tube at the TV rate. The denominator can be calculated analytically, but is more conveniently done on the computer by simulating the bar chart.

It should be mentioned that V(f) will have errors in it because of the noise which still was present in $\bar{v}(k)$. To minimize the effect of these errors, the amplitude C(f) should be high for all f and relatively constant. This is not the case with the present bar chart. Under investigation are new charts based on pseudo-random sequences which are better suited to our system.

Figures 8(a,b) show the results of some early experiments and are included to show the display capability of the system as well as its processing ability. The photographs were taken at the display terminal. Figure 8a shows the set of 100 TVL/PH bars of the Westinghouse test chart which were obtained after averaging 32 lines of data, each line containing 512 points. Fig. 8b shows a 10nA calibration pulse also after 32 averagings to reduce the noise. On the A-scope this pulse was barely visible. Signals as small as 3nA in noise of RMS value equal to 12nA can be resolved with only 32 lines of averaging.

References

1. Miller, L.D., in "Photo-Electronic Imaging Devices", ed. by L. M. Biberman and S. Nudelman, Vol. I, p. 267, Plenum Press, New York, 1971.
2. Nudelman, S. and Hickmott, J.T., Bull. Am. Phys. Soc., 4, 153 (1959).
3. Holter, M.R., Nudelman, S., Suits, G.H., Wolfe, W. L. and Zissis, G.J., "Fundamentals of Infrared Technology", p. 299, MacMillan, New York (1962).
4. Jensen, A.S. and Fawcett, J.M., in "Advances in Electronics and Electron Physics", ed. by J. D. McGee, D. McMullan, E. Kahan and B. L. Morgan, Vol. 28A, p. 289, Academic Press (1969).
5. Bergland, G. D., IEEE Spectrum, p. 41, July, 1969.

Figure Captions

Figure 1a - Box Car Integrator Simplified Block Diagram

Figure 1b - System Block Diagram

Figure 2 - Typical A Scope Presentation with a Vidicon

Figure 3 - Box Car Integrator Output for 300 and 400 TVL/PH

Figure 4 - Block Diagram RMS Noise Measuring Circuit

Figure 5 - Distribution of Errors for 53 Measurements

Figure 6 - Block Diagram of Interface System

Figure 7 - Frequency Response Characteristics of Interface

Figure 8a - 8b - Examples of Video Data Collected Using System

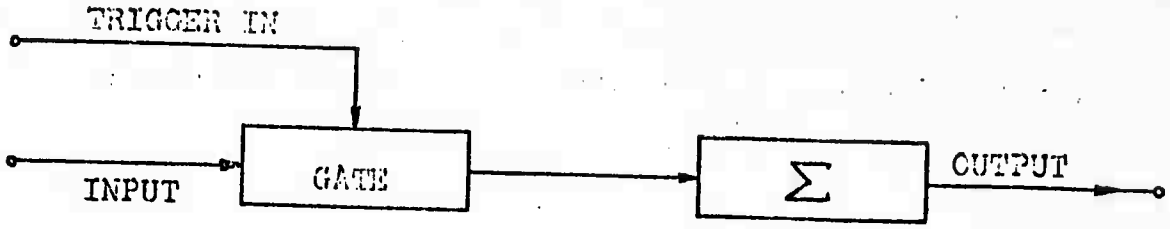

Fig. 1a.

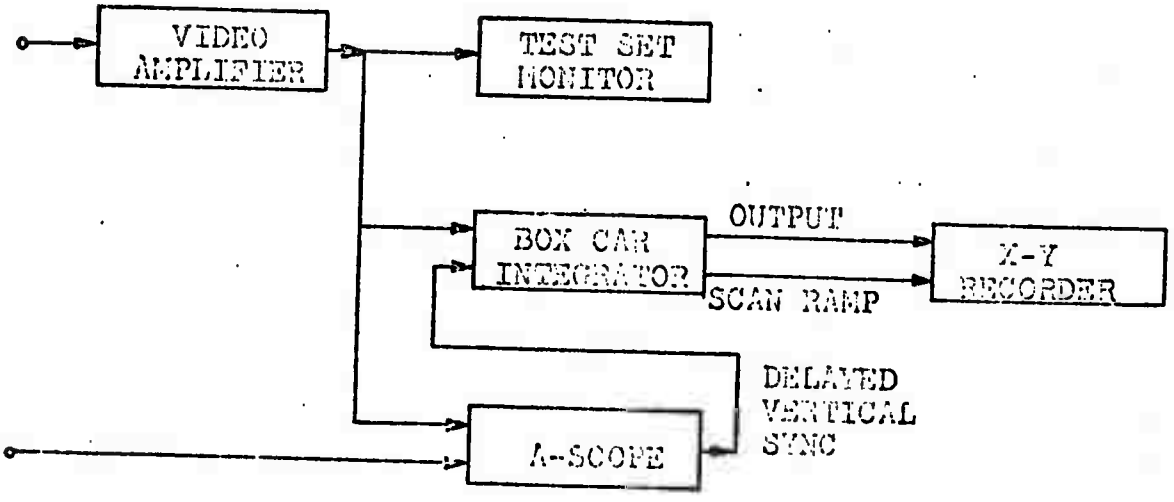

Fig. 1b.

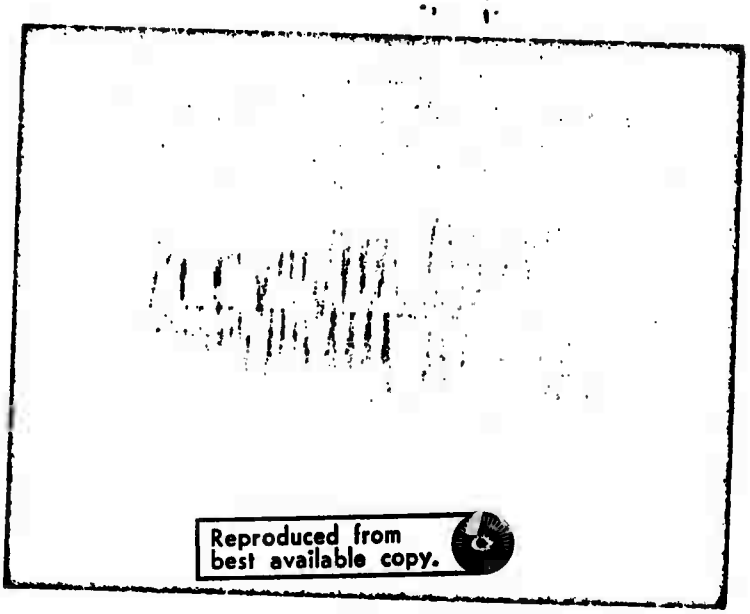

Figure 2

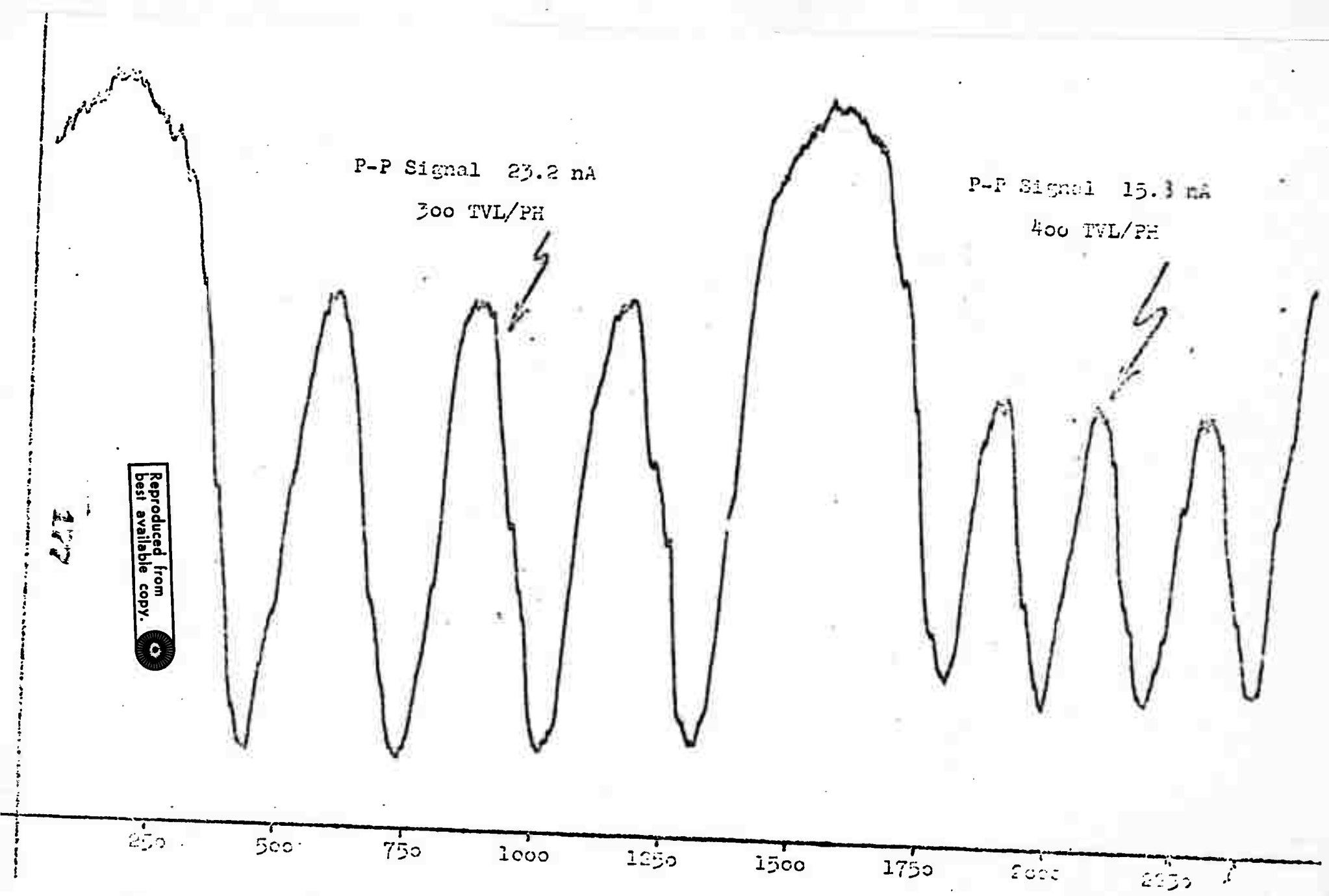

Fig. 3 TIME (Nanoseconds - referred to A-scope)

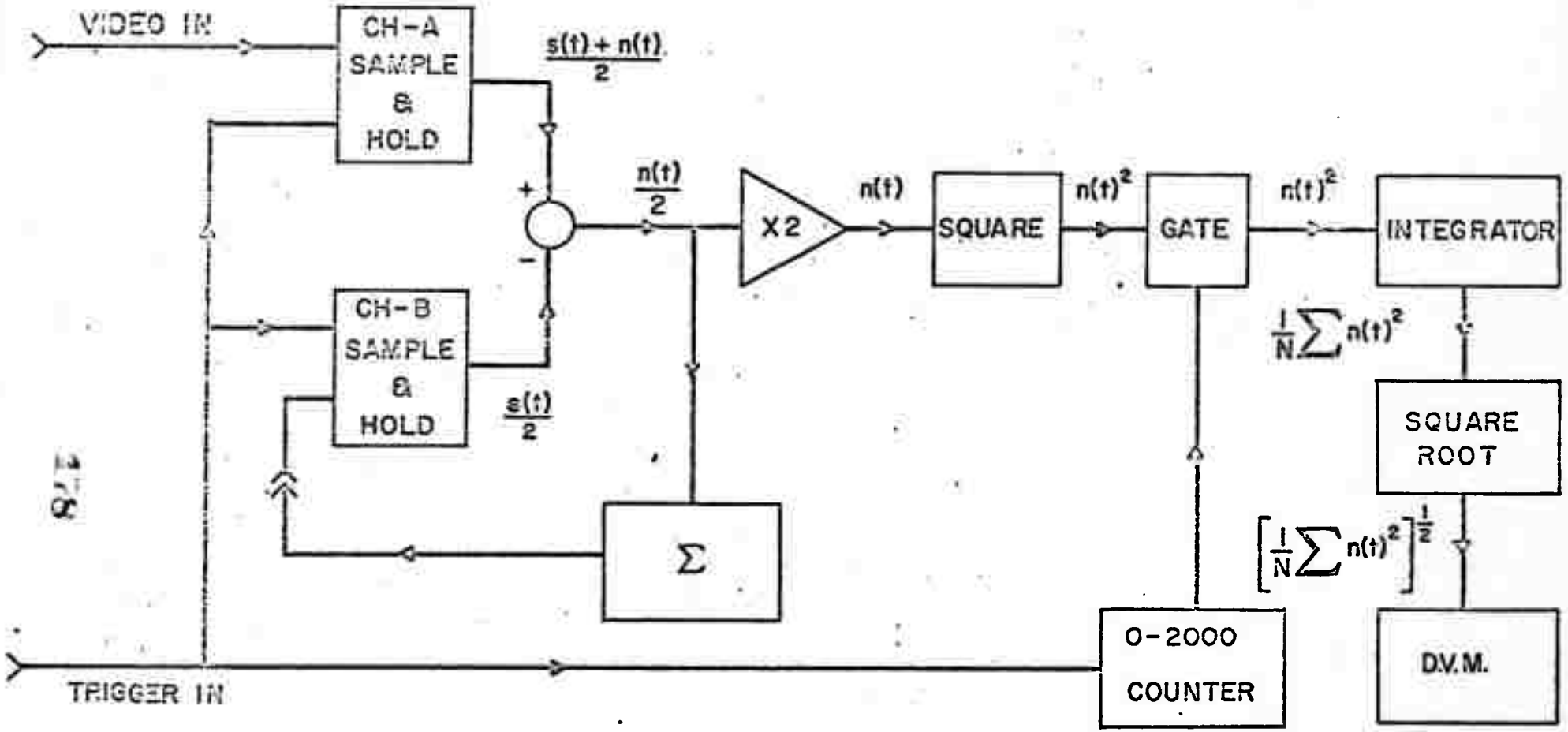

BLOCK DIAGRAM, RMS NOISE MEASURING CIRCUIT

FIGURE 4

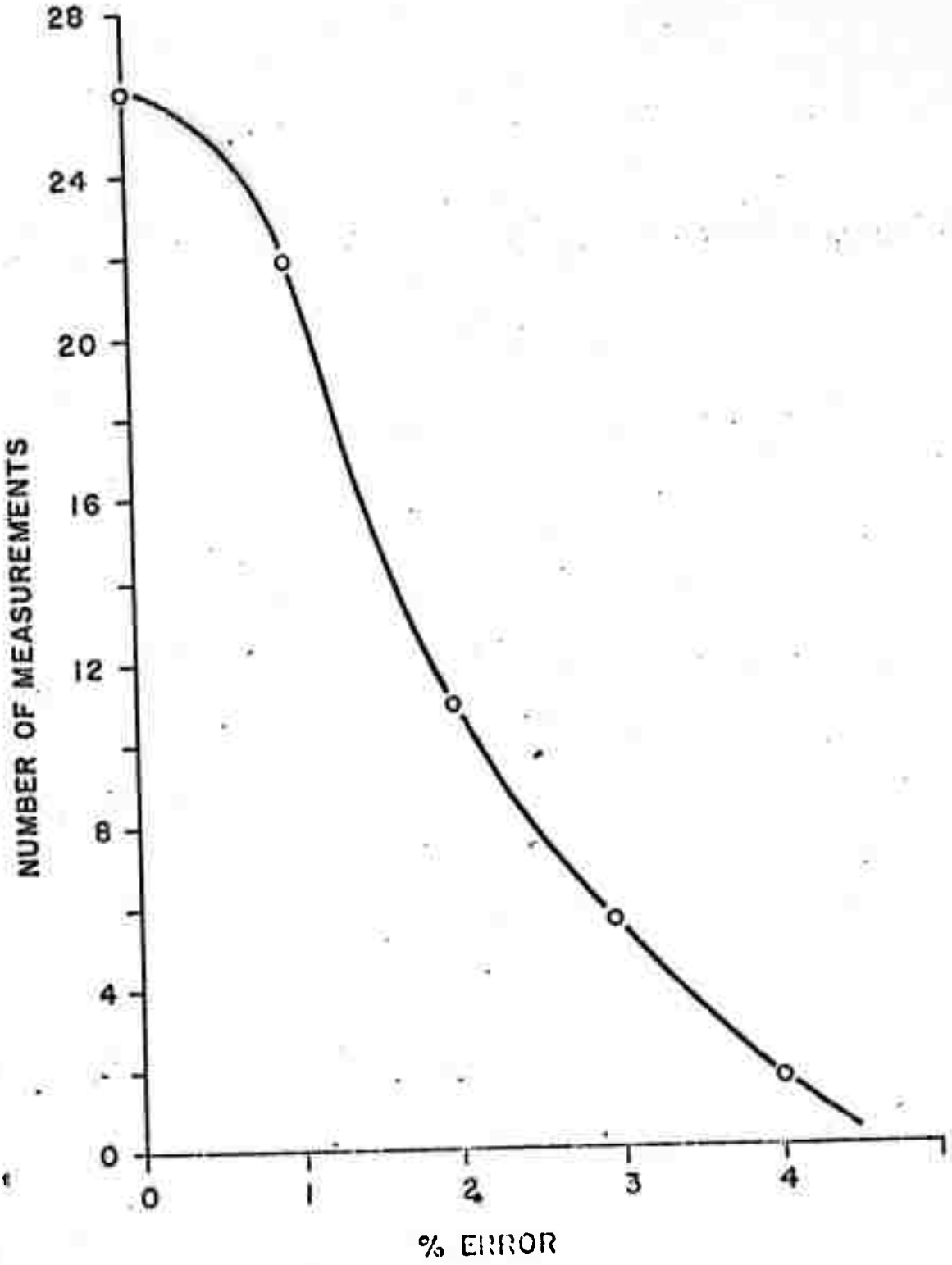

FIGURE 5

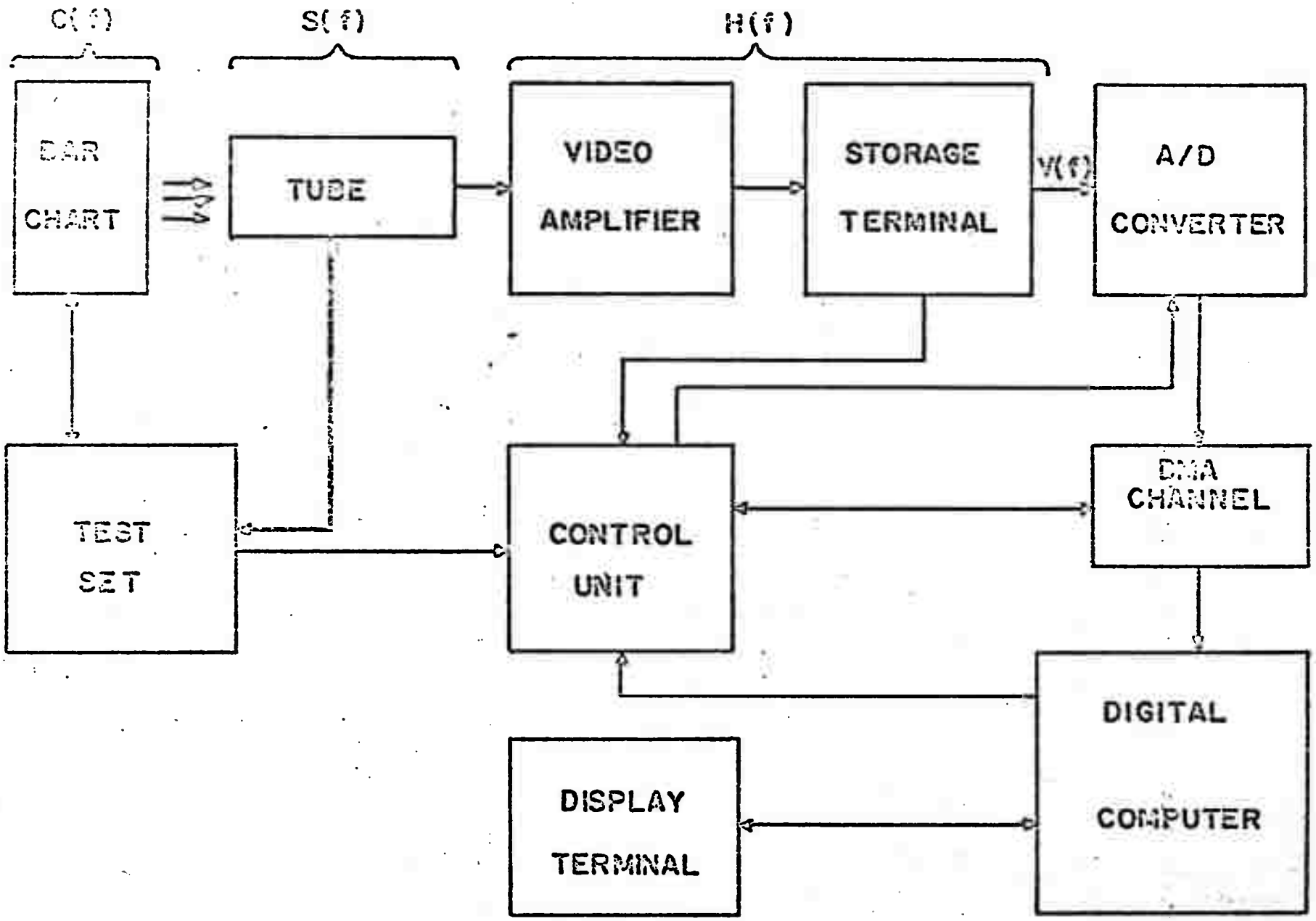
C(f)
S(f)
H(f)
BAR CHART
TUBE
VIDEO AMPLIFIER
STORAGE TERMINAL
V(f)
A/D CONVERTER
TEST SET
CONTROL UNIT
DMA CHANNEL
DIGITAL COMPUTER
DISPLAY TERMINAL

FIGURE 6

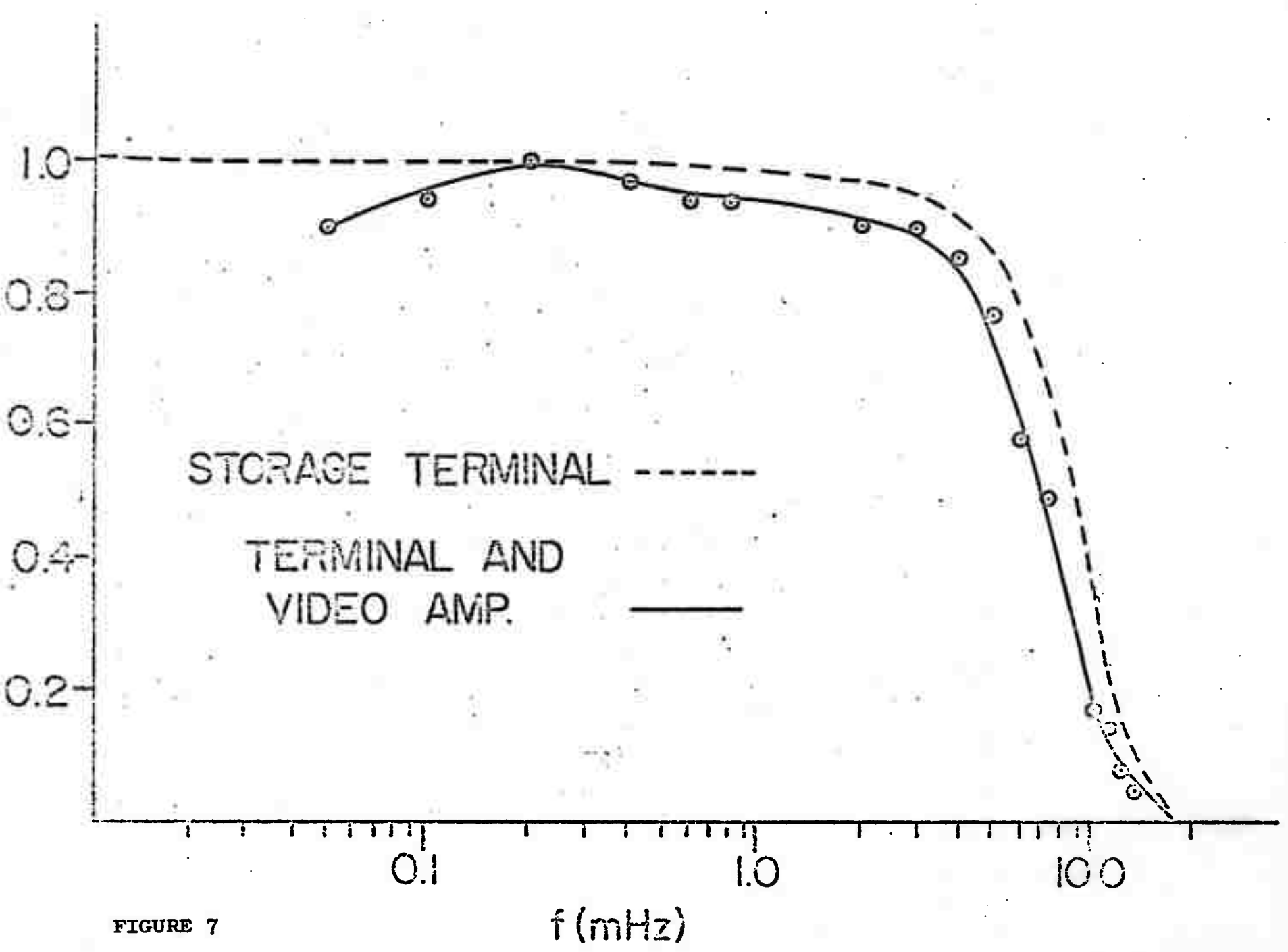
RELATIVE RESPONSE
1.0
0.8
0.6
0.4
0.2
STORAGE TERMINAL -----
TERMINAL AND
VIDEO AMP. ——
0.1
1.0
10.0
f (mHz)

FIGURE 7

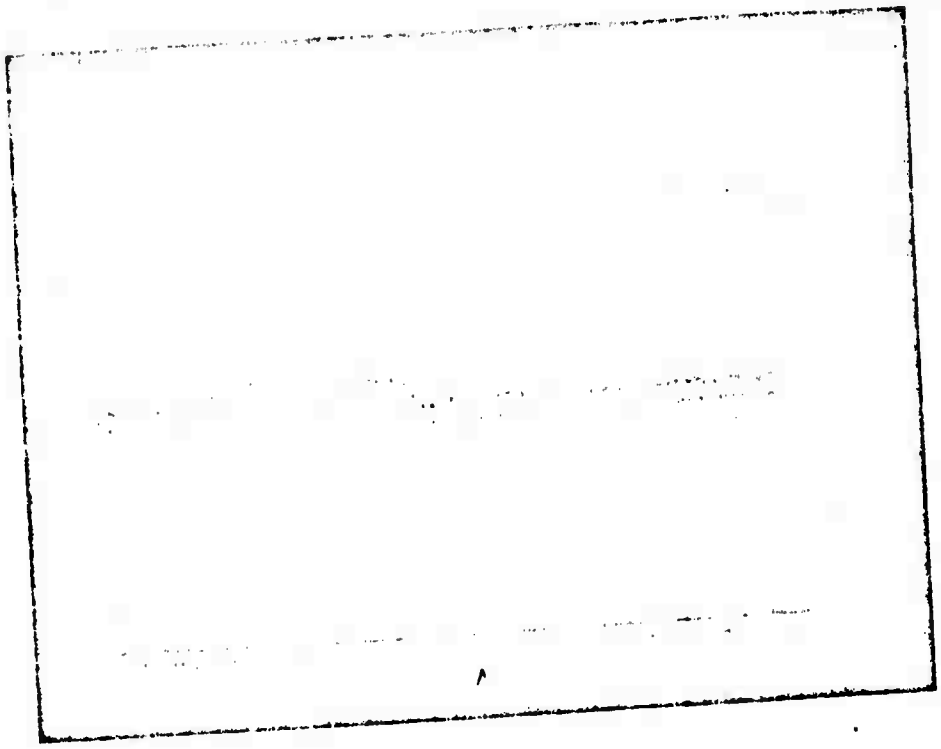

FIGURE 8a

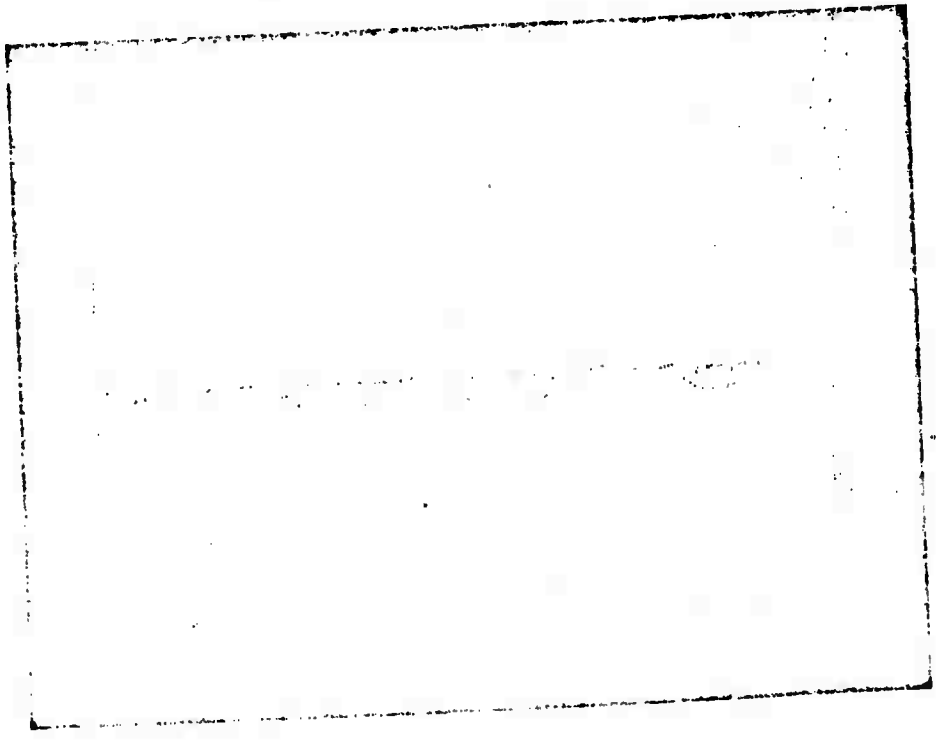

FIGURE 8b

Appendix III

MEASUREMENT OF NOISE IN THE VIDEO SIGNAL

1. Introduction

Noise is here defined as a varying current or voltage observed in the video channel which is random in both time of occurrence and amplitude. As shown in figure 1, it normally appears mixed with the video signal, including synchronizing, blanking, and shading signals which occur at both line and field rates. The measurement of rms noise amplitude or of noise power, therefore, requires separating the random noise from the video signal. Principal noise sources in the system, including the tube and the video preamplifier include, see figure 2, Johnson-Nyquist noise in the camera tube load resistor; shot noise in the first stage of the preamplifier; and in the camera tube under test, beam shot noise, shot noise in the target, and for an E. B. S. Tube, shot noise in the stream of photo-electrons leaving the photo cathode. Of these noise contributions, the largest is usually the video preamplifier shot noise, then the load resistor Johnson noise. Although these are not noise sources within the tube under test, they are always present and sufficiently large so that only very accurate noise measurements will permit separating and estimating the noise contributions from the tube under test from those external to the tube. Further, it can be shown that in most cases the size of the preamplifier noise contribution depends on the capacitance between the tube signal output electrode and ground, combined with the wiring and preamplifier input capacitance. Hence the accurate measurement of the preamplifier noise contribution is a proper concern of one who would measure the noise amplitude associated with the tube under test.

2. Measurement of Preamplifier Noise

Since noise is a set of randomly occuring pulses, whose amplitude distribution is approximately gaussian, the measurement should be in terms of noise power or equivalently in terms of an r.m.s. voltage or current derived from a true r.m.s. reading device. Further, since the noise spectra from the primary sources are thought to be essentially white[1], that is uniform noise power spectral density throughout the video spectrum, the measurement of noise current or power must be referred to an effective bandwidth, usually to the bandwidth of the video amplifier between the tube under test and the point where signal and noise measurements are made. Since the gain vs frequency characteristics of most video preamplifiers depend strongly on the shunt capacitance connected at the input terminal, all video amplifier noise measurements, and all gain vs. frequency measurements, should be made with the camera tube in place ready for operation and connected to the video amplifier. To eliminate the video signal, one may cutoff the electron beam either by biasing negatively the control grid of the electron gun or by interrupting the power supply to the cathode heater.

Accurate noise measurements will require elimination of the effect of synchronizing and blanking pulses. In some cases, the preamplifier noise can be measured easily by simply disabling or disconnecting the pulse generator circuits from the preamplifier, leaving at the test point only the preamplifier noise currents or voltages with no line or field rate signals. If removing these pulses does not change, e.g. the

1. The primary noise sources are white, but the rising gain vs. frequency characteristic of a typical video preamplifier means that the amplifier shot noise contribution is peaked toward higher frequencies, having an approximately triangular distribution.

operating point or the gain of the amplifier up to the test point, one may measure the noise current or voltage at the test point directly with a true r.m.s. reading meter, for example a thermocouple type r.f. milliammeter, then divide the measured value by the gain of the amplifier between the input terminal and the test point. If the signal is a voltage signal, it is then divided by the effective value of the load resistor to convert it to an equivalent noise current, referred to the input of the video preamplifier.

3. Measurement of Noise from either Camera Tube or Preamplifier

In some cases, however, the synchronizing and blanking pulses cannot be disabled without changing the operating point of the amplifier, or one may wish to measure preamplifier noise in the same configuration in which camera tube noise is measured so that the pulses and even the video signal must be present. Four methods have been used, and two are recommended.

3.1. Historically, the most popular method, which is not recommended, is to display the video signal at the test point from one or a few lines of the raster using a "line selector" oscilloscope. The observer selects a region corresponding to constant video signal and estimates the width of the apparent noise envelope, as shown in figure 3. The visual envelope is then assumed to correspond to either the $\pm 3\sigma$ or $\pm 2\sigma$ points in a Gaussian distribution and the rms noise voltage at the oscilloscope input is stated to be 1/6 or 1/4 of the envelope voltage, using the calibration means provided with the oscilloscope. This value is then divided by the preamplifier gain and the load resistor or other appropriate factors to convert it to an equivalent noise current referred to the preamplifier input.

This method has the advantage that the human observer can usually

separate the noise signal in the scope display from the gross video signal and from synchronizing or blanking pulses or from shading signals, although not from finely textured "fixed pattern noise", which see. Its great disadvantage is poor accuracy. The apparent noise envelope amplitude will depend on the brightness of the scope display and on the ambient illumination at the observer's position. Repeatability will not in general permit separating tube and system noise. Further, the uncertainty about the factor 1/6 or 1/4, makes quantitative measurements uncertain by ±10 to ±15°/o. Hence this measurement, though widely used, is not recommended.

3.2 A refinement on method 3.1., was described in IEEE Standard 158, Part 8, Methods of Test for Television Camera Tubes, corrected to 1965. As shown in figure 4, the oscilloscope display is viewed through a movable slit by a photo tube sensitive to the light emitted by the phosphor-screen of the display. The long dimension of the slit is oriented parallel to the horizontal, time, axis of the scope, and the photo tube output is measured and plotted as the slit is moved in the y or amplitude direction. Assuming that each noise pulse can be represented by a half sine wave and that its light output is concentrated near its peak, the light intensity profile is equated with the noise pulse amplitude distribution, and the value of σ, the r.m.s. noise pulse excursion amplitude with respect to the average video signal is determined by comparing the measured bell shaped curve with a standard Gaussian distribution.

This method is now considered relatively cumbersome, and the assumed relation between the brightness profile and the distribution of noise pulse amplitudes is only approximate. It is however, significantly better founded than method 3.1.

3.3. A way of making a direct rms noise measurement without disabling the synchronizing and blanking pulses was suggested by Jensen and Fawcett, Advances in Electronics and Electron Physics, Volume 28A.

In this method the tube under test is exposed to a uniform white or gray field so that the video signal is constant except for shading effects. The video channel is then keyed to select the video signal from only the central portion of the central scanning lines in each field. During the blanking intervals and when the beam is scanning the edges of the target where shading may be significant, the video signal is gated off, and a signal of the same average value as the center line video signal is substituted. The resulting noise and signal waveform shown in figure 5, is then presented to a true rms. reading meter. The reading must be corrected for the low duty cycles, but except for switching transients is a measure of rms noise at the test point in the video amplifier chain. As before, it is divided by amplifier gain to refer it to the preamplifier input terminal, and by the load resistance to convert it to an equivalent noise current.

Under ideal circumstances, this method should be far more accurate than either method 3.1 or method 3.2. Most TV camera systems, however, have shading due to falling irradiance off axis from the optical lens, because of sensor non-uniformities, and because of electron optical defects like non-normal landing of the deflected electron beam. Any shading signal appears as a line or field rate signal which the rms meter measures indistinguishably with the noise. To minimize this effect, the selected area from which signal is extracted is made smaller. However, this decreases the duty cycle and makes the effect of switching transients and of duty cycle inaccuracies more severe. Jensen estimates this method is at best accurate to only a few percent. Note

also that it does not distinguish between true random noise and fine grain fixed pattern noise.

3.4. The most accurate noise measuring method devised to date is in use at the University of Rhode Island. To truly measure rms noise in the presence of virtually any signal, data is taken from a single image element sampled once in each frame. Sampling is accomplished with a Hewlett Packard Model 140A sampling oscilloscope keyed to take its sample a selected number of microseconds after the start of a chosen line in the odd, or the even, field of the TV frame. The sampling gate width is typically 10^{-11} sec., virtually an instantaneous sample on the scale of the period of even the highest frequency handled by a 10mHz video channel. One data sample, the instantaneous value of signal plus noise, is taken from the same point in each frame and entered in a computer. Typically 2000 such samples are analyzed as an ensemble to determine the average value, the signal, and the rms deviation from that average value. The accuracy and reproducibility of this method are excellent, provided that the samples are taken from accurately the same location on the tube, and provided that the tube power supply and video amplifier circuitry produce no significant variations in gain or d.c. level during the 66 second measurement time. Note that these requirements, especially those of an accurately unvarying d.c. level, are often not met by standard television circuitry, and that slow variations of the order of the noise amplitude will usually not be visible on a TV display, but can interfere significantly with this measurement. Also note that the measurement time is significant. However, this appears to be the only method described to date which is accurate enough so that tube noise contributions can even be estimated

in the presence of preamplifier noise which is up to ten times larger. Assuming the stringent stationarity requirements can be met, it is also the only method which can ignore the effects of fixed pattern noise, and the only one which also establishes the distribution of noise amplitudes.

4. Evaluation of Tube Noise Contribution

The noise contribution from the camera tube and that from the preamplifier are independent, hence uncorrelated, and the total noise power is simply the sums of the noise powers considered separately. This means that if they could be measured separately

$$i_{nt}^2 = i_{na}^2 + i_{ns}^2$$

where i_{nt} = total rms noise current

i_{na} = rms noise current from the amplifier

i_{ns} = rms noise current from the sensor (tube under test)

In fact, all one can measure is i_{nt}, but by measuring it alternately with the tube operating normally and then with the lens capped or the electron beam current cutoff so that $i_{ns} = 0$, one can determine i_{nt} and i_{na}. At the present state of the art, i_{na} is about 2 to 4 x 10^{-9} amp for a typical 6 to 8 MHz bandwidth preamplifier. i_{ns} may be of the order of 5 x 10^{-10} amperes. To measure i_{ns} to significant accuracy, say 1 x 10^{-10} amp, 1/20 i_{na}, will require that changes in i_{nt} be measured to about 0.1%. This accuracy is completely beyond any of the other suggested methods. This suggested method is therefore recommended whenever critical noise measurements must be made, or as a standard against which other methods can be compared.

Figure 1 Video signal including noise

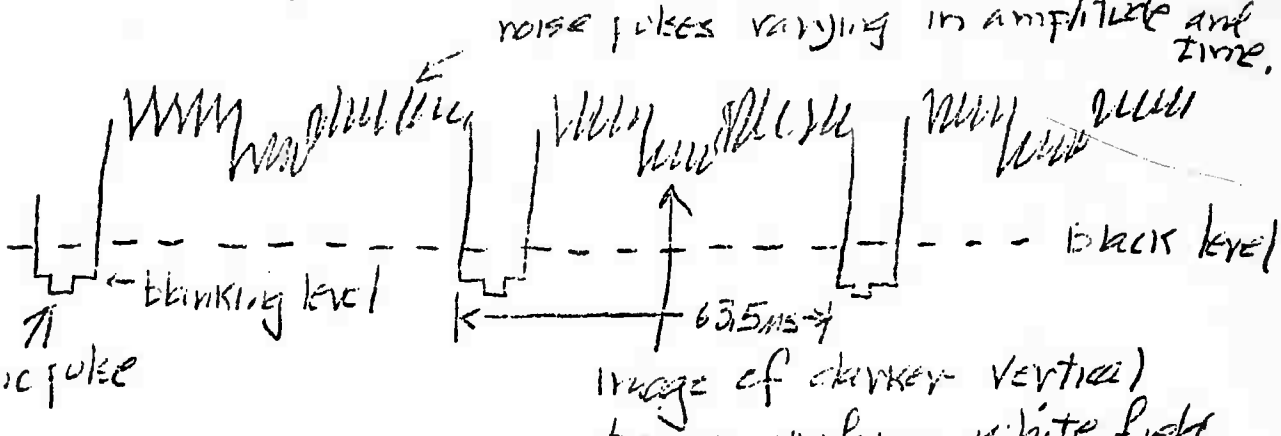

Figure 2 Principal television system noise sources.

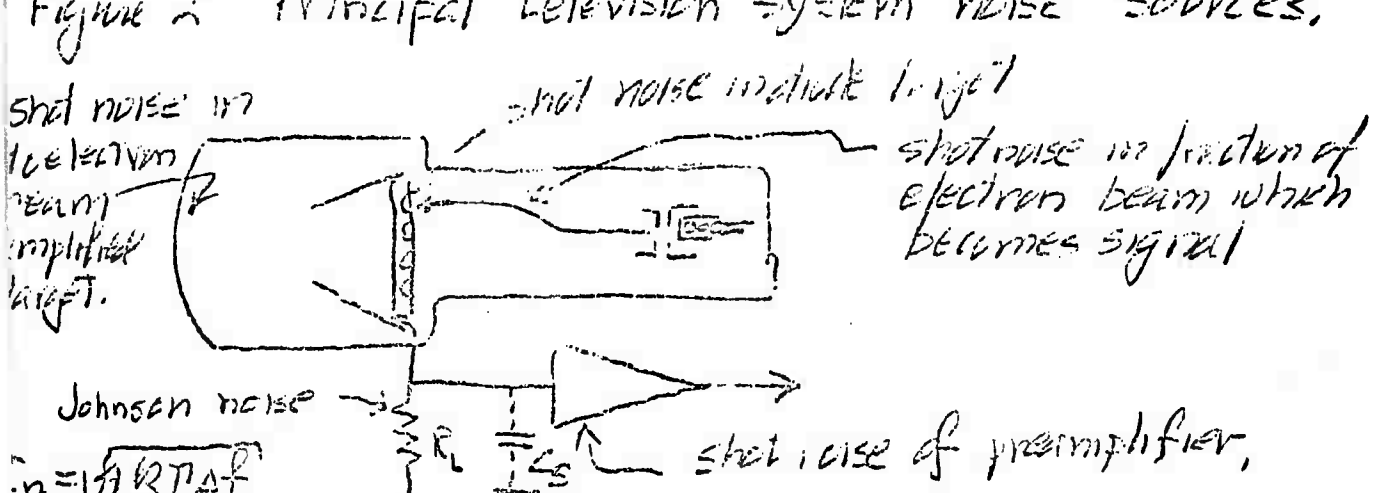

Figure 3 Noise estimation with a line selector scope.

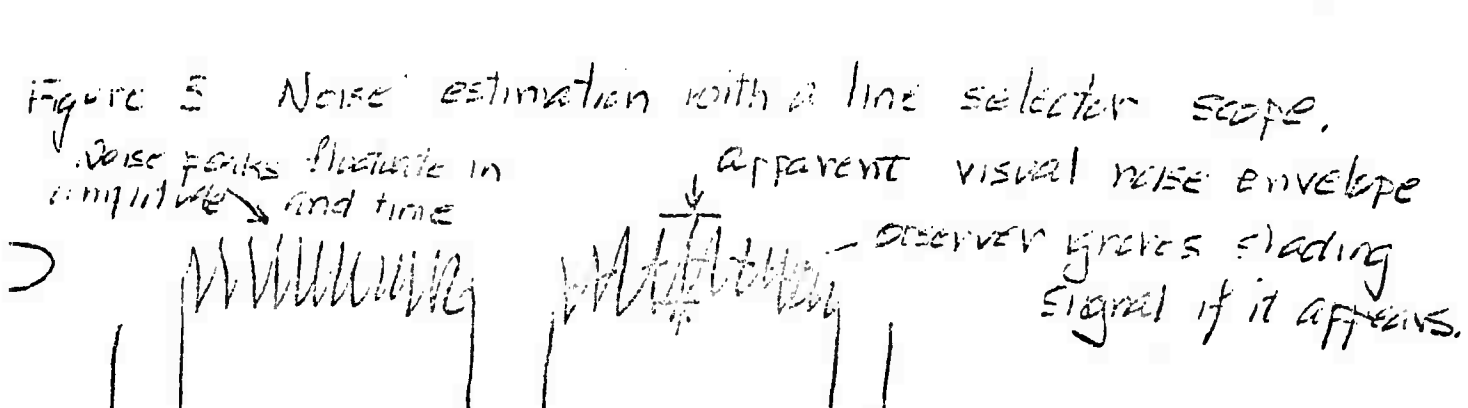

Figure 4. Old IEEE method for Noise Measurement.

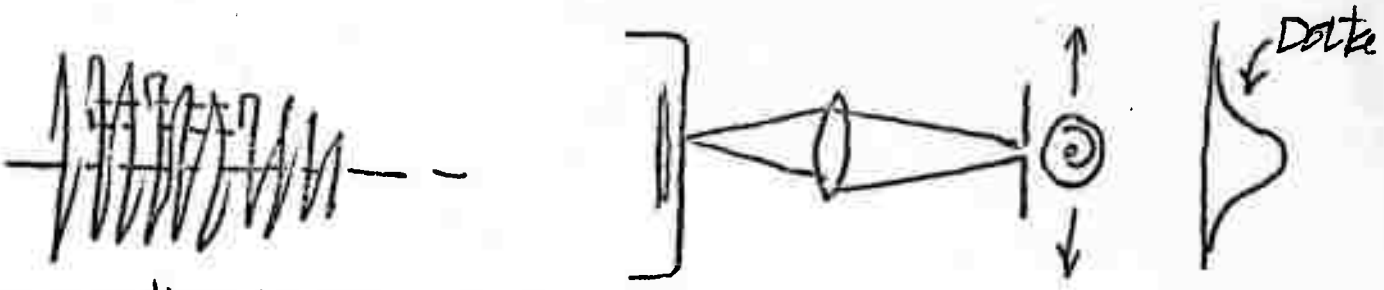

Noise pattern is scanned by slit indicated by dotted lines,

Slit, lens, and photocell are scanned as a unit over noise pattern. Resulting plot of brightness vs. displacement is identified with noise pulse distribution

Figure 5 Noise sampled from center of each scan line.

Raw signal:

After Sampling

This signal is fed to rms reading meter.